

AD-A021 201

A METHOD FOR PREDICTING HELICOPTER HUB DRAG

Thomas W. Sheehy, et al

United Technologies Corporation

Prepared for:

Army Air Mobility Research and Development
Laboratory

January 1976

**Reproduced From
Best Available Copy**

DISTRIBUTED BY:

NTIS

National Technical Information Service
U. S. DEPARTMENT OF COMMERCE

20000726027

USAAMRDL-TR-75-48

064091



A METHOD FOR PREDICTING HELICOPTER HUB DRAG

United Technologies Corporation
Sikorsky Aircraft Division
Stratford, Conn. 06602

ADAC 21201

January 1976

Final Report

Approved for public release;
distribution unlimited.

Prepared for

EUSTIS DIRECTORATE

U. S. ARMY AIR MOBILITY RESEARCH AND DEVELOPMENT LABORATORY

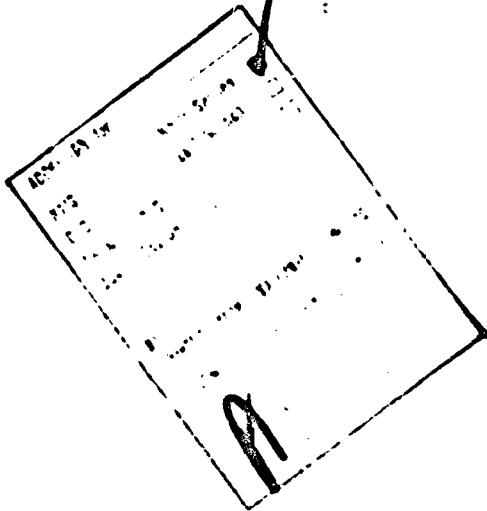
Fort Eustis, Va. 23604

Reproduced by
NATIONAL TECHNICAL
INFORMATION SERVICE
U. S. Department of Commerce
Springfield VA 22131

EUSTIS DIRECTORATE POSITION STATEMENT

This report has been reviewed by the Eustis Directorate, U. S. Army Air Mobility Research and Development Laboratory and is considered to be technically sound. The purpose of the program was to develop a procedure to predict the drag of a basic helicopter rotor and hub pylon.

The program was conducted under the technical management of William D. Vann of the Technology Applications Division.



DISCLAIMERS

The findings in this report are not to be construed as an official Department of the Army position unless so designated by other authorized documents.

When Government drawings, specifications, or other data are used for any purpose other than in connection with a definitely related Government procurement operation, the United States Government thereby incurs no responsibility nor any obligation whatsoever; and the fact that the Government may have formulated, furnished, or in any way supplied the said drawings, specifications, or other data is not to be regarded by implication or otherwise as in any manner licensing the holder or any other person or corporation, or conveying any rights or permission, to manufacture, use, or sell any patented invention that may in any way be related thereto.

Trade names cited in this report do not constitute an official endorsement or approval of the use of such commercial hardware or software.

DISPOSITION INSTRUCTIONS

Destroy this report when no longer needed. Do not return it to the originator.

Unclassified

SECURITY CLASSIFICATION OF THIS PAGE(When Data Entered)

20. ABSTRACT (cont'd)

A review of available rotor hub drag test data was conducted in order to identify the factors affecting helicopter rotor hub drag. The data base established was used in the development of the hub drag prediction method and also to define a systematic wind tunnel test program to refine and verify the drag prediction method and to investigate in detail the parameters affecting the drag contribution of the rotor hub.

The results of the data review indicate that the primary factors affecting the rotor hub drag and its associated interference drag are the swept frontal area, the increase in the local dynamic pressure due to the fuselage/pylon configuration, and the pylon shape.

2

Unclassified

SECURITY CLASSIFICATION OF THIS PAGE(When Data Entered)

PREFACE

This program was sponsored by the Eustis Directorate, U. S. Army Air Mobility Research and Development Laboratory (Contract DAAJ02-74-C-0050) and was monitored by Mr. William D. Vann. The authors express their appreciation to Mr. Vann for his assistance during the course of this study.

TABLE OF CONTENTS

	<u>Page</u>
PREFACE	3
LIST OF ILLUSTRATIONS	6
INTRODUCTION	9
HUB DRAG DATA REVIEW	10
HUB DRAG PREDICTION METHOD	18
Method Development	18
Aerodynamic Analysis Technique	25
Method Application and Correlation	29
HUB FAIRING DESIGN	34
WIND TUNNEL TEST DEFINITION	35
CONCLUSIONS	39
REFERENCES	41
BIBLIOGRAPHY	43
APPENDIXES	
A. DESCRIPTION AND USE OF AUTOMATED PANELING TECHNIQUE - PROGRAMS Y179A, Y179C	71
B. DESCRIPTION AND USE OF THE THREE-DIMENSIONAL AERODYNAMIC ANALYSIS TECHNIQUE - PROGRAM Y179L	89
C. DESCRIPTION AND USE OF THE HUB DRAG PREDICTION PROGRAM - Y179Z	105
LIST OF SYMBOLS	107

LIST OF ILLUSTRATIONS

<u>Figure</u>		<u>Page</u>
1	Trend of Rotor Hub Incremental Drag With Aircraft Gross Weight	45
2	Rotor Hub Drag Contribution to Total Helicopter Drag	46
3	Hub Drag Trend With Hub Frontal Area for Unfaired Hubs	47
4	Hub Incremental Drag Trend With Hub Frontal Area for Unfaired Hubs	48
5	General Types of Rotor Hub Fairings	49
6	Faired Hub Incremental Drag Variation With Fairing Thickness to Diameter Ratio	50
7	Effect of Hub-Pylon Separation Distance on Hub Interference Drag	51
8	Variation of Incremental Hub Drag With Body Attitude	52
9	Rotational Effects on Incremental Rotor Hub Drag	53
10	Effect of Mach Number Variation on Incremental Hub Drag	54
11	Comparison of Full-Scale and One-Sixth Scale Rotor Hub Drag Test Results	55
12	Pylon Drag Trends With Pylon Length-to-Height Ratio	56
13	Example of a General Helicopter Configuration With an Unfaired Rotor Hub	57
14	Example of a General Helicopter Configuration With an Ellipsoidal Faired Hub	58
15	Example of a General Helicopter Configuration With a Rigid Rotor Hub Fairing	59
16	Geometric Model of a Simulated Fuselage/Pylon Configuration	60

LIST OF ILLUSTRATIONS (Continued)

<u>Figure</u>		<u>Page</u>
17	General Pylon Configurations	61
18	Calculated Surface Pressures Along the Centerlines of Type A Pylons	62
19	Calculated Surface Pressures Along the Centerlines of Type B Pylons	63
20	Calculated Surface Pressures Along the Centerlines of Type C Pylons	64
21	General Ellipsoidal Fairing Characteristics	65
22	Calculated Surface Pressures Along the Tops of General Ellipsoidal Fairings	66
23	Calculated Surface Pressures Along the Sides of General Ellipsoidal Fairings	67
24	Calculated Equivalent Forebody Pressure Coefficients for General Ellipsoidal Fairings	68
25	Geometric Model of a Pylon/Simulated Fuselage Upper Surface Configuration . . .	69
26	Comparison of Calculated Surface Pressures for a Pylon Configuration With and Without a Complete Fuselage Simulation	69
27	Rigid Rotor Hub Fairing Designed to Reduce Rotor Hub Incremental Drag	70
A-1	CH-53E Fuselage Generated by Automated Paneling Technique.	83
A-2	Description of Segment Types and Input Points for APT	84
A-3	Sample Input Points and Resulting Output for Cross Section Generated by APT (Rear View)	85
A-4	Required Input Order for Segments Describing a Cross Section	86
A-5	Example of Fuselage Sections Combined to Form Complete Aircraft	87

LIST OF ILLUSTRATIONS (Continued)

<u>Figure</u>		<u>Page</u>
A-6	Required Input Order for Corner Points Describing an Input Panel	88
B-1	Panel Representation of Body Used in Three-Dimensional Aerodynamic Analysis Technique (Y179L)	100
B-2	General Arrangement of Lifting Section Vortex Lattice Network	101
B-3	Comparison of Experimental and Calculated Surface Pressures on RSRA One-Sixth Scale Model	102
B-4	Comparison of Experimental and Calculated Surface Pressures on a 45-Degree Swept Wing	102
B-5	Comparison of Experimental and Calculated Surface Pressures on Model 1 Fuselage (Reference: NASA TM X-3185)	103
B-6	Estimated CPU Time for Y179L on IBM 360 System	104

INTRODUCTION

The helicopter has traditionally been used to operate in and out of congested and remote areas. Because of the low flight speeds associated with this role, overcoming the aerodynamic drag of the fuselage has consumed a relatively small percentage of the total power required; consequently, errors in the design phase parasite drag estimate did not have a crucial impact on the overall aircraft performance. Today's helicopters, however, require relatively high speed and long range capabilities, making low drag an important design criterion and an accurate drag estimate in the design process a necessity.

The rotor hub is a high-drag component of the helicopter and represents a significant percentage of the total aircraft drag. Efforts to reduce the drag of the helicopter, therefore, must necessarily include a reduction in the drag of the rotor hub. Several wind tunnel test programs have been conducted in an effort to identify low-drag hub configurations. To date, no mechanically sound, practical solution has been found.

In an effort to better define the parameters affecting the contribution of the rotor hub to the total drag and to facilitate accurate prediction of the hub drag, a review of available hub drag test data was conducted and a method developed to predict the hub drag. The data obtained from the review were used, along with the hub drag prediction method, to define a systematic wind tunnel test program to further investigate the parameters affecting the hub drag and to refine and verify the hub drag prediction method.

HUB DRAG DATA REVIEW

Before discussing the parameters associated with the drag of the rotor hub, it is appropriate that its significance be well established. A summary of rotor hub drag trends with gross weight is shown in Figure 1. The geometric complexity of the rotor hub (i.e., articulated, hingeless, faired) is shown to be a strong influencing factor in determining the contribution of the hub drag to the total helicopter drag. Figure 2 demonstrates the magnitude of the hub drag contribution. The hub and its associated interference drag (i.e., the drag created by the alteration of the flow conditions about a body due to the proximity of another body) is responsible for between 20% and 23% of the total drag of current production helicopters. Most current helicopter fuselages have not been designed for high-speed operation, and consequently low drag was not a primary design consideration. For this reason most helicopter fuselages are aerodynamically "unclean"; consequently, the potential exists for a considerable reduction in the fuselage drag itself.¹ The line in Figure 2 also demonstrates the penalty paid for the rotor hub drag if the drag of the fuselage alone is reduced by 50% without a proportionate reduction in rotor hub drag. It is apparent from Figure 2 that every effort should be expended in reducing the drag contribution of the rotor hub and that it is imperative that the drag of the hub be accurately predicted.

The hub drag data presented herein represent the data supporting the major conclusions drawn. The results of the hub drag data review are identified in greater detail in References 1 and 2. The data identified by circle symbols in the figures represent data drawn from internal Sikorsky Aircraft and United Technologies Research Center reports. For the purpose of clarity and since most of the reports are not generally available, the individual data points are not identified by a reference; however, the bibliography includes the titles and authors of the reports from which the data were obtained.

Hub Frontal Area

The rotor hub swept frontal area is the most significant parameter affecting the hub drag. Use of the term frontal

- 1 ROTORCRAFT PARASITE DRAG; Special Report Presented to the 31st Annual National Forum by the Ad Hoc Committee on Rotorcraft Drag, American Helicopter Society, Washington, D. C., May 14-15, 1975.
- 2 Sheehy, Thomas W., A GENERAL REVIEW OF HELICOPTER ROTOR HUB DRAG DATA; Sikorsky Aircraft, SER-50890, September 23, 1974.

area related to the rotor hub refers to the "swept" frontal area which represents the total projected frontal area of a rotating rotor hub. Figure 3 shows the trend of rotor hub drag with hub swept frontal area for a range of unfaired rotor hubs. The rotor hub drag (f_H) represents only the drag of the hub itself and does not include interference effects. The data shown in Figure 3 indicate that approximately 1 square foot of drag can be saved for each square foot reduction in frontal area. It should be pointed out that the scatter in this figure and in other figures concerned with hub frontal area can be partially attributed to errors in estimating the value of hub frontal area. This parameter was simply not identified in some reports, and frontal areas were measured from sketches or photographs.

The effect of including interference drag associated with the rotor hub is demonstrated in Figure 4, which shows the variation in rotor hub incremental drag with frontal area. The rotor hub incremental drag (\bar{f}_H) represents the difference in drag of the helicopter configuration with the hub and the configuration without the hub, and consequently includes the interference drag.

Although no consistent variation with hub frontal area is apparent, there is a general increase in incremental hub drag with increasing frontal area. The curve in Figure 3 has been duplicated in Figure 4 to demonstrate the potentially large differences between hub drag (f_H) and rotor hub incremental drag (\bar{f}_H). The values obtained from the hub drag curve have also been increased by 25% in Figure 4 to simulate a 25% increase in the dynamic pressure such as might be encountered at the hub location on a fuselage/pylon configuration. It is apparent that not even a 25% increase in the local dynamic pressure can account for the difference in rotor hub f_H and \bar{f}_H .

The scatter in the incremental hub drag values and the large differences between f_H and \bar{f}_H are indicative of the magnitude of the hub interference drag and imply that the interference drag is dependent on the individual fuselage/pylon configuration tested.

Rotor Hub Fairings

Several types of rotor hub fairings have been used in attempts to reduce the rotor hub incremental drag. The general categories into which these fairings can be divided are shown in Figure 5. The "beanie" fairing does not enclose the hub but merely sits on top. This type of hub has not been demonstrated to yield any significant drag reduction, but it has been used with some success to alter the flow separation process such that vibration due to the hub wake is reduced. The

ellipsoid fairing is designed to fully enclose the rotor hub in an effort to make the hub configuration a more streamlined aerodynamic shape.

The ellipsoid fairing rotates with the blades and is normally designed to tilt with the blade motions. Because of this rotational and tilting motion, this type of fairing is sometimes referred to as a "floating" fairing. Since the hub fairing floats, a greater hub shaft length is normally required to provide the proper clearance between the fairing and the pylon. In some cases shaft fairings have been used to enclose the extended shaft, and boundary layer control with blowing on the sides of the shaft fairing has successfully reduced the hub incremental drag. The rigid fairing shown in Figure 5 also rotates with the hub, but is not designed to tilt with the blade motions. The blade hinges are enclosed by rigid bearing type seals or flexible cuffs which allow blade motion.

The variation of faired hub incremental drag coefficient with thickness-to-diameter ratio is shown in Figure 6. A large amount of scatter in drag coefficient is evident in this figure for ellipsoidal type fairings, indicating that the interference effects associated with this type of fairing are quite large. Most of the data found for this type of fairing were for a $t/d \approx .3$. This thickness appears to be the minimum required to enclose current articulated hubs.

The data shown in Figure 6 for rigid fairings show essentially no variation in hub drag coefficient with thickness-to-diameter ratio, which implies that the interference effects for this type of fairing are much less severe than in the case of the ellipsoidal fairing. Because of the limited amount of data for this type of hub fairing, the implication should not be considered conclusive.

Hub/Pylon Clearance

Figure 7 demonstrates the variation of the hub/pylon interference drag as hub/pylon separation distance is changed. As the hub/pylon separation distance is increased, the hub interference effects on the pylon are reduced. In addition, more of the hub itself is removed from the region of potentially large increases in local dynamic pressures caused by the fuselage/pylon configuration. The separation distance required to remove the hub from the region of increased dynamic pressures is dependent on the individual fuselage/pylon geometry involved.

Unfortunately, although the interference effects of the hub on the pylon are reduced by increasing the hub/pylon separation, the drag of the additional exposed shaft (and possibly control

rods) area may offset the interference drag reduction. Because of this trade-off between interference drag and drag due to increased frontal area, there is an optimum hub/pylon separation distance which will yield the minimum incremental hub drag for a given hub/pylon/fuselage configuration.

Fuselage Angle of Attack

The data reviewed indicate that the incremental hub drag of faired or unfaired hubs is not significantly affected by changes in the fuselage angle of attack over a relatively wide range of body attitudes. This is demonstrated in Figure 8, which represents only a part of the data supporting this conclusion. The reason the hub incremental drag is not affected by body attitude appears to be that the presence of the fuselage/pylon configuration tends to suppress changes in the flow conditions, such as local dynamic pressure and flow direction at the hub location, due to a change in body attitude. It is interesting to note that this is generally true of test configurations not incorporating a full fuselage simulation although the angle-of-attack range for which this holds is somewhat reduced.

Hub Rotation

The effect of rotating the hub on the hub incremental drag is shown in Figure 9. Several tests have shown that rotational effects on unfaired rotor hub incremental drag are negligible. Wind tunnel tests conducted by Sikorsky also indicate that blade azimuth position for nonrotating hubs does not significantly affect the hub incremental drag. Both of these conclusions are based on tests of rotor hubs having four blades or more. However, for two- or three-bladed hub configurations, it is recommended that tests be conducted with the hub rotating or with the blades at the 0° , 90° , 180° and 270° azimuth positions.

The data from Reference 3 shown in Figure 9 indicates that the incremental hub drag increases when the hub is rotated. The test results from Reference 3 shown were not consistent over the range of Mach numbers tested, and other tests (such as that presented in Figure 9) showed little variation in hub incremental drag as the hub rotation increased. Because of the discrepancies between different test data, it should not be assumed that rotation does not affect the hub incremental drag of faired hubs.

3 Linville, J. C., AN EXPERIMENTAL INVESTIGATION OF HIGH-SPEED ROTORCRAFT DRAG, Sikorsky Aircraft; USAAMRDL Technical Report 71-46, Eustis Directorate, U. S. Army Air Mobility R & D Laboratory, Ft. Eustis, Virginia, February, 1972, AD740771.

Mach Number

Because the helicopter has traditionally been designed for low speeds, very little data is available on the effects of Mach number on rotor hub drag. An exception is the data presented in Reference 3, which tested a proposed high-speed transport helicopter configuration over a range of Mach numbers from .2 to .6. This test represents a thorough investigation of the effects of Mach number on an unfaired hub, a hub with a rigid fairing, and an ellipsoidal fairing with and without boundary layer control (BLC) by tangential blowing. The test results from this reference, presented in Figure 10, indicate that the drag of the unfaired hub and the ellipsoidal fairing using BLC are not significantly affected by Mach numbers between .2 and .4. The incremental drag of the ellipsoidal fairing and the rigid fairing increases with increasing Mach number over the range tested. This can probably be attributed to extremely high local Mach numbers occurring around the bluff fairing shape and probably eventually to local shocks. In any case, the large increases in incremental drag for the hub configurations representing practical hub configurations (i.e., the unfaired, rigid faired, or ellipsoidal faired hub with BLC) occur at $M > .4$, which is not applicable to pure helicopter configurations, but may be relevant for compound helicopters.

Scale Effects/Reynolds Number

A large amount of test data has been obtained on the effects of Reynolds number and on scale effects for streamlined shapes. Consequently, the scale corrections for test data on these shapes is relatively well understood. Unfortunately, this is not the case for bluff bodies and for nonaerodynamic shapes representative of many helicopter components and in particular for helicopter rotor hubs.

Results from Sikorsky Aircraft tunnel tests indicate that small-scale tests generally underpredict the drag increments due to unfaired rotor hubs. However, for faired rotor hubs, representative hub drag increments can generally be obtained from small-scale tests. This is illustrated in Figure 11, which presents test results from full-scale and 1/6-scale tests of a configuration consisting of a simulated fuselage upper surface, a pylon, and a faired and an unfaired rotor hub.

Test data for helicopter configurations indicate that for the basic fuselage shape, reasonably small-scale (Reynolds number >1 million/foot) tests yield accurate drag measurements as discussed in References 4 and 5. The data presented in these references did not include comparisons of the configurations with rotor hubs, however.

Basically, two factors influence the validity of small-scale test data. The proper flow conditions must be modeled as closely as possible and the model tested should accurately represent the geometric characteristics of the actual configuration. The fuselage and pylon region of a helicopter usually presents no difficulties in this respect provided the scale is large enough to obtain Reynolds numbers above sub-critical for the configuration.

The drag of small-scale rotor hubs appears to follow the basic hub drag trends in Figure 3, which includes some small-scale data, provided the hub geometric properties are accurately modeled. Recent tests by Sikorsky showed that a crude geometric model of a rotor hub resulted in only 75% of the drag measured on an accurate geometric model. It can be concluded from the data that a true geometric model is a necessity if an accurate drag estimate is to be obtained.

As far as Reynolds number is concerned, usually a value sufficient to yield adequate fuselage drag modeling is sufficient to insure an accurate hub drag. For a rotating hub the turbulence level is probably adequate to alleviate sub-critical flow on the small components such as pushrods even in very small scale tests.

Aerodynamic Sealing

The necessity of good aerodynamic seals in the hub region depends on the particular hub configuration. Test data indicate that the ellipsoidal type of fairing must be well sealed at the juncture of the fairing and the pylon to achieve any potential drag reduction. On the other hand, the available data on rigid type fairings indicate that sealing in the pylon/fairing juncture region is not particularly required. For unfaired hubs, the pylon cutout (i.e., the opening in the

⁴ Sweet, G. E., Julian, L., and Jenkins, J. L., WIND TUNNEL INVESTIGATION OF THE DRAG AND STATIC STABILITY CHARACTERISTICS OF FOUR HELICOPTER FUSELAGE MODELS, NASA TN D-1363, National Aeronautics and Space Administration, July 1962.

⁵ Biggers, J. C., McCloud, J. L., III, and Patterakis, P., WIND TUNNEL TESTS OF TWO FULL SCALE HELICOPTER FUSELAGES, NASA TN-1548, National Aeronautics and Space Administration, October 1962.

pylon required for the rotor shaft and controls) can cause additional drag depending primarily on the shape of the "lip" on the trailing edge of the cutout. Hoerner⁶ presents data on low drag shapes of holes in surfaces applicable to the pylon cutout.

As might be expected, the data on both ellipsoidal type fairings and rigid fairings demonstrated that the openings in the fairings for the blades should be sealed. This may present some difficulty for certain types of hubs because the cutout seals must be moveable or flexible to allow blade movement, but every effort should be made to seal this region.

Pylon Shape

Generally, the shape of the main rotor pylon has a strong influence on the incremental hub drag. The pylon influence manifests itself in two ways. First, the presence of the pylon (and the fuselage) alters both the local velocity magnitude and the direction in the hub region. The local flow direction will, of course, be parallel to the local surface; however, the magnitude of the velocity can be considerably higher than the freestream velocity with consequent increases in the local dynamic pressure. For many pylon configurations, the increase in local dynamic pressure can be the predominant factor in determining the interference between the pylon and the hub. For instance, hub incremental drag calculations based on frontal area and accounting for the increased local q were reported in Reference 7 to account for the difference between the hub drag alone and the measured hub incremental drag for unfaired hubs. Accounting for the local q failed to account for the drag differences for the faired hubs tested, however.

The second contribution is through the interference drag. The flow about the pylon can be significantly changed by the presence of the hub. Assuming that the flow is not initially separated on the aft pylon, the addition of the rotor hub will almost certainly induce separation of the flow over the aft pylon to some extent, thereby increasing its base drag. For some fuselage/pylon configurations, the effects of the hub may extend even further to influence the aft fuselage region. Unfortunately, no systematic test data was found which

⁶ Hoerner, Dr. - Ing S. F., FLUID-DYNAMIC DRAG, Second Edition, Bricktown, New Jersey, Hoerner Fluid Dynamics, 1965.

⁷ Jenkins, J. L., Winston, M. M., A WIND TUNNEL INVESTIGATION OF THE LONGITUDINAL AERODYNAMIC CHARACTERISTICS OF TWO FULL SCALE HELICOPTER FUSELAGE MODELS WITH APPENDAGES, NASA TN-1364, National Aeronautics and Space Administration, July 1962.

quantified the extent to which the hub interference affected the drag of the fuselage itself (i.e., what percentage of the interference drag acts on the pylon and fuselage respectively). Although many hub drag tests are conducted using a pylon configuration with only a simulated fuselage upper surface, it is felt by the authors that the validity of this approach should be substantiated by a systematic test program.

Generally speaking, a clean aerodynamic pylon design should yield a shape which will yield small hub/pylon interference drag. However, even clean pylon shapes can produce high local velocities in the hub region. Although not directly applicable to hub incremental drag, the trends of pylon drag coefficient with pylon length-to-height ratio are shown in Figure 12. There is a significant variation in pylon drag coefficient for a constant l/h which can be attributed to differences in the pylon nose shapes and the lengthwise position of maximum height as well as differences in interference drag associated with the individual configurations. Reference 8 presents the results of a rather detailed investigation of canopy configurations representative of pylon shapes. These data are presented merely to demonstrate that generally the pylon length-to-height ratio (comparable to fineness ratio) should be as large as is practical. Analytical studies, which will be discussed later in this report, indicate that this criterion also yields relatively low supersonic velocities along the pylon and consequently reduced pylon/hub interference.

⁸ Robinson, R. G., Delano, J. B., AN INVESTIGATION OF THE DRAG OF WINDSHIELDS IN THE 8 FOOT HIGH SPEED WIND TUNNEL, NACA Report 730, National Advisory Committee for Aeronautics, 1944.

HUB DRAG PREDICTION METHOD

The helicopter rotor hub operates in a region of confused flow with strong viscous interactions and unsteady local velocities. As a consequence of the complexity of the aerodynamic flow in this region, a purely analytical approach to determine the rotor hub drag and its associated interference drag is not only difficult, but is probably impossible considering the current state of the art. For this reason, an analytical method for calculating the flow field about arbitrary configurations has been combined with empirical data identified in the hub drag data review in an effort to predict the incremental drag of faired and unfaired rotor hubs. The method incorporates the primary factors identified as having controlling influence on the rotor hub incremental drag.

METHOD DEVELOPMENT

Unfaired Hubs

The primary factor influencing the incremental drag of unfaired hubs is the swept frontal area. The trending equation for the curve shown in Figure 3 nondimensionalized by hub swept frontal area is

$$C_{DH} = .582 + .0349 A_p - .00057 A_p^2 \quad (1)$$

The C_{DH} obtained from Equation (1) represents the drag of the hub in free flow and does not include the various interference effects associated with a hub/pylon combination.

The effect of an increase in the local dynamic pressure in the hub region is relatively straightforward. If one considers a pylon/fuselage configuration as shown in Figure 13, the flow velocity to which the hub is subjected differs from the free-stream velocity. Since the drag coefficient given by Equation (1) is based on free-stream dynamic pressure acting on the hub, C_{DH} must be corrected to account for the local dynamic

pressure. The extent of accelerated or decelerated flow in the hub region is dependent on the particular configuration involved. However, it is possible that sections of the hub may be outside the region of influence associated with the pylon/fuselage induced velocities. To account for that portion of the hub which may be considered outside of this region of influence, the ratio of pylon width to hub diameter is used as a generalizing parameter. The effective drag coefficient of the rotor hub is then

$$C_{DH}'' = C_{DH} (1 - K_2) + C_{DH} (1 - C_{pz}) K_2 \quad (2)$$

where $K_2 = \frac{\text{pylon width}}{\text{hub diameter}}$ (maximum value = 1.)

and C_{pz} is the local pressure coefficient at the hub location. Equation (2) assumes that the shaft height is insufficient to extend the hub itself vertically outside of the local increased velocity region. For certain hub configurations, this assumption may not be valid (methods to determine the validity of this assumption will be discussed in a later section).

To determine the drag of a hub configuration for which the shaft height can be considered sufficient to remove the hub itself from the increased dynamic pressure region, the shaft and hub frontal areas are considered separately. The drag of the shaft, in this instance, is given by

$$C_{DS}' = \frac{A_S}{A_S + A_P} [C_{DS} (1 - K_3) + C_{DS} K_3 (1 - C_{pz})] \quad (3)$$

where $K_3 =$ the ratio of pylon width to shaft height ($K_3 \leq 1$)
 $C_{DS}' =$ the two-dimensional drag coefficient for the shaft in free flow determined empirically.
 Values for C_{DS} for most shaft configurations can be found in the literature. Reference 6 is a useful source.

The equivalent drag coefficient for the hub and shaft combination not including the interference drag due to the rotor hub or the shaft is then

$$C_{DH}' = C_{DH}'' \frac{A_P}{A_P + A_S} + C_{DS}' \quad (4)$$

Having determined the effective drag coefficient of the hub, the interference drag must be determined for the particular hub/pylon configuration. The magnitude of the interference drag is dependent on the individual pylon/fuselage shape and the location of the rotor hub on the pylon. The method used to evaluate the interference drag is similar to that given in Reference 6 for determining the effects of adding a plate or disc to a streamlined body.

As the flow moves around the pylon and fuselage, it accelerates, causing local regions of reduced pressure. Following these regions of low pressure (higher velocity), the flow decelerates, resulting in a rise in pressure. With such an unfavorable pressure gradient the tendency for the boundary layer to separate from the surface is increased. This susceptibility to flow separation is heightened by the presence of any disturbance generated by an obstruction such as the rotor hub or shaft. Consequently, the interference drag can be evaluated if the strength of the flow disturbance is known and the stability of the flow on the pylon is gauged from the pressure gradients on the pylon. A function has been identified which relates the interference drag to the strength of the flow disturbance generated by the hub or shaft and the general flow stability on the pylon. This function is expressed as

$$\Delta C_{DH} = K_1 (\Delta C_{pz}) (l/\Delta Z) C_{Da} \quad (5)$$

where K_1 = an empirical constant equal to .2
 ΔC_{pz} = the potential flow pressure differential ($C_{p1} - C_{p2}$) between the pressure coefficient at the end of the pylon and the pressure coefficient at the location at which the hub is placed (see Figure 13).

The method of determining C_{p2} and C_{p1} will be discussed in a later section.

C_{Da} in Equation (5) represents the drag coefficient of the body creating the disturbance. If the shaft height is not sufficient to remove the hub from the region of increased velocity caused by the pylon/fuselage configuration, then $C_{Da} = C_{DH}$. However, if the shaft height is sufficient, then the shaft can be considered the component creating the disturbance and $C_{Da} = C_{DS}$.

The relationship given by Equation (5) indicates that as ΔZ decreases (i.e., the hub is moved toward the end of the pylon), the interference drag increases. This is as would be expected since the boundary layer on the pylon would become more susceptible to flow separation for a given ΔC_{pz} due to the increased boundary layer thickness. The data in Reference 6 indicates that the relationship given by Equation (5) will not be adequate for hub locations near the end of the pylon (i.e., small ΔZ). This is considered to be irrelevant for helicopter rotor hub/pylon configurations since this would imply a rearward tilting shaft if the hub were parallel with the local surface.

Equation (5) also shows that as the pressure differential ΔC_{p2} increases, the interference drag will increase. As stated previously, the pressure gradient is indicative of the flow stability. If a strong adverse pressure gradient exists on the configuration without the hub, then the flow will be more susceptible to separation for a given flow disturbance than if the pressure gradient were small. The pressure gradient can be an indicator not only of the flow stability, but also of the effectiveness of the pylon/fuselage shape. For instance, a strong adverse pressure gradient would indicate that the pylon aft closure is quite sharp and consequently, a loss in pressure recovery due to a flow separation would significantly increase the base pressure drag.

Accounting for the local velocity increases in the hub region and using the relationship for interference drag given in Equation (5), the total incremental drag coefficient for the rotor hub is given by

$$\bar{C}_{DH} = C_{DH}' + \Delta C_{DH} \quad (6)$$

Ellipsoidal Faired Hubs

Although the ellipsoidal fairing is a much more aerodynamic shape than the unfaired hub, the combination of a hub fairing, shaft fairing, pylon and fuselage shown in Figure 14, represents a configuration which taxes the capabilities of even the most sophisticated aerodynamic analyses. The interference effects associated with this type of configuration are quite large and more complex than those associated with an unfaired hub. Consequently, the approach used to predict the incremental drag of ellipsoidal faired hubs combines analytical techniques with empirical relations and is somewhat similar to the method for unfaired hubs. The method is divided into three major parts: the drag force acting on the hub fairing, the drag of the shaft or shaft fairing, if applicable, and the associated interference drag of the components.

The ellipsoidal fairing alone is amenable to the same potential flow aerodynamic technique as the fuselage/pylon configuration, which will be discussed later. This technique allows the potential pressure distribution and surface velocities over the surface of the fairing to be determined analytically. This information combined with the local velocities at the location on the pylon at which the hub is located allows the superposition of the local velocities on the fairing surface for the complete configuration. The surface pressure test data for faired hubs with blade shanks and a full pylon simulation are rather limited, but the available data indicates that the presence of the pylon, rotor shaft and

particularly blade shanks induce almost total separation on the fairing afterbody. Based on this, the base drag of the fairing accounting for the increased velocity due to the pylon/fuselage is given by

$$C_{DFB} = (1 - C_{pZ}) C_{PF} - (C_{PC} + C_{pZ}) \quad (7)$$

where C_{PF} = an equivalent forebody pressure coefficient (defined in the next section) which is indicative of the forebody suction force
 C_{PC} = the crest point pressure coefficient on the fairing alone (Figure 14)

This relationship assumes that the pressure in the base region of the fairing is equal to the pressure at the crest of the fairing with the induced velocity due to the pylon/fuselage superimposed. The absence of blade shanks on the fairing appears to allow some pressure recovery on the aft portion of the fairing, making the assumed base pressure invalid; however, the requirement for blade shanks makes this discrepancy rather academic.

Since the fairing may have a significant amount of surface area, the drag due to surface skin friction should be included in the total drag. Only the surface skin friction increment acting on the forebody of the fairing is applied since the afterbody flow is assumed separated. The skin friction drag increment is given by

$$C_{DSF} = C_f (1 - C_{pZ}) (A_w/2A_f) \quad (8)$$

where C_f = the skin friction coefficient
 A_w = the wetted area of the fairing
 A_f = projected frontal area of fairing

For standard unfaired configurations, there is little influence of the hub on the blade shank drag. For the ellipsoidal faired hubs, however, it is more appropriate to include in the fairing drag the drag of any sections of the blade shanks which operate in the region of influence of the increased velocities due to the presence of the fairing. For many configurations, the drag of these blade shank sections can be considered negligible. However, for a configuration with a significant area of shanks exposed, a drag increment must be included for the shanks. This drag increment is given by

$$C_{DBS} = 2 C_{DBS} (A_{BS}/A_f) (1 - C_{pS}) \quad (9)$$

where C_{pS} = the local pressure coefficient at the 90° and 270° azimuth position on the hub
 C_{DBS} = an empirical drag coefficient determined for the particular shank configuration

If a shaft or shaft fairing is used in conjunction with the ellipsoidal fairing, then an additional drag increment must be included to account for this component. This increment is given by

$$C_{DS}' = C_{DS} (1 - (C_{pZ} + C_{pC})/2) (A_S/A_P) \quad (10)$$

where again C_{DS} = an empirical drag coefficient for the particular shaft or shaft fairing

The shaft drag is corrected for a local velocity increase based on an average of the velocity at the crest of the fairing and the velocity at the hub location on the pylon without the shaft or hub.

The magnitude of the interference drag associated with an ellipsoidal faired hub is determined in the same manner as for an unfaired hub. This drag increment is given by Equation (5). For a faired hub then

$$C_{DF} = K_1 (\Delta C_{pZ}) (t/\Delta Z) C_{Da} \quad (11)$$

where again, if a shaft or shaft fairing is used, C_{Da} is equal to C_{DS}' , and if a shaft is not applicable, then

$$C_{Da} = C_{DFB} + C_{DSF} + C_{DBS}'$$

Consequently, the total incremental drag for an ellipsoidal faired hub is

$$\bar{C}_{DF} = C_{DFB} + C_{DSF} + C_{DBS}' + C_{DS}' + C_{DF} \quad (12)$$

Rigid Fairing

The rigid fairing represents an aerodynamic shape more similar to an unfaired hub than to an ellipsoidal faired hub. The method of predicting the incremental drag of a rigid fairing is, therefore, very similar to that used for the unfaired hub. Figure 15 shows that the shape of the basic rigid fairing (i.e., without the blade cuffs) is similar to a circular "can" on the surface. Data presented in Reference 6 on the drag of surface imperfections (although much of the data is presented

for subcritical flow) indicates that a realistic drag coefficient for a basic rigid fairing shape is about .38. The drag increment for the basic rigid fairing is given by

$$C_{DF}' = C_{DF} (1 - C_{pZ}) \quad (13)$$

where $C_{DF} = .38$.

This expression assumes that the entire basic fairing is subjected to the increased velocity field at the hub location. The value of C_{DF} used appears to be valid for thickness-to-

diameter ratios (t/d) less than .6, but for $t/d > .6$ or for fairing shapes significantly different from that shown, the value of C_{DF} used should be reevaluated.

The blade cuffs associated with a rigid fairing usually represent a significant portion of the exposed area and consequently must be included as a drag increment. The drag of the blade cuffs must also be corrected for the local q . Again the ratio of pylon width to hub diameter is used as a general parameter to account for this effect, and the resulting expression for the blade cuff drag increment is

$$C_{DBS}' = (C_{DBS} (1 - K_2) + C_{DBS} (1 - C_{pZ}) K_2) \left[\frac{2 A_{BS}}{A_F} \right] \quad (14)$$

where C_{DBS} = an empirical drag coefficient based on the shape of the blade cuff.

The interference drag is given by Equation (11) using

$$C_{Da} = C_{DF}' + C_{DBS}'$$

The total incremental drag of the rigid fairing is then

$$\bar{C}_{DF} = C_{DF}' + C_{DBS}' + \Delta C_{DF} \quad (15)$$

AERODYNAMIC ANALYSIS TECHNIQUE

Determining Local Surface Pressures

The local pressure coefficients required in the hub drag prediction methods are determined analytically by use of a three-dimensional aerodynamic technique developed at Sikorsky Aircraft and described in Reference 9. This technique calculates the incompressible, inviscid flow field on and about the surface of arbitrary lifting or nonlifting bodies in steady flow. The technique uses a combination of the classical approach for nonlifting bodies developed by Hess and Smith^{10, 11} and a vortex lattice method for lifting sections of the body (i.e., wings, tail surfaces, etc.) developed by Rubbert and Saaris¹² combined with a modified Multhopp lifting surface analysis.¹³

The technique uses a finite element type of approach to solve for the flow about the body. The surface of the configuration of interest (including the lifting section if applicable) is described by a finite number of approximately flat panels as shown in Figure 16. A constant strength source of uniform density is distributed over the surface of each panel and, in addition, lifting sections of the body are modeled by a vortex lattice distribution on the mean camber line. The surface singularity distribution and the vorticity distribution are then computed as a solution to a set of integral

- ⁹ Sheehy, Thomas W., A SIMPLIFIED APPROACH TO GENERALIZED HELICOPTER CONFIGURATION MODELING AND THE PREDICTION OF FUSELAGE SURFACE PRESSURES, presented at the American Helicopter Society Symposium on Helicopter Aerodynamic Efficiency, Hartford, Connecticut, March 1975.
- ¹⁰ Hess, J. L. and Smith, A.M.O., CALCULATION OF POTENTIAL FLOW ABOUT ARBITRARY BODIES, Progress in Aeronautical Sciences, Vol. 8, The Pergamon Press, 1967.
- ¹¹ Hess, J. L. and Smith, A.M.O., CALCULATION OF NON-LIFTING POTENTIAL FLOW ABOUT ARBITRARY THREE-DIMENSIONAL BODIES, Journal of Ship Research, Vol. 8, No. 2, 1964.
- ¹² Rubbert, P. E., Saaris, G. R., et al., A GENERAL METHOD FOR DETERMINING THE AERODYNAMIC CHARACTERISTICS OF FAN-IN-WING CONFIGURATIONS, Boeing Aircraft; USAAVLABS Technical Report 67-61A, Vol. 1, U. S. Army Aviation Materiel Laboratories, Ft. Eustis, Virginia, December 1967.
- ¹³ Lamar, J. E., A MODIFIED MULTHOPP APPROACH FOR PREDICTING LIFTING PRESSURES AND CAMBER SHAPE FOR COMPOSITE PLANFORMS IN SUBSONIC FLOW, NASA TN DO4427, National Aeronautics and Space Administration, July, 1968.

equations satisfying the known flow conditions at the trailing edge of lifting sections and the requirement that there must be no flow normal to the surface of the body unless fluid ejection or suction has been specified by the user. Once the singularity strengths have been determined, the flow direction and magnitude can be computed at the surface control points and at any arbitrary points located off the body. The procedures for determining the singularity strengths are described in detail in References 10 - 12, and a more detailed description of the technique can be found in Reference 9. The use of the three-dimensional aerodynamic analysis computer program (designated Y179L) is described in Appendix B.

The aerodynamic technique is quite general in application. The bodies acceptable for solution are not required to be slender, can be lifting or nonlifting, and the body itself or the flow conditions can be nonsymmetric (i.e., yawed flow). In addition, the aerodynamic flow field about multiple bodies can be computed to determine the mutual body interference. The numerical algorithm used accepts the surface panel descriptions as individual entities, and, consequently, the panels may be input in random order and panels may be concentrated in regions of primary interest which increases the accuracy of the solution in those regions. This feature is demonstrated in Figure 16 where the pylon region has been modeled more accurately than the fuselage surface.

The number of bodies and the complexity of the configurations acceptable are limited only by the size of the computing facility available and the inherent assumptions of incompressible, inviscid, steady potential flow. As a consequence of these assumptions, computed results in or very near regions of separated flow are not meaningful. Calculated results near sharp corners will also be inaccurate.

By use of the aerodynamic technique, the local velocities and, therefore, the local pressures can be determined at the positions required in the hub drag prediction method described. To determine the values of C_{p2} and C_{p1} the pylon/fuselage configuration of interest is modeled and an aerodynamic analysis is performed. The resulting output of the surface pressures and velocities on the surface can then be interpolated (if necessary) to obtain the pressures at the required locations. If desired, the velocities at selected off-body points in the hub region may also be determined to identify the region of influence of increased velocities for the particular configuration. The pylon width to hub diameter ratio used in Equation (2) appeared adequate in this study, and the precise identification of the width of the region of influence was not deemed necessary.

The required pressures for predicting the drag of an ellipsoidal hub fairing are determined in the same manner as the values of C_{p7} and C_{p1} . The ellipsoidal fairing of interest is geometrically modeled and an analysis performed. The values of C_{pC} and C_{pS} are obtained directly from the output. The determination of the equivalent forebody pressure (C_{pF}) is not quite as straightforward. Since the fairing is modeled by a finite number of surface panels, the forebody of the fairing has an incremental area for each panel on which the local pressure is assumed equal to the calculated pressure for that panel. The resultant equivalent pressure coefficient (C_{pF}) acting on the forebody of the fairing in the drag direction can then be obtained by numerically integrating these incremental forces and C_{pF} is given by

$$C_{pF} = \frac{1}{A_F} \sum_{i=1}^N C_{pi} A_{di} \quad (16)$$

where N = the number of panels describing the fairing forebody (i.e., to the point of maximum thickness)

C_{pi} = the local C_p on each panel

A_{di} = the component of each panel area perpendicular to the drag direction

The aerodynamic program automatically performs the summation of nondimensionalized forces in the X, Y and Z directions as well as calculating the moments about each axis. The summation of forces about the entire body in potential flow without vorticity, assuming the body description is exact, will be zero although the distribution of incremental forces will yield moments whose accuracy depend on the extent of the viscous flow effects on the particular configuration. Consequently, although the potential flow program will inaccurately predict total pressure recovery on the fairing afterbody, the C_{pF} determined by the above procedure will be accurate since the forebody flow is well represented by potential flow.

Geometric Modeling

Although the potential flow solution method is basically the same for any arbitrary shape, properly modeling the configuration poses a new problem for each body of interest. The generation of a proper model would normally be a time-consuming and tedious task for four principal reasons: the number of panels required to model most shapes is large, regions of high curvature require more panels than those of low curvature, panel size should vary smoothly from one adjacent panel to another, and the total number of panels must be minimized to

fit within computing facility constraints of time and size.

To minimize the manual effort in this area, a computerized method has been developed at Sikorsky Aircraft to complement the three-dimensional aerodynamic program. The method developed simplifies the generation of a suitable model for an arbitrary shape by reducing both the time required to model the shape and the amount of effort required of the user in preparing the input.

The body shape is generated by describing relatively few input cross sections by combinations of various types of simple curves which are then divided into straight line increments based on specific constraints related to the accuracy of the straight line approximation to the true curve and the basic requirements of the aerodynamic analysis technique. The curvature along the input axis (i.e., the axis on which cross sections are defined) determines the number of cross sections which are required. In the nose region where the axial curvature is normally large, several sections may be required, whereas in the cabin and tail regions, few input sections are required and the length of individual panels in these regions is controlled by requesting intermediate cross sections to be generated by linear interpolation. Because each surface panel is described as a separate entity, sections of the body may be generated independently and the resulting output combined to form the complete body.

A description of the Automated Paneling Technique (APT; Deck Y179A) can be found in Appendix A. The geometry program (APT) has been successfully used to model configurations ranging from simple cylindrical shapes to complex compound helicopters such as the U. S. Army/NASA/Sikorsky Rotor Systems Research Aircraft (RSRA). As compared to traditional methods, the geometry modeling technique used demonstrates a significant reduction in time and effort required to model aircraft configurations.

The surface pressures calculated by the three-dimensional potential flow program (Y179L) using shapes generated by APT have been successfully correlated with test data over a wide range of fuselage configurations, angles of attack and yaw attitudes. Several examples of the correlation achieved with test data are presented in Appendix B, Figures B-3 to B-5. Both the APT and potential flow program have been demonstrated to be extremely useful tools in the design and analysis of rotorcraft configurations.

METHOD APPLICATION AND CORRELATION

The hub drag prediction methods described previously require information about the flow field in the pylon region and about the ellipsoidal fairing if applicable. Because the drag prediction method is relatively sensitive to the local flow velocities in the hub region and the potential pressure recovery indicated by ΔC_{p2} , it is recommended that the particular pylon/fuselage configuration of interest (and the ellipsoidal fairing, if applicable), be geometrically modeled and an aerodynamic analysis performed to obtain the required information.

Unfortunately, even with the simplified modeling technique, this may require more effort than is warranted for a quick drag estimate, particularly if the fuselage/pylon configuration has not been finalized. To alleviate this difficulty, several pylon configurations have been analyzed in conjunction with a basic fuselage representation as well as several general ellipsoidal fairing configurations. An example of the geometric model of one pylon configuration on the fuselage underbody used is shown in Figure 16.

The basic pylon shapes used in the analysis are shown in Figure 17 and are designated A, B and C. For each pylon shape, the maximum pylon height-to-length ratio and the axial position of maximum height were varied in order to obtain the matrix of thirty-six general pylon configurations identified in Table 1. The surface pressures obtained from the potential flow program (Y179L) for the matrix of pylon shapes are shown in Figures 18 to 20.

The ellipsoidal fairing shapes which were analyzed are shown in Figure 21. The thickness-to-diameter ratios of the fairings vary from .1 to .4. Predicted surface pressures along the top centerline and the lateral centerline for the fairings are shown in Figures 22 and 23, respectively.

In application, the user is required to identify the various frontal areas associated with the hub configuration of interest (i.e., A_p or A_f , A_g and A_{gg}) as well as the hub position, shaft height, and the various empirical drag coefficients of individual components as needed. The particular pylon geometric characteristics such as length, width, maximum height, and axial position of maximum height must be known. The values of the local surface pressures must be determined in one of two ways. If the particular pylon/fuselage or fairing configuration has been modeled and analyzed, then these values are obtained from the potential flow analysis. The alternative to this is to identify a pylon or fairing configuration from the matrix identified in Table 1 and Figure 21, respectively, which most closely represents the

TABLE 1. PYLON CONFIGURATIONS USED IN CONJUNCTION WITH SIMULATED FUSELAGE TO OBTAIN SURFACE PRESSURES.

Maximum Height (h/l)	Position of Maximum Height (Z _M /L)		
	.25	.50	.75
.05	A,C*	A,C	A,C
.10	A,B,C	A,B,C	A,B,C
.15	A,C	A,C	A,C
.20	A,B,C	A,B,C	A,B,C
.25			
.30	B	B	B
.35			
.40	B	B	B

*Designates Pylon Type

particular shape of interest. The values of C_{p2} , C_{p1} and/or C_{pC} , C_{pS} can then be obtained from Figures 18 to 20 and Figures 22 and 23. Interpolation may be required to obtain the required pressure coefficients if the maximum height and position of maximum height or fairing thickness to diameter ratio of the particular shape do not correspond to any of the configurations available. Values of C_{pF} for the particular fairings shown in Figure 21 can be obtained from Figure 24.

A generalized hub drag prediction computer program (Y179Z) has been developed which accepts the required geometric characteristics of the pylon, hub and the shaft and blade shanks (if applicable), along with the required empirical drag coefficients. The predicted aerodynamic data for the pylon matrix and the ellipsoidal fairings have been incorporated in the program in order that an estimated pylon surface pressure distribution for an arbitrary pylon shape, and C_{pC} and C_{pS} for an arbitrary ellipsoidal fairing can be computed if required in the hub drag prediction. The hub type is specified and the appropriate equations (i.e., unfaired, ellipsoidal fairings, rigid fairing) are solved to identify the drag of the hub itself, the interference drag, and subsequently, the total incremental drag of the rotor hub. The use of the hub drag prediction computer program is described in Appendix C.

The procedure required for predicting the drag of a particular hub/pylon/fuselage configuration is summarized in the following steps:

1. Determine A_p or A_F and A_w , A_S and A_{BS}
2. Determine factors K_2 and K_3
3. Determine C_{DS} , C_{DBS} and C_f
4. Determine C_{p2} , C_{p1} and C_{pC} , C_{pS} , C_{pF} (if applicable) using the aerodynamic analysis or values from the pylon and fairing configuration matrix
5. Use the information in the appropriate drag calculations outlined for unfaired, ellipsoidal faired or rigid fairing hub.

The rotor hub drag prediction method has been correlated with test data for several unfaired and faired hub configurations. The comparison between predicted hub incremental drag and measured hub incremental drag for these hub configurations is shown in Table 2. The predicted drag is within 8% of the measured drag for all the configurations except for the unfaired hub test data from Reference 3. The reason for the larger difference between predicted and measured hub incremental drag is not known. In any case, a predicted incremental hub drag within 13% of the actual corresponds to only

a 4% error in total aircraft drag of conventional helicopters. However, for exceptionally clean helicopters, an incremental hub drag error of this size could represent about a 7% error in aircraft drag.

Some of the hub configurations identified in Table 2 were tested with only a pylon and fuselage upper surface representation and not a full fuselage component. The predicted incremental drag coefficient values for these hubs (with the effect of the fuselage included) are shown in Table 2 also. The large differences between the drag values with and without the fuselage present deserve further discussion.

The local pressures and velocities in the hub region are dependent upon the full configuration. The hub configurations tested without a fuselage were tested with a pylon and fuselage upper surface simulation similar to the configuration shown in Figure 25. The local velocities along the pylon are expected to be lower for this type of configuration than for a complete pylon/fuselage shape. Although no test data was identified during the course of this study which substantiates this conclusion, the differences in the calculated surface pressures for a pylon/fuselage combination and the same pylon with only a simulated fuselage upper surface are shown in Figure 26. The difference between the pressures is essentially equal to the surface pressures along the top of the fuselage body without the pylon or, in essence, the fuselage surface pressures are superimposed on the pylon surface pressures except at the end of the pylon where the pressure differences are small.

The predicted hub incremental drags for the hub configurations tested with a pylon and fuselage upper surface are based on the pressure distributions on a pylon/fuselage upper surface configuration, and good correlation with test data is obtained. Since good correlation was achieved with the configurations tested with a full fuselage component and those without a full fuselage, provided the appropriate local pressures are used, it is reasonable to expect that the predicted incremental hub drags based on the complete pylon/fuselage configurations shown in Table 2 are accurate.

The differences in the predicted incremental drags with and without a fuselage component demonstrate that the incremental drag of ellipsoidal faired hubs is quite sensitive to the fuselage presence and that the drag of rigid fairings, and probably unfaired hubs, are not nearly so sensitive to the presence of the fuselage. This tends to further support the earlier conclusion that the interference effects associated with ellipsoidal fairings are much greater than for the other hub configurations.

TABLE 2. COMPARISON OF EXPERIMENTAL AND PREDICTED INCREMENTAL ROTOR HUB DRAG.

Helicopter Configuration	Type of Fairing	Predicted C_{DH} or C_{DF}	Experimental C_{DH} or C_{DF}	$\frac{\text{Predicted-Experimental}}{\text{Experimental}}$
S-65	None	1.24	1.30	-4.6%
S-61	None	1.25	1.24	+ .8%
High-Speed Helicopter (Reference 3)	None	1.27	1.12	+13.4%
(Reference 7)	None	.80	.75	+6.7%
BO-105 (Reference 1)	None	1.17	1.26	-7.1%
S-61	Ellipsoidal	.382(.51)*	.37	+3.2%
High-Speed Helicopter (Reference 3)	Ellipsoidal	.53	.56	-5.4%
(Reference 7)	Ellipsoidal	.93	.90	+3.3%
(Reference 31)	Ellipsoidal	.43(.55)	.44	-2.3%
(Reference 31)	Ellipsoidal	.53(.67)	.52	+1.9%
High-Speed Helicopter (Reference 3)	Rigid	.507	.515	-1.6%
(Reference 39)	Rigid	.52(.59)	.56	-7.1%

*The predicted drag values in parentheses represent the predicted incremental drag of the rotor hub if tested with a complete fuselage simulation.

HUB FAIRING DESIGN

A rotor hub/pylon configuration representative of current U. S. Army designs was identified and analyzed during the course of this study. In addition, a rotor hub fairing designed to reduce the incremental hub drag was identified and analyzed. The basic hub/pylon shape is shown in Figure 27.

The basic unfaired hub shown in dashed lines in Figure 27 is typical of a fully articulated, elastomeric, four-bladed rotor hub; and the basic pylon configuration is similar to pylon type "A" identified in Figure 17. This type of rotor hub represents a relatively low drag configuration because elastomeric rotor hubs yield lower values of frontal area for a given hub design requirement. Because of this feature, this type of hub allows a more compact fairing design, although this feature may also reduce the potential drag reductions to be obtained by fairing the hub for some configurations.

The rigid rotor hub fairing shown in Figure 27 was chosen for this configuration for several reasons. The low profile characteristics of this type of helicopter make the floating characteristics required for ellipsoidal type fairings less attractive than the rigid fairing characteristics. Ellipsoidal fairings also require a significant amount of flexible aerodynamic sealing in the pylon/fairing juncture region and the blade cutout region. Even with proper sealing, the ellipsoidal type fairing may not yield a net drag reduction due to the increase in frontal area required and the strong interference effects. The reduction of the interference effects is difficult and requires either a redesign of the pylon/hub region or using boundary layer control which is impractical because of the mechanical complexity involved.

The rigid fairing shown avoids the mechanical complexities associated with an ellipsoidal fairing and the boundary layer control devices. The fairing consists of a rigid nonrotating base, a rotating fairing component, and flexible blade cuffs enclosing the shank/hub juncture and the pushrod linkages. A comparison of the predicted drag of the basic unfaired hub and the rigid fairing is shown below.

	<u>Unfaired Hub</u>	<u>Faired Hub</u>
Frontal Area	4.0 ft ²	4.667 ft ²
Predicted Incremental Drag	4.4 ft ²	2.74 ft ²

WIND TUNNEL TEST DEFINITION

A systematic wind tunnel test program which is designed to further investigate the parameters affecting the contribution of the rotor hub to the total helicopter drag and to refine and verify the hub drag prediction method has been identified. The required wind tunnel test program based on results from this study is outlined below.

Models Required:

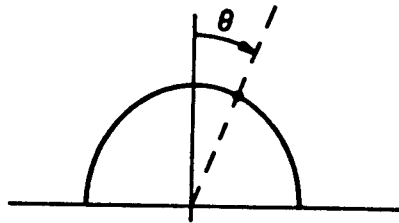
1. A simulated fuselage upper surface
2. A complete fuselage underbody
3. Eighteen pylon configurations
 - a. Three pylon types similar to types A, B and C shown in Figure 18
 - b. Two maximum heights for each pylon configuration ($h/t = .1, .2$)
 - c. Three maximum height positions for each configuration, preferably at 25, 50 and 75% of the pylon length
4. One rotating rotor hub configuration
 - a. Unfaired hub with component buildup
 - b. Hub with a rigid fairing as shown in Figure 27
 - c. Variable shaft height for unfaired hub configuration
5. A representative set of rotor blades (not necessarily scaled).

Balances Required:

1. Balance for fuselage/pylon configuration
2. Rotor hub balance.

Recommended Data:

1. Fuselage/pylon forces and moments
2. Rotor hub forces
3. Flow visualization on fuselage/pylon
 - a. Oil
 - b. Tufts
4. Rotor hub wake definition
 - a. Wake survey
 - b. Laser velocimeter
5. Surface pressures
 - a. Pressure taps on fuselage upper and lower surfaces and along lateral centerline
 - b. Pressure taps on pylon as shown below



Taps located on surface of pylon for
 $\theta = 0^\circ, \underline{+20^\circ}, \underline{+40^\circ}, \underline{+60^\circ}, \underline{+80^\circ}$

Wind Tunnel Required:

1. Test section area should be a minimum of approximately 250 square feet
2. Test section airspeed should be approximately 200 mph.

Model Scale:

Reynolds number based on hub diameter should be greater than 1.5 million. This yields a minimum diameter of approximately .8 feet based on the wind tunnel described above. If the scale is based on the configuration shown in Figure 27, the minimum scale is one-sixth, which yields a low tunnel blockage factor of approximately .17%.¹⁴

In light of the results presented in the previous section, the wind tunnel test program should attempt to verify the validity of rotor hub drag tests without a full fuselage simulation. Even if this approach is demonstrated to yield lower values for the hub incremental drag than with a complete fuselage underbody, this does not preclude the possibility of obtaining meaningful data provided that the mechanism responsible for the differences in hub drag magnitude is identified and understood in greater detail.

Several pylon configurations are proposed for the test program to permit study of how the pylon shape itself affects the hub incremental drag. In addition, a matrix of pylon configurations such as the one proposed will provide a better data base for the design of low drag pylon configurations. Testing selected pylon configurations with the simulated fuselage upper surface as well as with the complete fuselage underbody would help better identify the interference effects associated with a pylon/fuselage configuration.

The axial location of the unfaired rotor hub should be varied for each pylon shape to aid in refining and verifying the hub drag prediction method. The positions tested should be located forward of the maximum height position or at the maximum height position. The basic hub position should allow the hub to be rotated, but rotating the hub for the hub position study is not considered necessary.

A component buildup (i.e., control rods, etc.) should be performed for the basic hub configuration and a systematic study of the effects of shaft height should be done at the basic axial hub position (i.e., the position at which the hub balance is located). It is not considered particularly necessary to rotate the rotor hub for the basic hub position and height studies, but the hub should be rotated to verify this.

A representative set of rotor blades should be included in this study as well. No data were found in the literature which demonstrate how the rotor blades and the rotor wake may affect the way in which the presence of the hub interferes with

¹⁴ Pope, A. and Harper, J. J., LOW-SPEED WIND TUNNEL TESTING, John Wiley and Sons, Inc., New York, 1966.

the pylon/fuselage configuration. One would suspect that the rotor wake dominates the flow field in the hub/pylon region and that the mechanism of the interference drag is significantly altered. The surface pressure data and the oil flow studies will aid in identifying the rotor wake effects on the pylon/fuselage region.

The rotor hub has additional undesirable effects on the helicopter overall performance other than increasing the parasite drag. The wake from the hub can interfere with the tail surfaces and the tail rotor, causing undesirable handling qualities and vibration. Reducing the drag of the rotor hub should reduce the magnitude of this interference, and properly designed pylon shapes can alleviate the possibility of this interference by altering the wake trajectory. For this reason, a wake survey is recommended for the faired and unfaired hubs on the three types of pylons to investigate the potential reduction in the hub wake interference effects.

Laser velocimeter measurements are also recommended in order to obtain off-body velocities both with and without the rotor wake present. This will not only aid in defining the region of influence of induced velocities due to the fuselage/pylon configuration, but also aid in determining the unsteady flow characteristics associated with the rotor wake effects and the rotor hub wake.

Although some of the test program characteristics are not inherently necessary to refine and verify the hub drag prediction method, these features will significantly increase the understanding of the entire hub/pylon/fuselage flow characteristics. This will aid in the design of efficient high-speed rotorcraft. This test program also offers the potential to provide a data base directly applicable to two contracts recently awarded by the U. S. Army Air Mobility Research and Development Laboratory, Eustis Directorate, concerning three-dimensional aerodynamic analysis techniques in extensive use to predict flow velocity and direction off the surface of the body. This analytical capability is essential for predicting flow interference on external stores and identifying potential body/rotor interference.

The wind tunnel test outlined is rather extensive in scope, and consequently, the estimated cost of the program is high (\$415,000). This cost is comprised of approximately \$112,000 for the design and fabrication of the model, \$44,000 for the design and fabrication of the rotor hub (assuming a properly scaled hub is not available), and \$259,000 for the wind tunnel program and documentation. The cost estimate is based on the use of existing balance systems and rotor blades compatible with the test outlined.

CONCLUSIONS

Results of the helicopter rotor hub drag data review indicate that:

1. The rotor hub swept frontal area is the primary factor influencing the contribution of the rotor hub to the total aircraft drag. Reducing the frontal area offers the greatest potential to reduce the hub drag.
2. Changing fuselage angle of attack does not significantly affect the incremental drag of unfaired or faired hubs.
3. The effect of rotation on the incremental drag of unfaired hubs, having four or more blades, is negligible. The data reviewed on the effects of rotation on faired hubs was inconsistent and no conclusions were drawn.
4. Increasing the separation distance between the rotor hub and the pylon can reduce the incremental drag of the rotor hub only if the drag of the increased exposed shaft and control rods is less than the reduction in interference drag caused by removing the hub from the higher dynamic pressure region around the pylon and the resultant smaller flow disturbance on the aft pylon/fuselage region. This conclusion is based on test data obtained without the effects of the rotor wake present. Due to insufficient data, no conclusions have been drawn concerning the effects of increased shaft height on the airframe/rotor mutual interference.
5. Small-scale tests can yield accurate hub drag values only if the actual rotor hub geometric properties are properly modeled.
6. Rotor hub fairings offer the potential to yield significant hub incremental drag reductions. For ellipsoidal type fairings, care should be taken to guarantee that the fairing causes a minimal increase in frontal area. This is particularly important if boundary layer control is not used in conjunction with the fairing.
7. The drag reductions available using rotor hub fairings are decreased as flight Mach number is increased due probably to local shocks occurring on the bluff aerodynamic shape of the fairings.

8. The rotor hub and its associated interference effects contribute 20 to 30% of the total airframe drag of current helicopters. If the magnitude of incremental hub drag is not reduced, the hub could potentially contribute 40 to 60% of the airframe drag for aerodynamically clean fuselage configurations.

It has been demonstrated that a semiempirical procedure using three-dimensional analytical aerodynamic techniques combined with empirical data can be used to predict the incremental drag of rotor hub configurations. The method developed correlates within $\pm 14\%$ with test data for a wide range of hub configurations, but is within $\pm 8\%$ for most hubs.

A rigid fairing, compatible with a hub/pylon configuration representative of current designs, has been identified which should yield a 37% reduction in hub incremental drag compared to the unfaired hub configuration, and a wind tunnel test program has been defined to verify and refine the method developed.

REFERENCES

1. ROTORCRAFT PARASITE DRAG; Special Report Presented to the 31st Annual National Forum by the Ad Hoc Committee on Rotorcraft Drag, American Helicopter Society, Washington, D. C., May 14-15, 1975.
2. Sheehy, Thomas W., A GENERAL REVIEW OF HELICOPTER ROTOR HUB DRAG DATA; Sikorsky Aircraft, SFR-50890, September 23, 1974.
3. Linville, J. C., AN EXPERIMENTAL INVESTIGATION OF HIGH-SPEED ROTORCRAFT DRAG, Sikorsky Aircraft; USAAMRDL Technical Report 71-46, Eustis Directorate, U. S. Army Air Mobility R&D Laboratory, Ft. Eustis, Virginia, February 1972, AD 740771.
4. Sweet, G. E., Julian, L., and Jenkins, J. L., WIND TUNNEL INVESTIGATION OF THE DRAG AND STATIC STABILITY CHARACTERISTICS OF FOUR HELICOPTER FUSELAGE MODELS, NASA TN D-1363, National Aeronautics and Space Administration, July 1962.
5. Biggers, J. C., McCloud, J. L., III, and Patterakis, P., WIND TUNNEL TESTS OF TWO FULL SCALE HELICOPTER FUSELAGES, NASA TN-1548, National Aeronautics and Space Administration, October 1962.
6. Hoerner, Dr. -Ing S. F., FLUID-DYNAMIC DRAG, Second Edition, Bricktown, New Jersey, Hoerner Fluid Dynamics, 1965.
7. Jenkins, J. L., Winston, H. H., A WIND TUNNEL INVESTIGATION OF THE LONGITUDINAL AERODYNAMIC CHARACTERISTICS OF TWO FULL SCALE HELICOPTER FUSELAGE MODELS WITH APPENDAGES, NASA TN-1364, National Aeronautics and Space Administration, July 1962.
8. Robinson, R. G., Delano, J. B., AN INVESTIGATION OF THE DRAG OF WINDSHIELDS IN THE 8 FOOT HIGH SPEED WIND TUNNEL, NACA Report 730, National Advisory Committee for Aeronautics, 1944.
9. Sheehy, Thomas W., A SIMPLIFIED APPROACH TO GENERALIZED HELICOPTER CONFIGURATION MODELING AND THE PREDICTION OF FUSELAGE SURFACE PRESSURES, Presented at the American Helicopter Society Symposium on Helicopter Aerodynamic Efficiency, Hartford, Connecticut, March 1975.
10. Hess, J. L., and Smith, A.M.O., CALCULATION OF POTENTIAL FLOW ABOUT ARBITRARY BODIES, Progress in Aeronautical Sciences, Vol. 8, The Pergamon Press, 1967.

11. Hess, J. L. and Smith, A.M.O., CALCULATION OF NON-LIFTING POTENTIAL FLOW ABOUT ARBITRARY THREE-DIMENSIONAL BODIES, Journal of Ship Research, Vol. 8, No. 2, 1964.
12. Rubbert, P. E., Saaris, G. R., et al., A GENERAL METHOD FOR DETERMINING THE AERODYNAMIC CHARACTERISTICS OF FAN-IN-WING CONFIGURATIONS, Vol. 1 - Theory and Application, Boeing Aircraft; USAAVLABS Technical Report 67-61A, U. S. Army Aviation Materiel Laboratories, Ft. Eustis, Virginia, December 1967, AD667980.
13. Lamar, J. E., A MODIFIED MULTHOPP APPROACH FOR PREDICTING LIFTING PRESSURES AND CAMBER SHAPE FOR COMPOSITE PLANFORMS IN SUBSONIC FLOW, NASA TN D04427, National Aeronautics and Space Administration, July, 1968.
14. Pope, A. and Harper, J. J., LOW-SPEED WIND TUNNEL TESTING, John Wiley and Sons, Inc., New York, 1966.
15. INVESTIGATION OF THREE-DIMENSIONAL FLOW SEPARATION ON FUSELAGE CONFIGURATIONS, RFQ DAAJ02-75-Q-0119, U. S. Army Air Mobility Research and Development Laboratories, Eustis Directorate, Ft. Eustis, Virginia, February 1975.
16. ROTOR WAKE EFFECTS ON HUB/PYLON FLOW SEPARATION, RFQ DAAJ02-75-Q-0138, U. S. Army Air Mobility Research and Development Laboratories, Eustis Directorate, Ft. Eustis, Virginia, February, 1975.
17. Key, C. N. and Wiesner, R., GUIDELINES FOR MINIMIZING HELICOPTER PARASITE DRAG, American Helicopter Society Preprint No. 805, May, 1974.
18. Churchill, G. B., and Harrington, R. D., PARASITE DRAG MEASUREMENTS OF FIVE HELICOPTER ROTOR HUBS, NASA Memo 1-31-59L, February, 1959.
19. Moser, H., FULL SCALE WIND TUNNEL INVESTIGATION OF HELICOPTER DRAG, American Helicopter Society Journal, Vol. 6, No. 1, January, 1961, pp. 27-33.

BIBLIOGRAPHY

1. Nozick, H. J., RESULTS OF FULL SCALE ROTOR DRAG TESTS IN THE UAC 18-FOOT WIND TUNNEL, SER-2525, Sikorsky Aircraft, May, 1953.
2. Hall, J. B., AN EXPERIMENTAL INVESTIGATION OF HELICOPTER ROTOR HEAD DRAG CHARACTERISTICS, UAC R-25588-2, United Aircraft Corporation.
3. Harrington, R. D., REDUCTION OF HELICOPTER PARASITE DRAG, NACA TN-3234, August, 1954.
4. Grose, R. M., EFFECTS OF PROTUBERANCES ON THE DRAG OF CYLINDERS, UAC R-25784-1, United Aircraft Corporation, February, 1955.
5. Lanz, H. K., PILOT WIND TUNNEL TESTS OF A 1/4 SCALE MODEL OF AN S-56 HELICOPTER MAIN ROTOR AND PYLON, UAC-R-0822-1, United Aircraft Corporation, March, 1956.
6. Wilson, J. C., PILOT WIND TUNNEL TESTS OF SUCTION BOUNDARY LAYER CONTROL TO A CYLINDER FOR PYLON AND ROTOR HEAD DEVELOPMENT, UAC R-1208-1, United Aircraft Corporation, March, 1958.
7. Lawton, T. D., PILOT WIND TUNNEL TESTS OF A 1/8 SCALE MODEL OF A SIMULATED SIKORSKY S-56 HELICOPTER ROTOR HEAD, UAC R-1234-2, United Aircraft Corporation, February, 1959.
8. Wilson, J. C., PILOT WIND TUNNEL TESTS OF A 1/6 SCALE MODEL OF THE SIKORSKY S-61 ROTOR HEAD AND PYLON, UAC R01234-4, United Aircraft Corporation, March 16, 1959.
9. Lawton, T. D., EFFECT OF HUB FAIRING ON ROTOR PERFORMANCE IN HOVER, UAC R-1234-3, United Aircraft Corporation, April, 1959.
10. Harper, T. E., WIND TUNNEL DRAG STUDY OF A FULL-SCALE ROTOR HEAD AND PYLON MODEL OF THE SIKORSKY HSS-2 HELICOPTER UAC R-1299-1, United Aircraft Corporation, April, 1959.
11. Olson, J. R., WIND TUNNEL DATA AND ANALYSIS OF FULL SCALE ROTOR HEAD AND PYLON DRAG INVESTIGATION, SER-61027, Sikorsky Aircraft, April, 1959.
12. Lawton, T. D., WIND TUNNEL TESTS OF A 1/6 SCALE MODEL OF A SIKORSKY S-61 TRANSPORT ROTOR HEAD AND PYLON, UAC R-0289, United Aircraft Corporation, May, 1959.
13. Wilson, J. C., WIND TUNNEL TESTS OF MODELS OF ROTOR HEAD FAIRINGS, UAC R-0495, United Aircraft Corporation, August, 1959.

14. Tanner, W. H., FULL SCALE S-61 ROTOR HEAD - PYLON DRAG AND WAKE SURVEY INVESTIGATION, Unpublished, Sikorsky, September, 1960.
15. Biggers, J. C., McCloud, J. L. III, and Patterakis, P., WIND TUNNEL TESTS OF TWO FULL SCALE HELICOPTER FUSELAGES, NACA TN-1548, October, 1962.
16. Carr, L. W., CH-53A WIND TUNNEL INVESTIGATIONS, SER-65110, Sikorsky Aircraft, February, 1963.
17. Lewis, R. B., ONE-HALF SCALE WIND TUNNEL TESTS OF A RIGID COAXIAL ROTOR HEAD, SER-50465, Sikorsky Aircraft, February, 1967.
18. Linville, J. C., A REVIEW OF ROTOR HEAD-PYLON DRAG REDUCTION, SER-50543, Sikorsky Aircraft, May, 1968.
19. Linville, J. C., AN EXPERIMENTAL INVESTIGATION OF THE EFFECTS OF ROTOR HEAD CONFIGURATION AND FUSELAGE YAW ON THE WAKE CHARACTERISTICS AND ROTOR PERFORMANCE OF A 1/8 SCALE HELICOPTER, USAAVLABS Technical Report 69-94, January, 1970.
20. Gifford, J., ONE-FIFTH SCALE WIND TUNNEL TESTS OF AN S-65 ROTOR HUB AND PYLONS, SER-65566, Sikorsky Aircraft, 1970.
21. Gifford, J. A. M., and Flemming, R., PARASITE DRAG STANDARD PROCEDURE, Sikorsky Aircraft, 1972 (unpublished).
22. Ruddell, A. J. and Kaplita, T. T., WIND TUNNEL TEST OF A 1/10 SCALE S-69 (ABC) FLIGHT DEMONSTRATOR, SER-69001, Sikorsky Aircraft, December, 1972.
23. Werner, J. V., and Flemming, R. J., YUH-60A QUARTER SCALE WIND TUNNEL TEST REPORT, SER-70531, Sikorsky Aircraft, April, 1973.

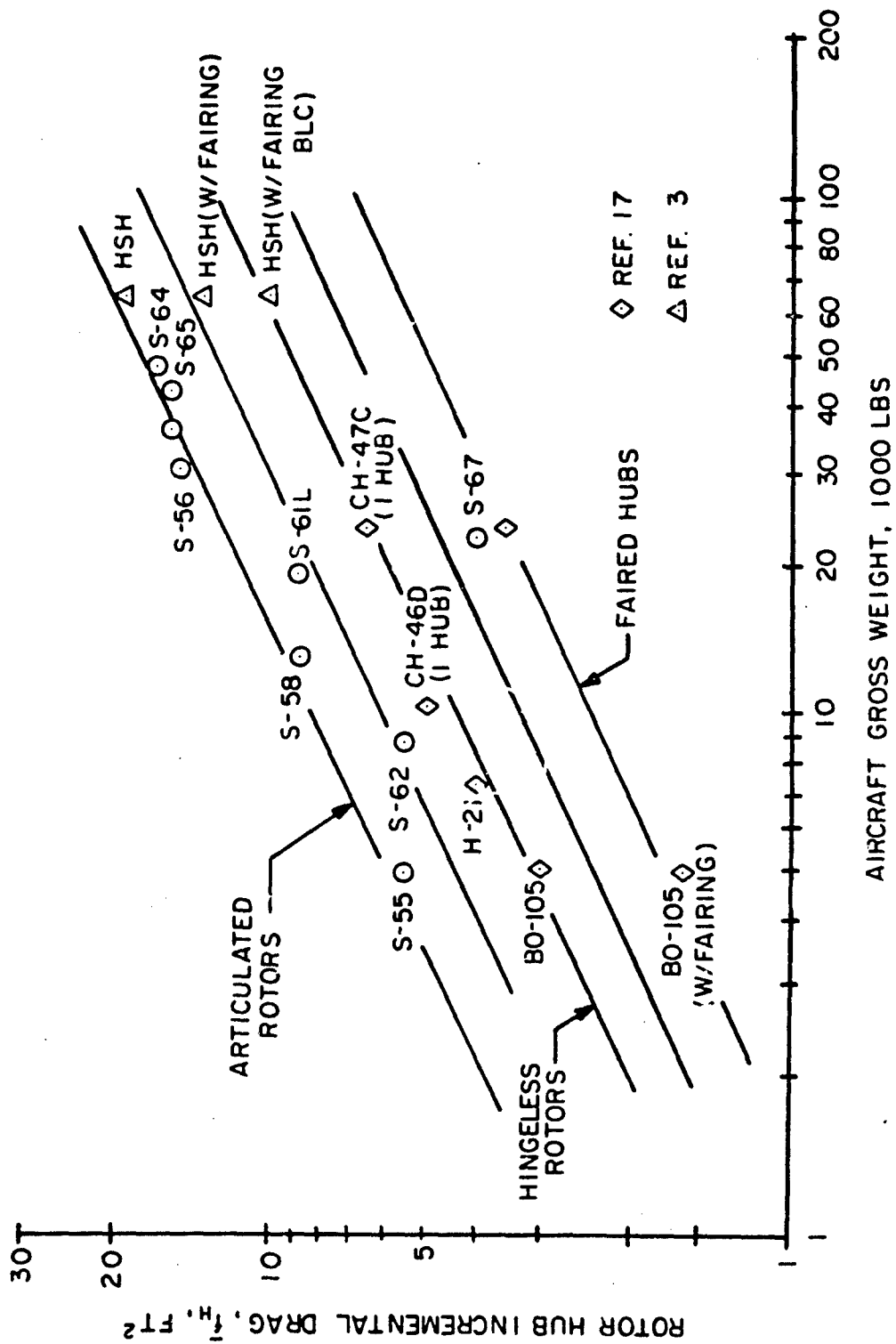


Figure 1. Trend of Rotor Hub Incremental Drag With Aircraft Gross Weight.

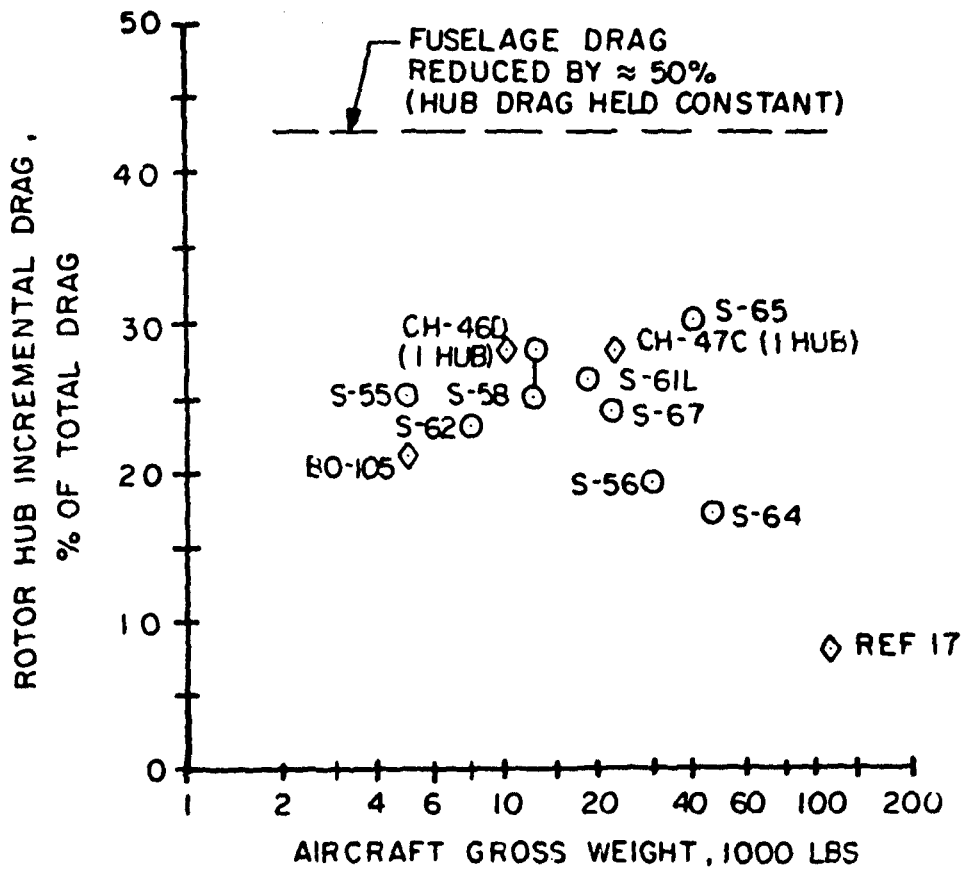


Figure 2. Rotor Hub Drag Contribution to Total Helicopter Drag.

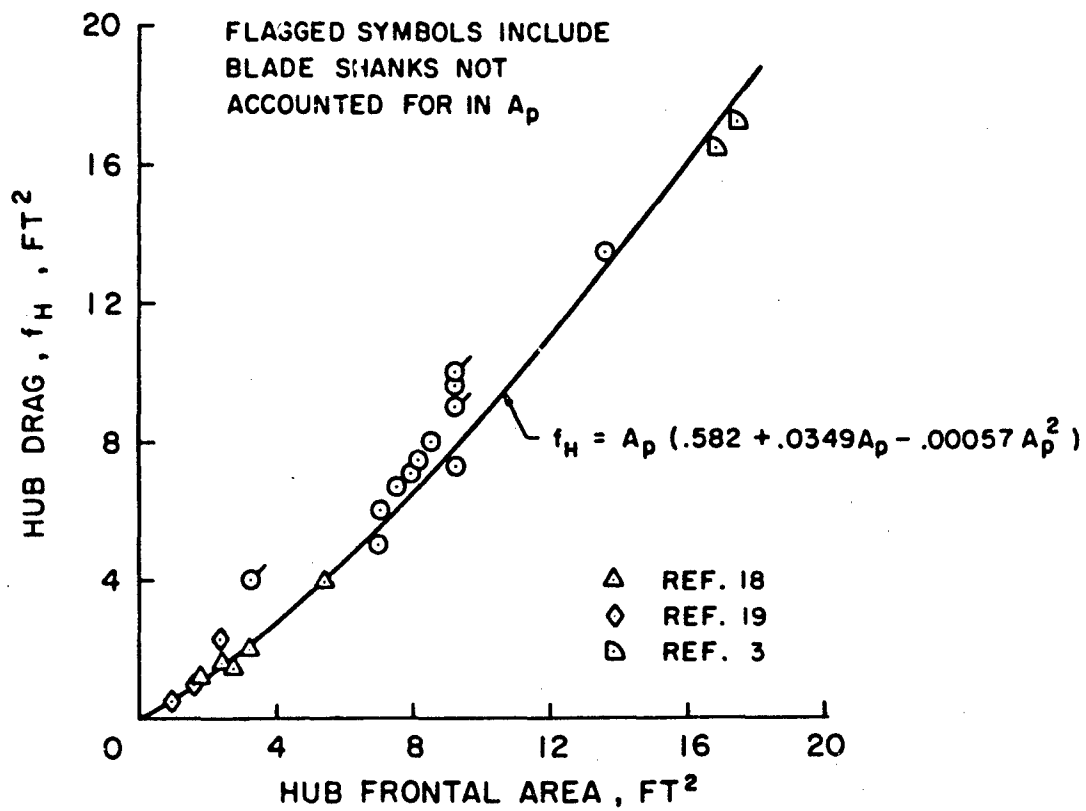


Figure 3. Hub Drag Trend With Hub Frontal Area for Unfaired Hubs.

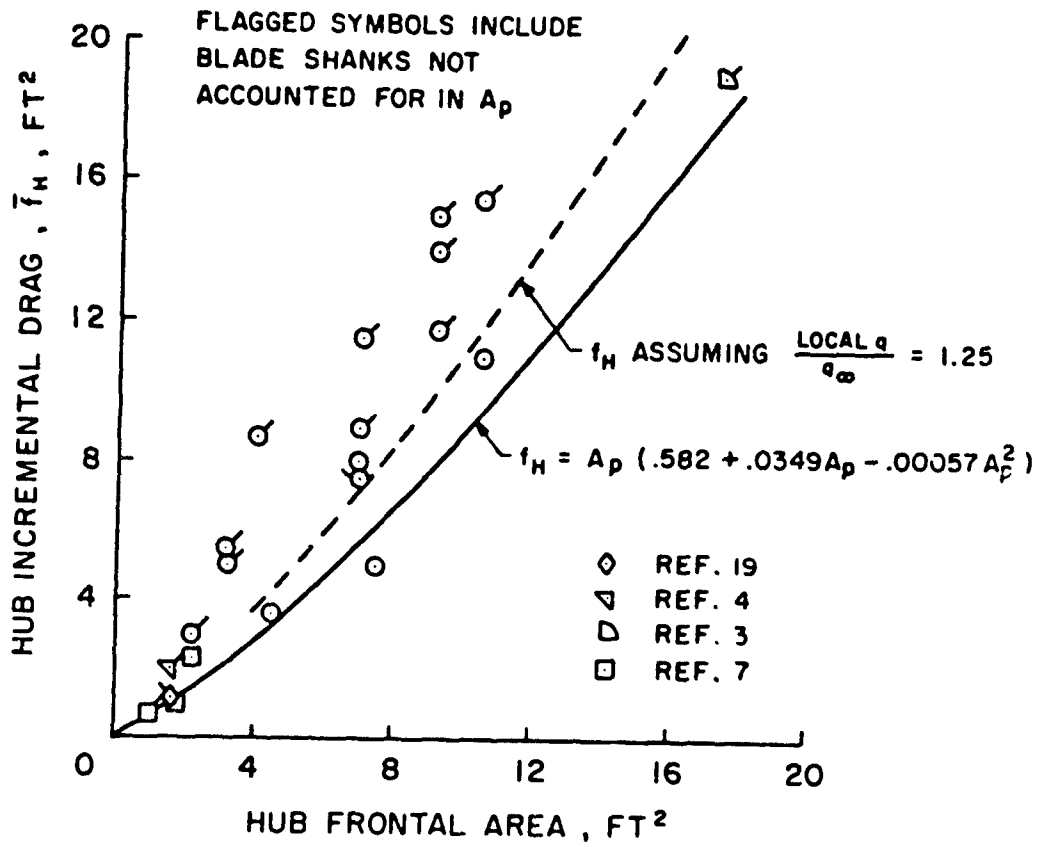
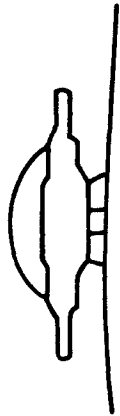
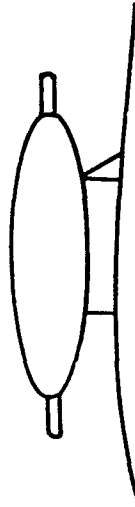


Figure 4. Hub Incremental Drag Trend With Hub Frontal Area for Unfaired Hubs.

BEANIE FAIRING



ELLIPSOIDAL FAIRING
FLOATING



RIGID FAIRING



Figure 5. General Types of Rotor Hub Fairings.

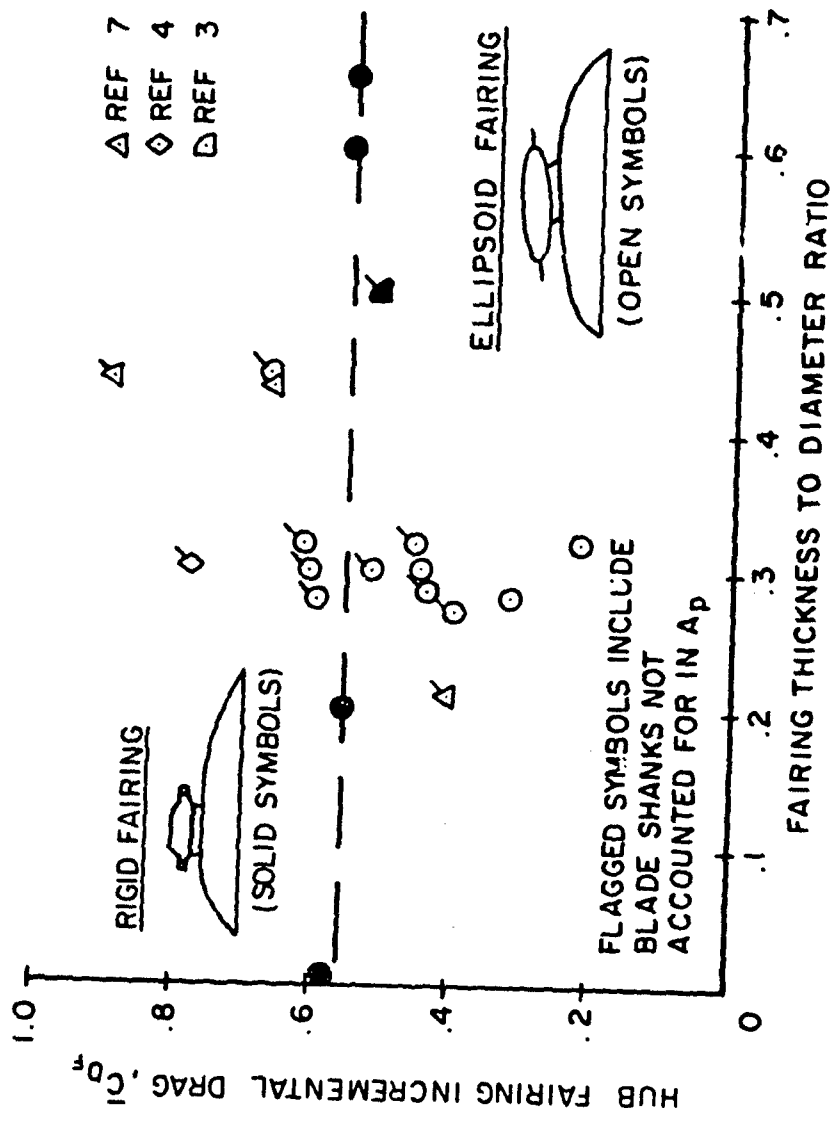


Figure 6. Fairing Hub Incremental Drag Variation With Fairing Thickness to Diameter Ratio.

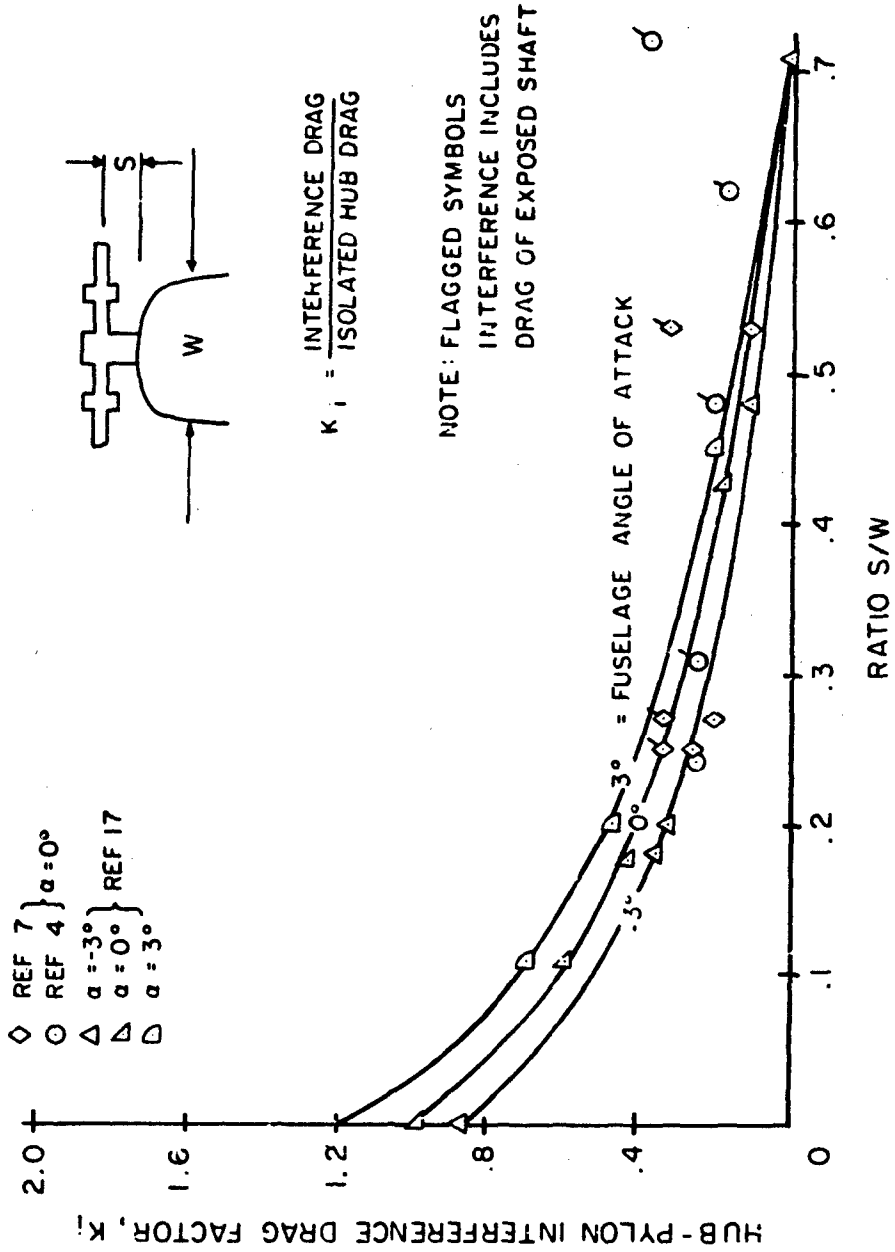


Figure 7. Effect of Hub-Pylon Separation Distance on Hub Interference Drag.

△◇ REF 18

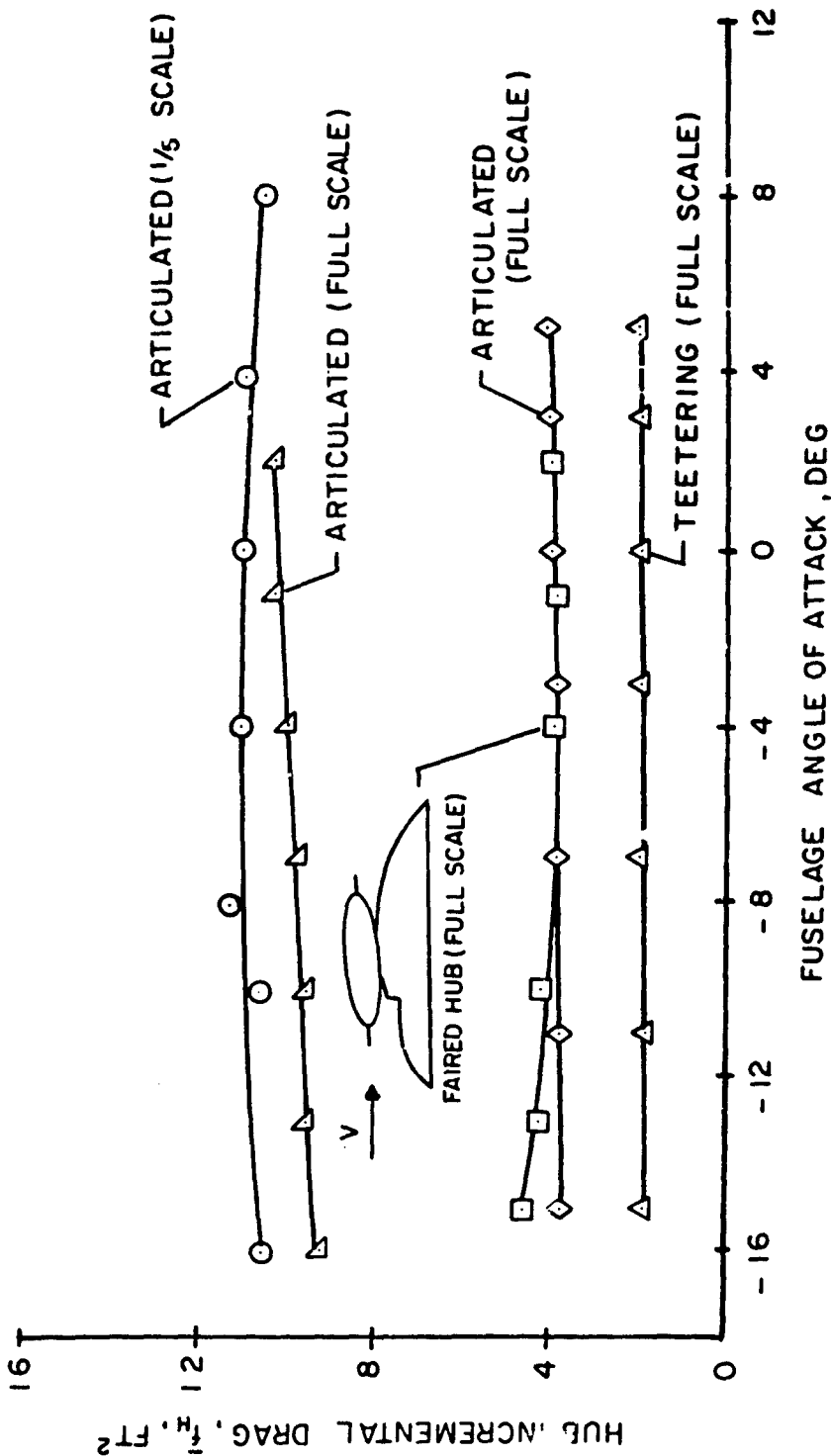


Figure 8. Variation of Incremental Hub Drag With Body Attitude.

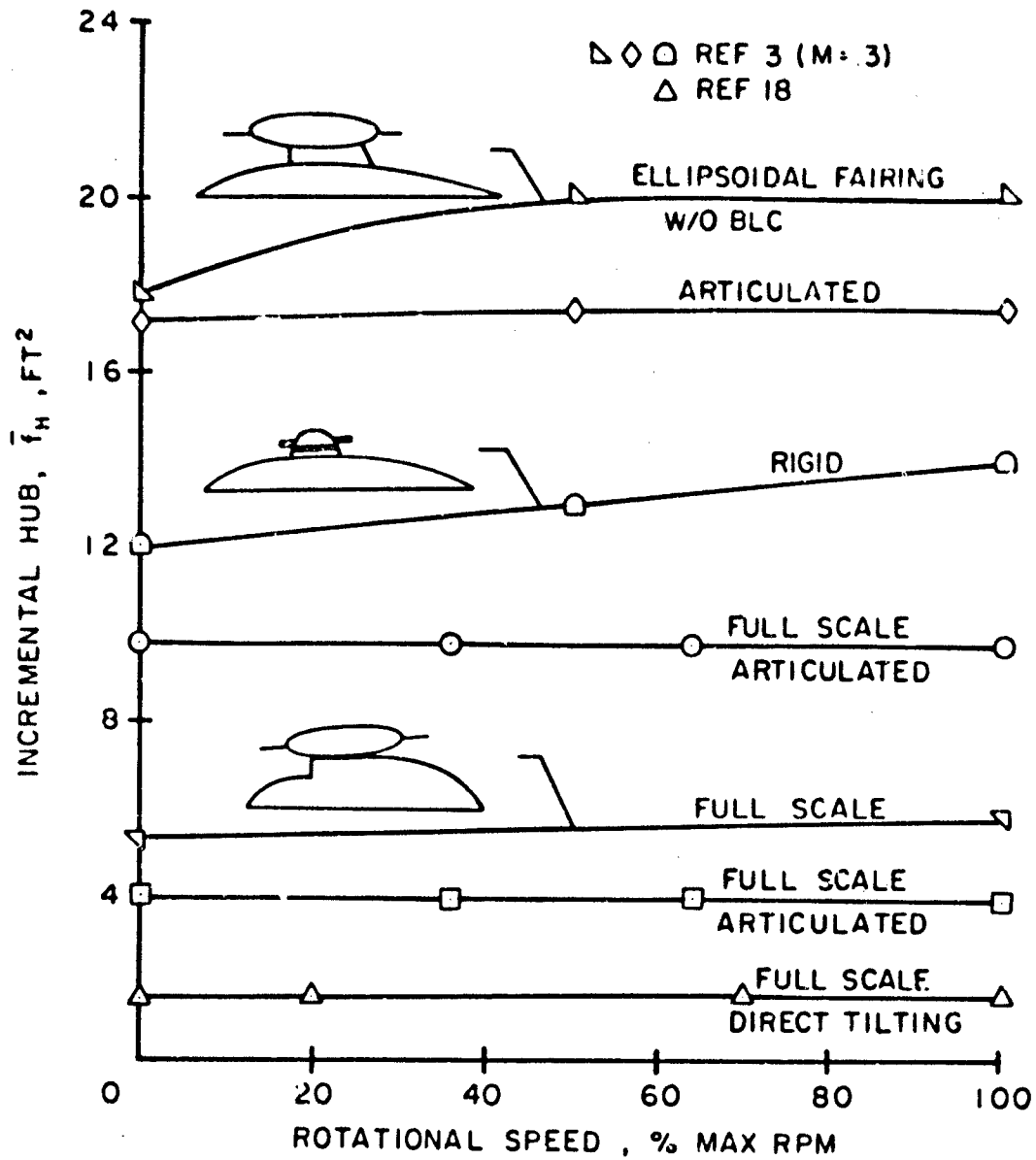


Figure 9. Rotational Effects on Incremental Rotor Hub Drag.

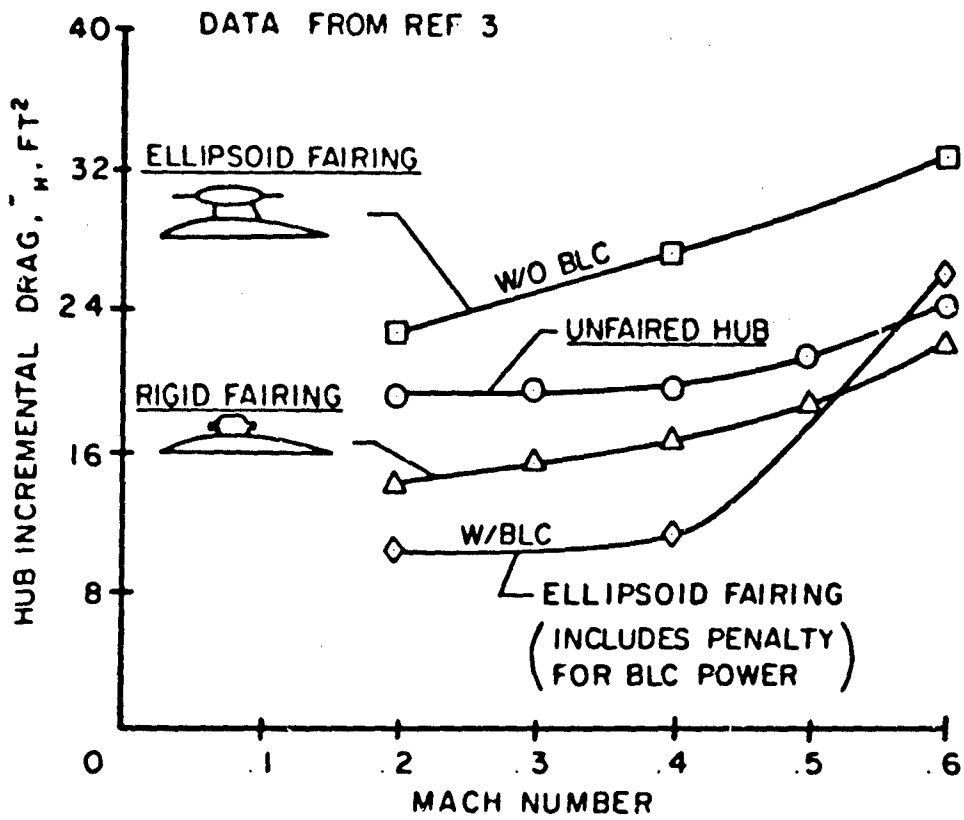


Figure 10. Effect of Mach Number Variation on Incremental Hub Drag.

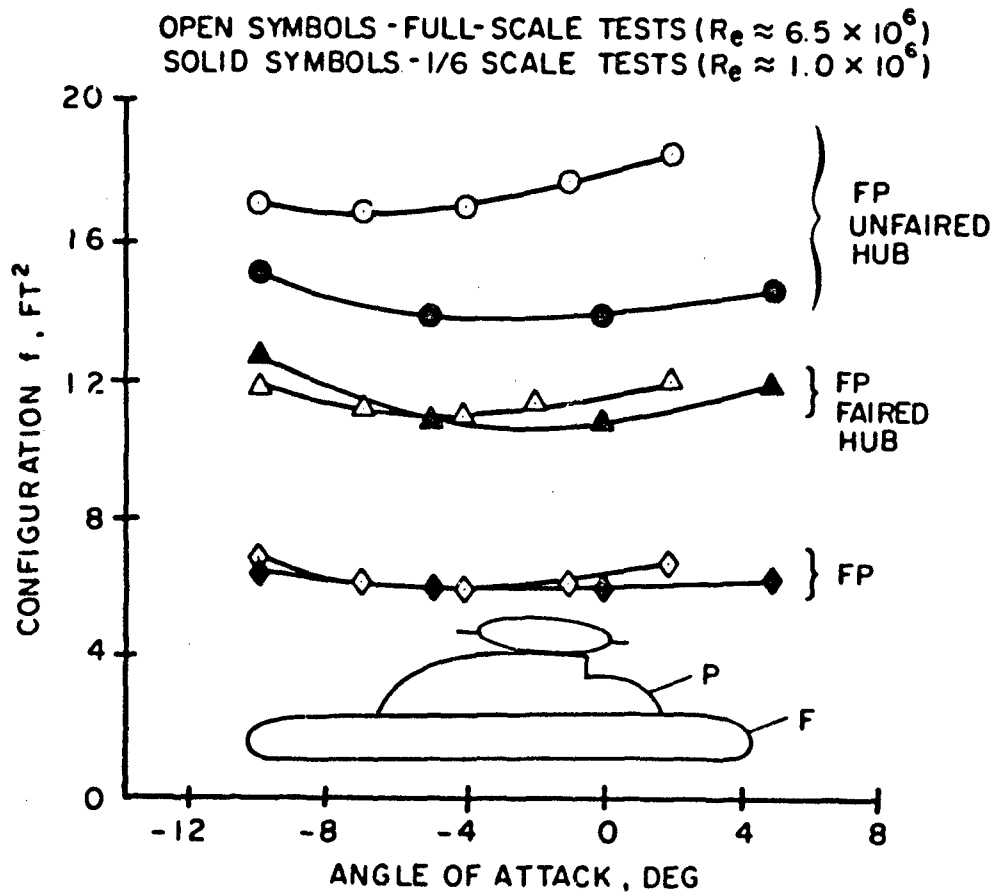


Figure 11. Comparison of Full-Scale and One-Sixth Scale Rotor Hub Drag Test Results.

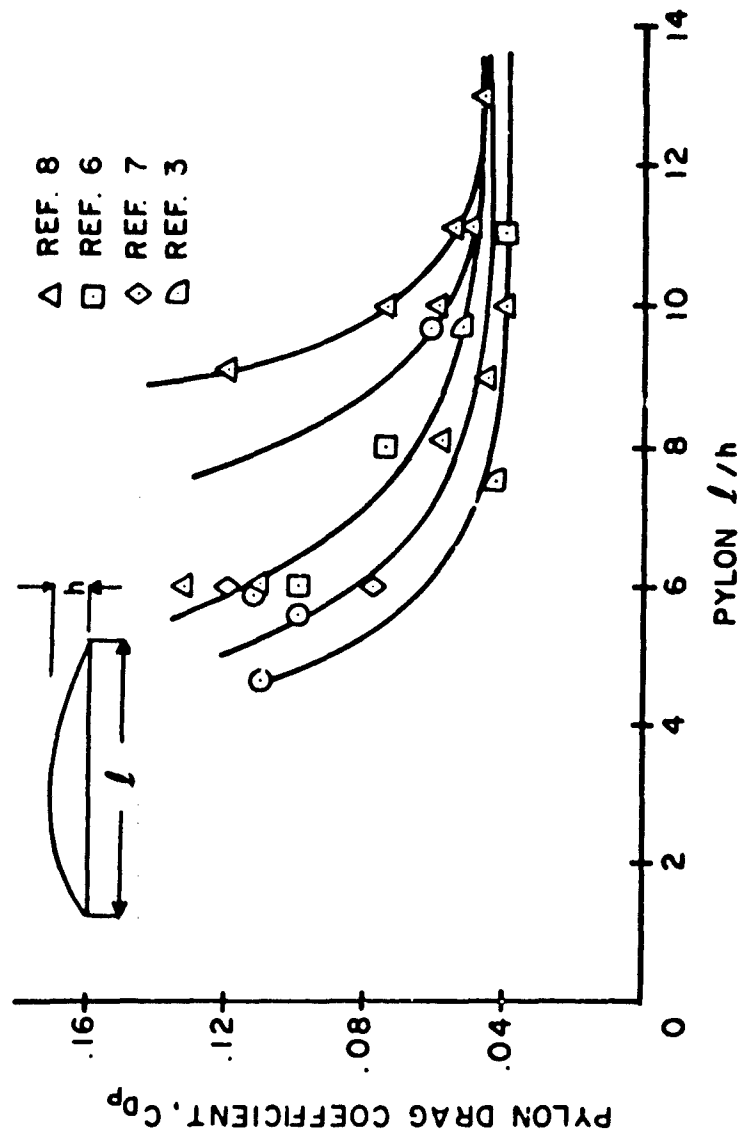


Figure 12. Pylon Drag Trends With Pylon Length-to-Height Ratio.

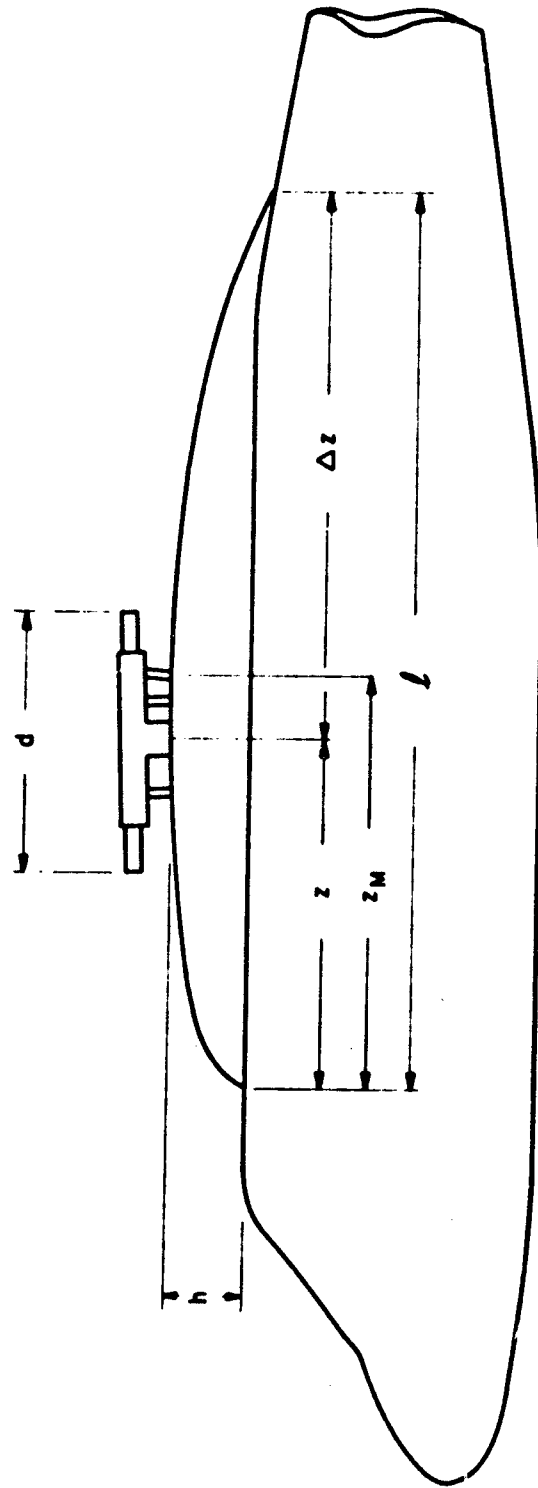


Figure 13. Example of a General Helicopter Configuration With an Unfaired Rotor Hub.

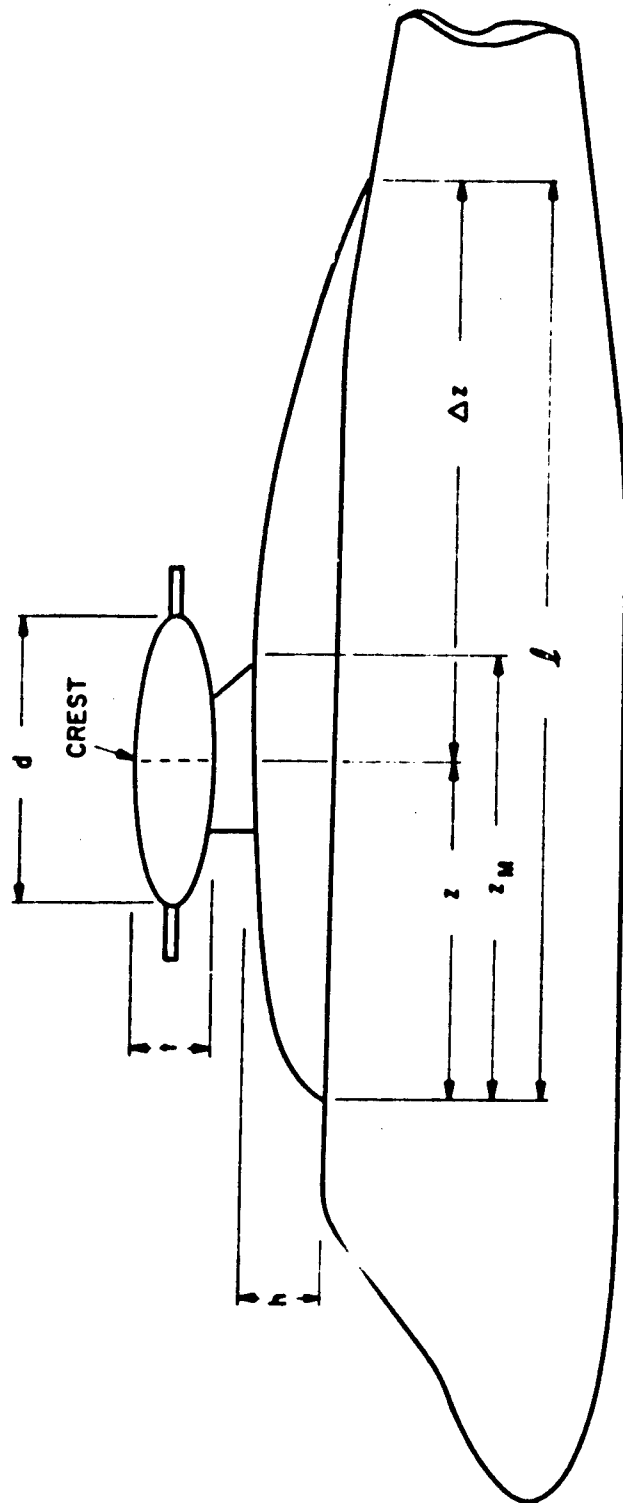


Figure 14. Example of a General Helicopter Configuration With an Ellipsoidal Paired Hub.

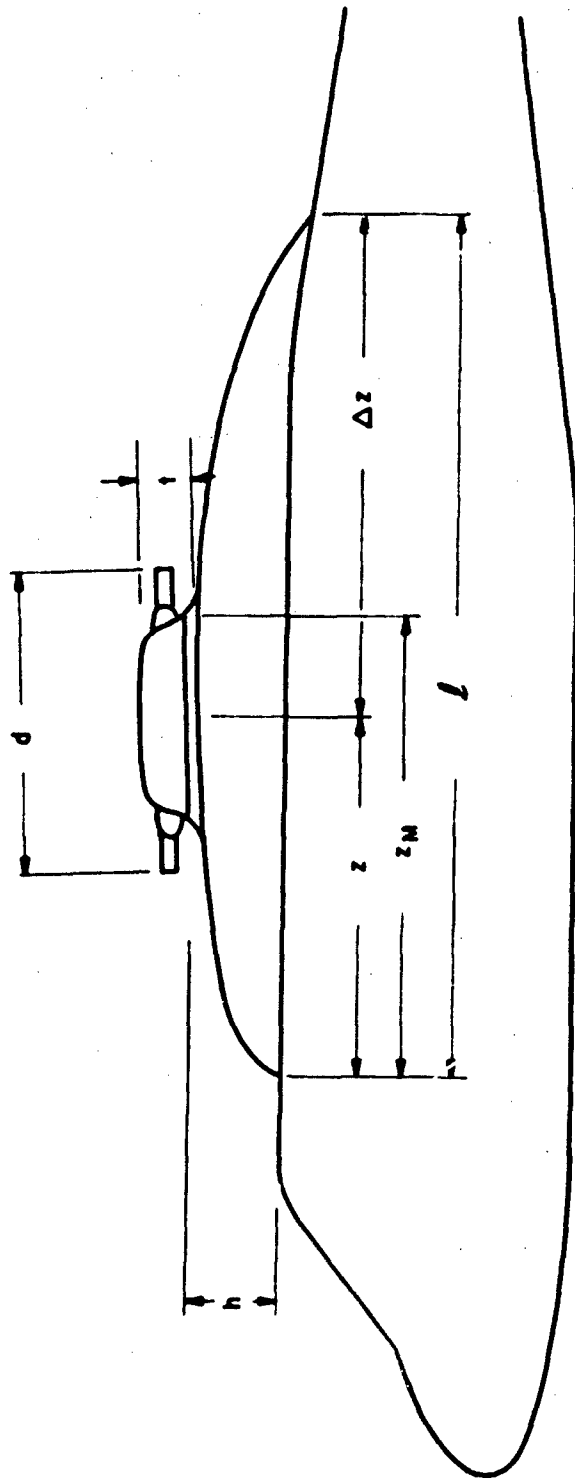


Figure 15. Example of a General Helicopter Configuration With a Rigid Rotor Hub Fairing.

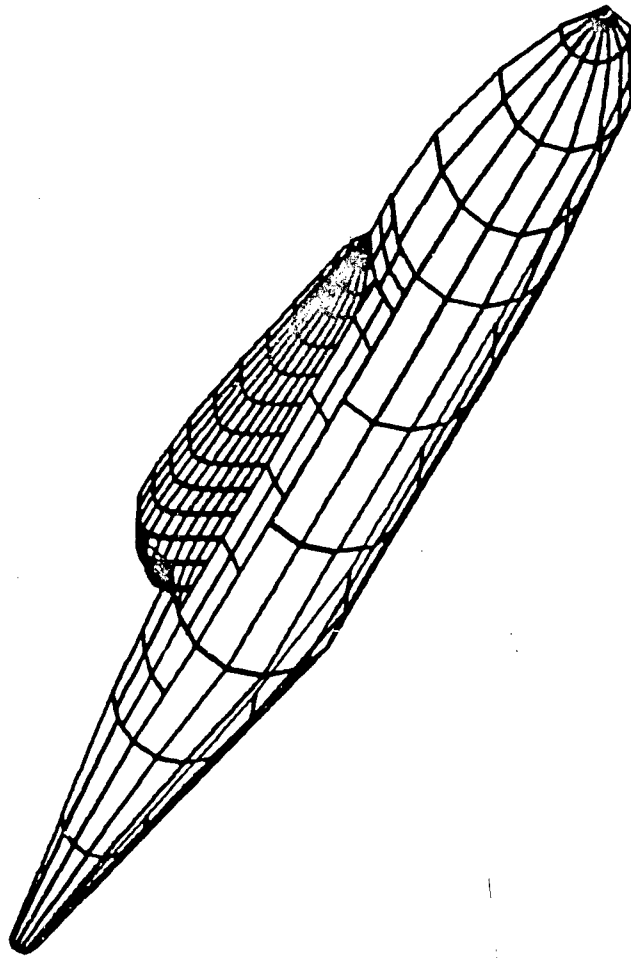
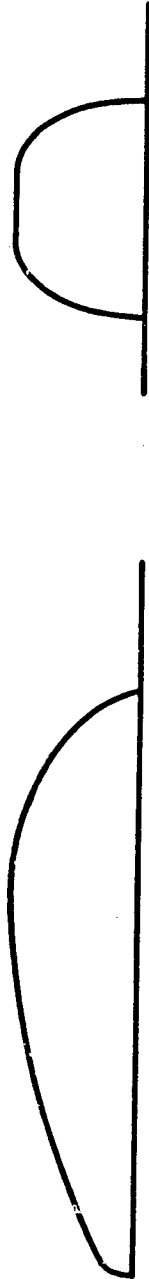


Figure 16. Geometric Model of a Simulated Fuselage/Pylon Configuration.

PYLON TYPE 'A'



PYLON TYPE 'B'



PYLON TYPE 'C'



PROFILE

FRONT

Figure 17. General Pylon Configurations.

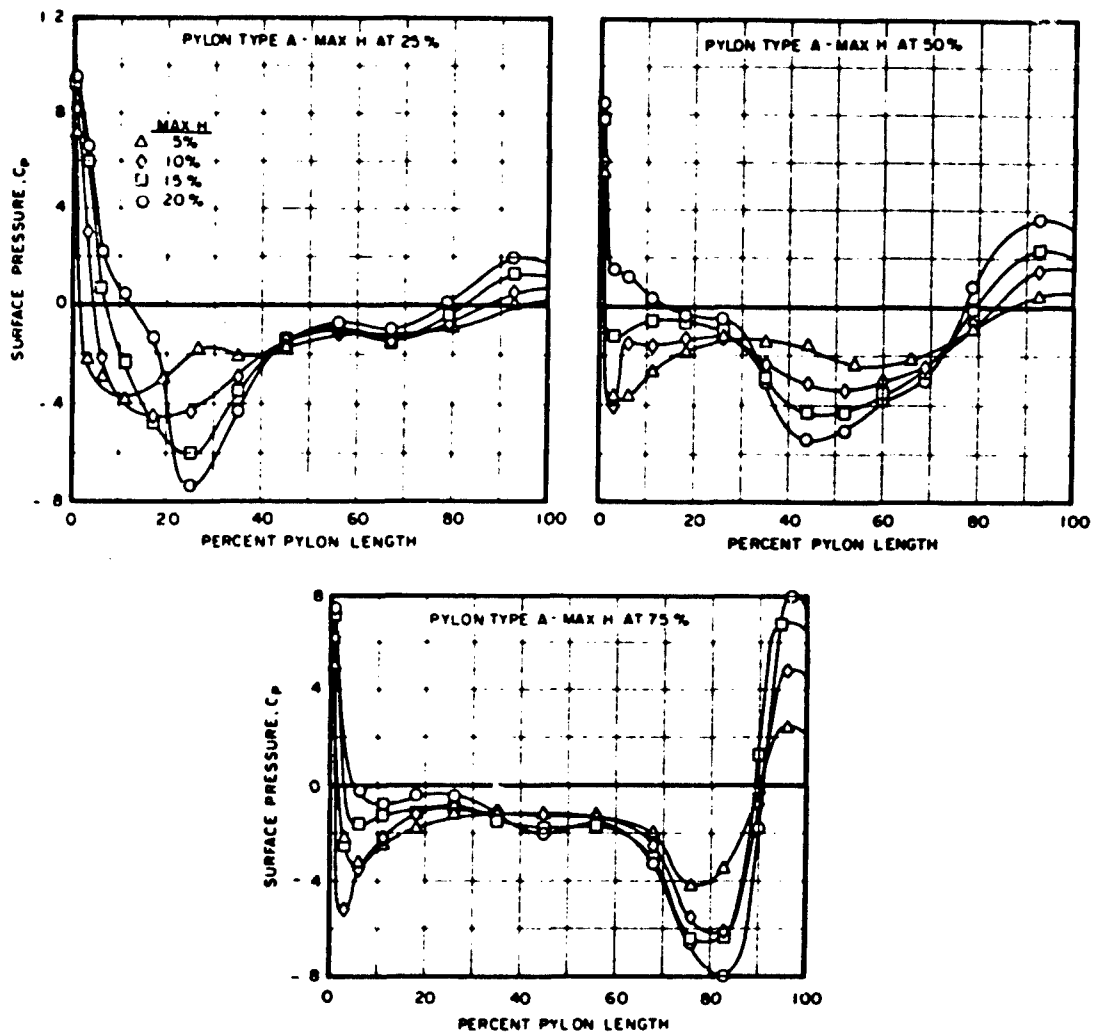


Figure 18. Calculated Surface Pressures Along the Centerlines of Type A Pylons.

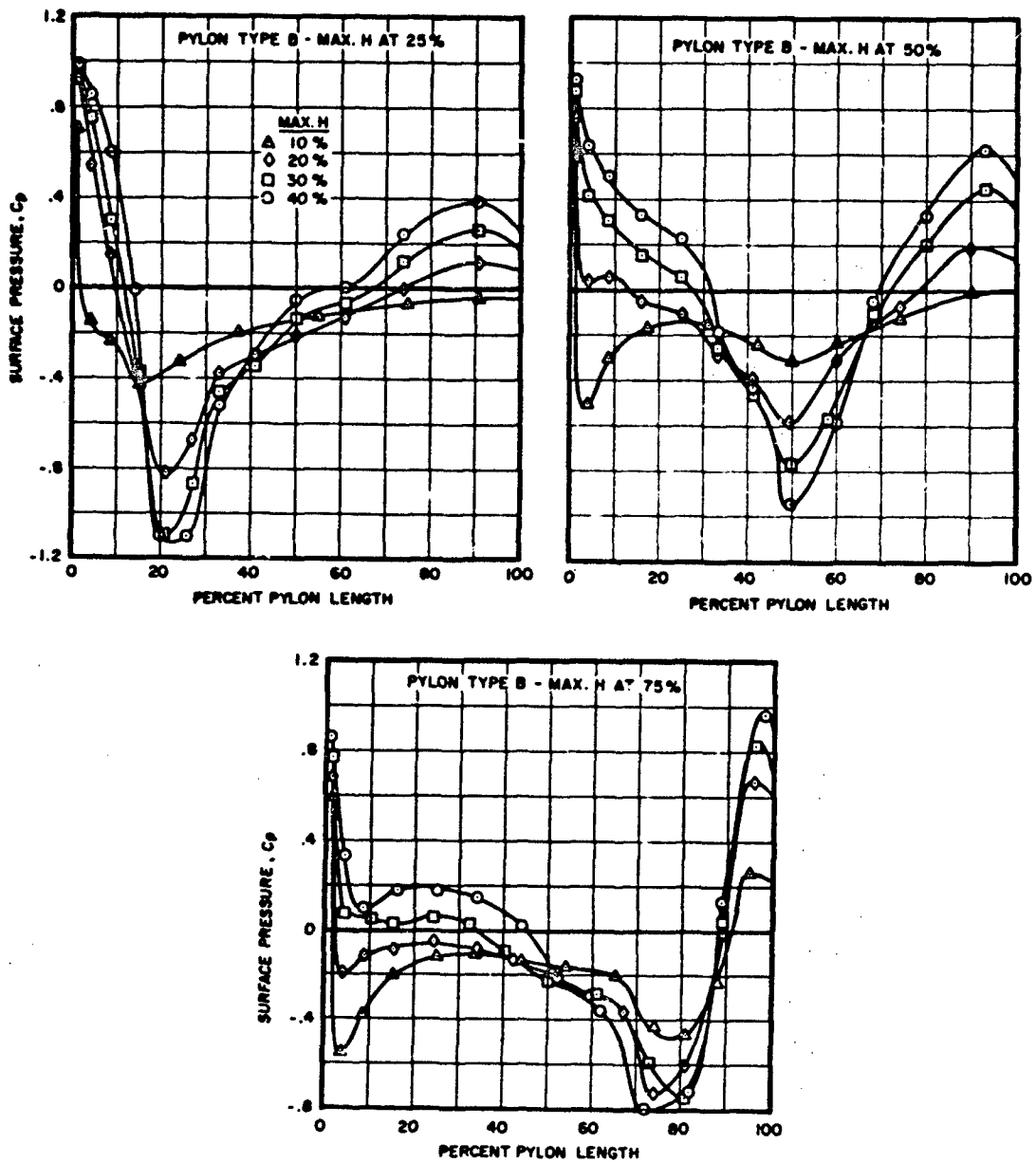


Figure 19. Calculated Surface Pressures Along the Centerlines of Type B Pylons.

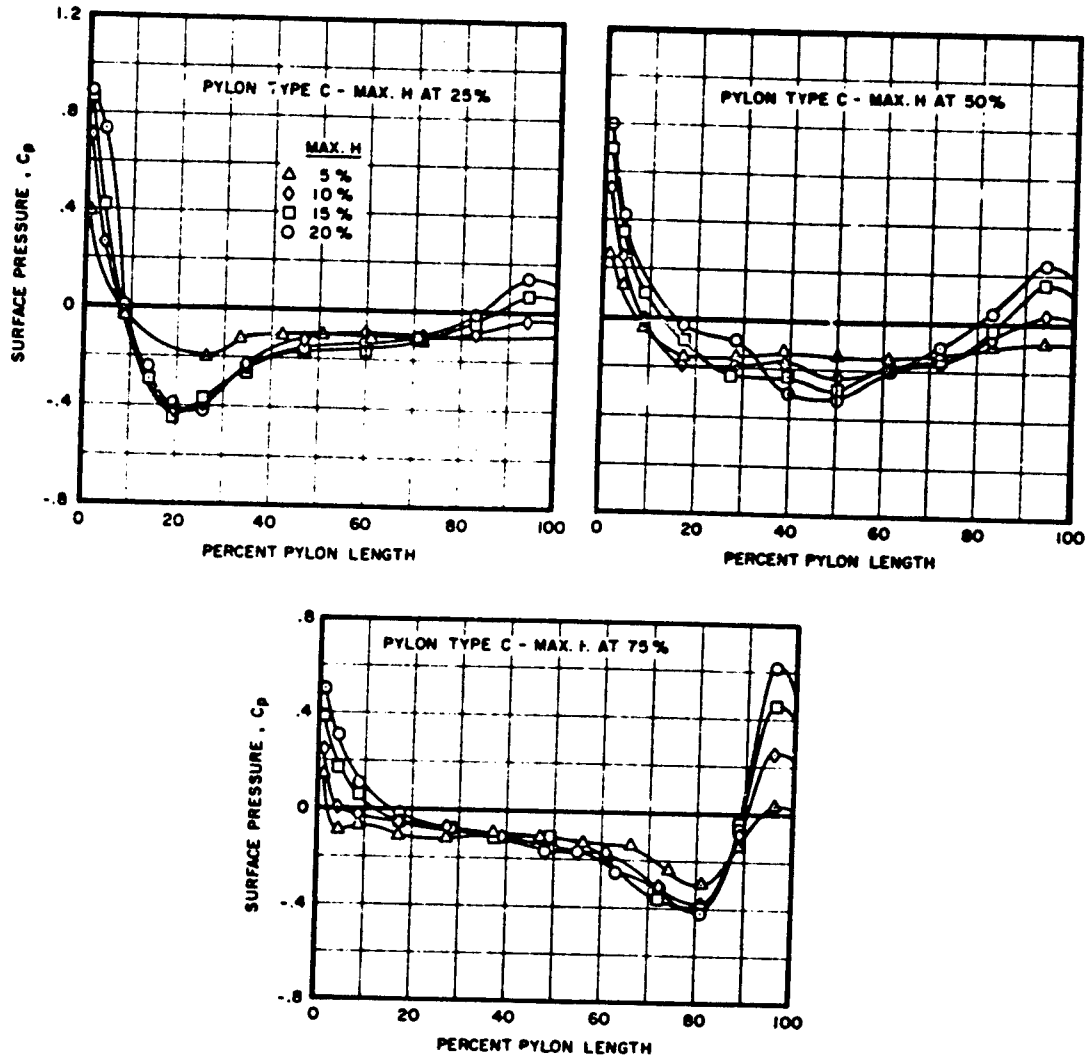


Figure 20. Calculated Surface Pressures Along the Center of Type C Pylons.

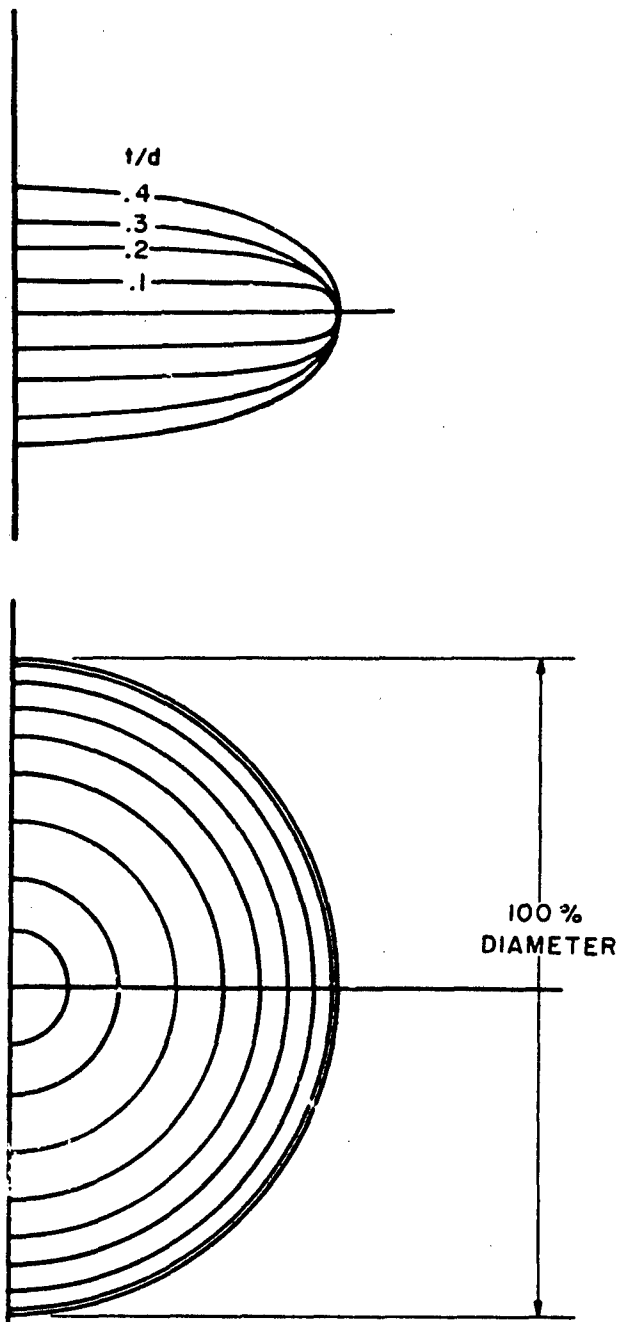


Figure 21. General Ellipsoidal Fairing Characteristics.

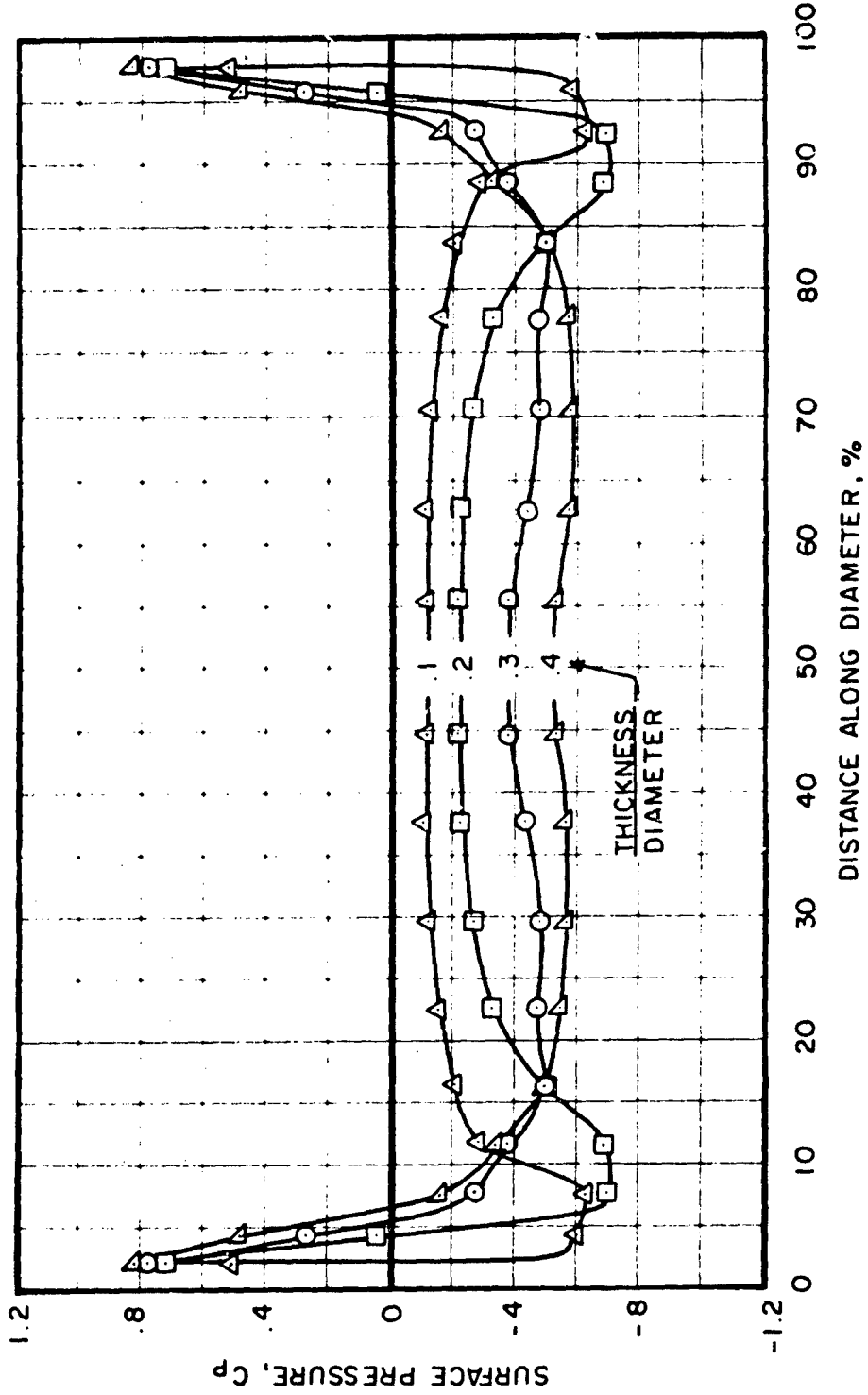


Figure 22. Calculated Surface Pressures Along the Tops of General Ellipsoidal Fairings.

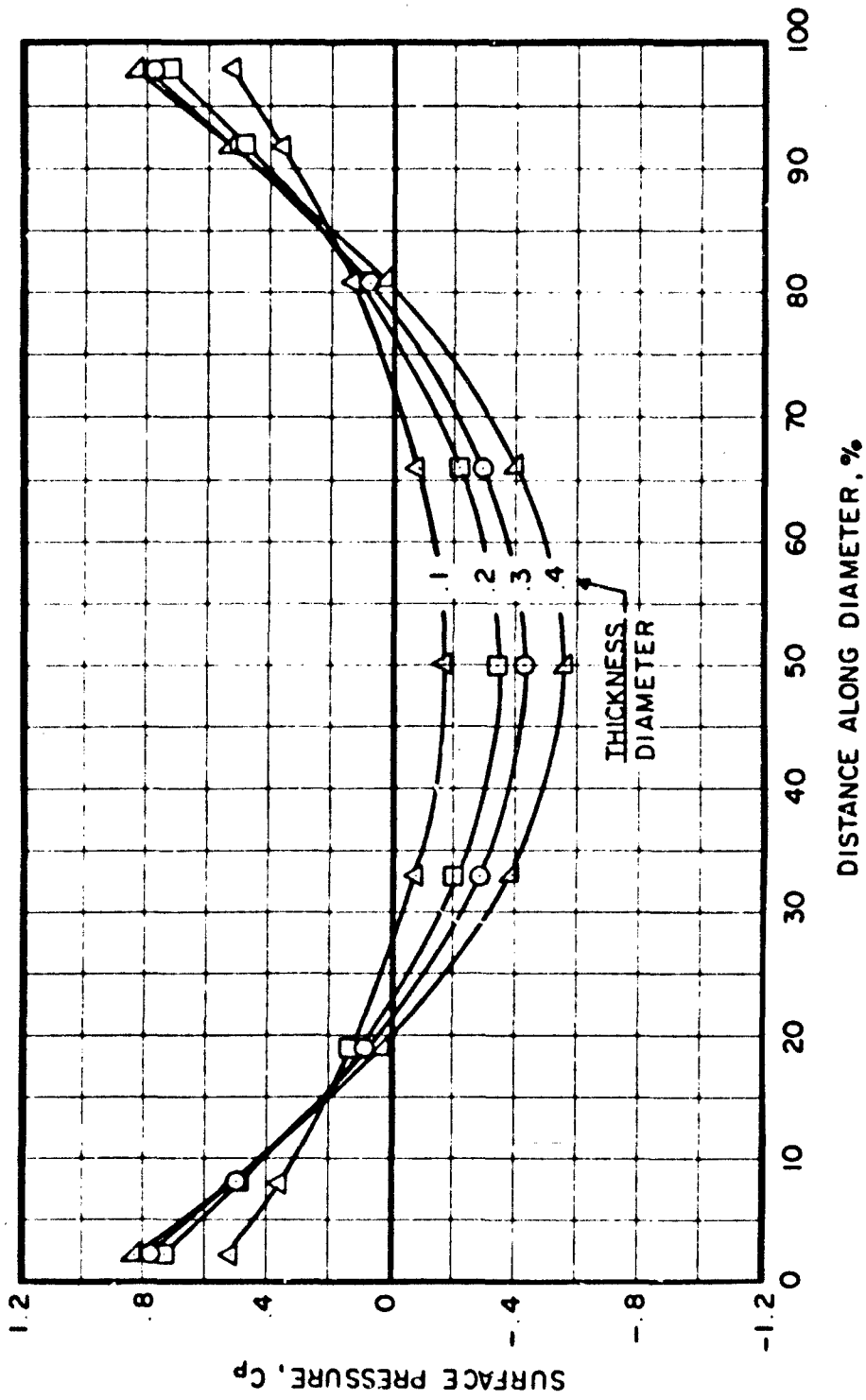


Figure 23. Calculated Surface Pressures Along the Sides of General Ellipsoidal Fairings.

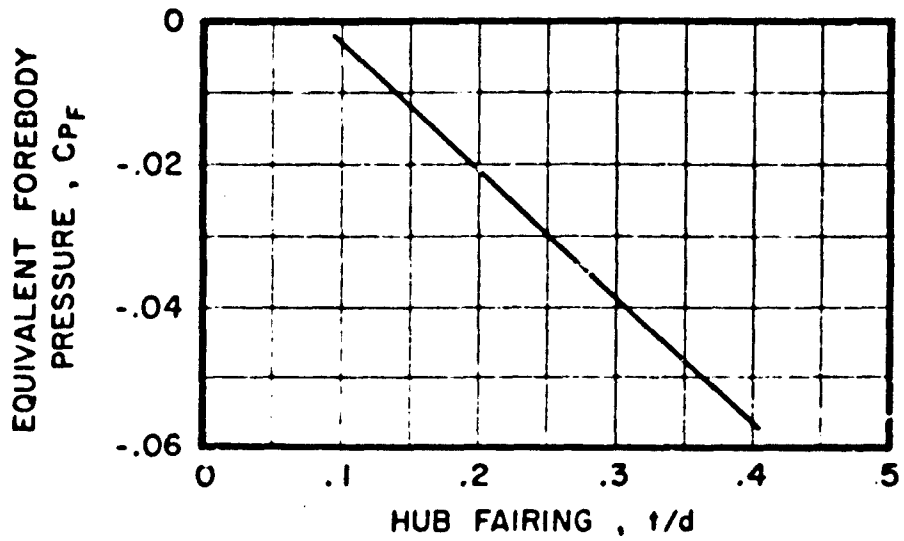


Figure 24. Calculated Equivalent Forebody Pressure Coefficients for General Ellipsoidal Fairings.

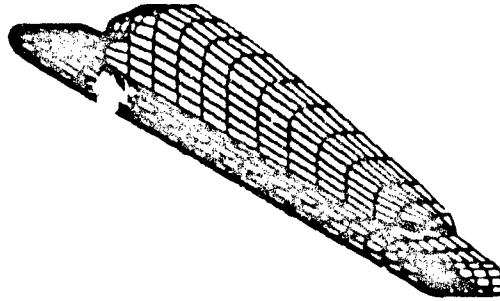


Figure 25. Geometric Model of a Pylon/Simulated Fuselage Upper Surface Configuration.

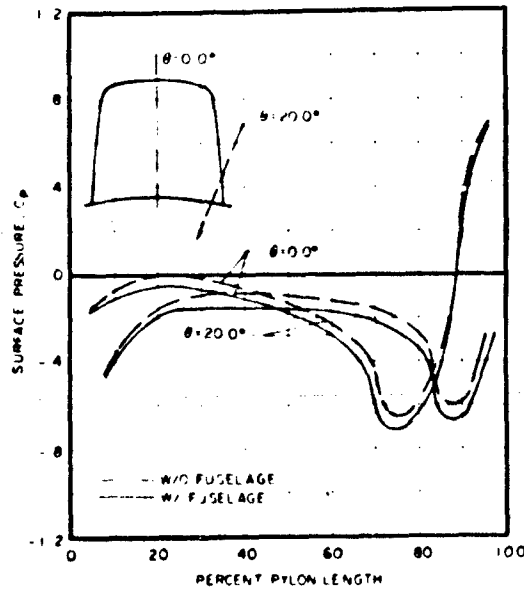
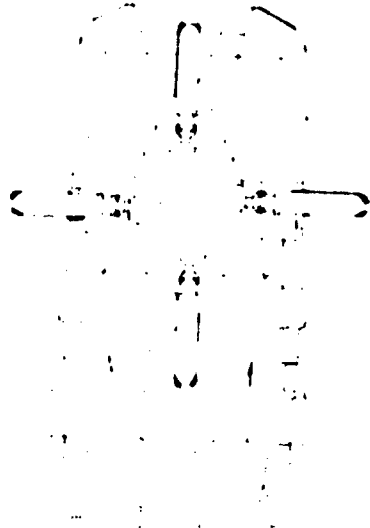
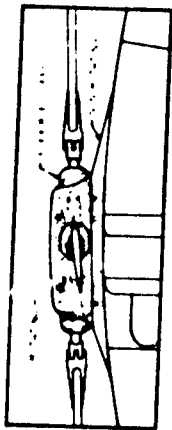


Figure 26. Comparison of Calculated Surface Pressures for a Pylon Configuration With and Without a Complete Fuselage Simulation.



50 56



50 56

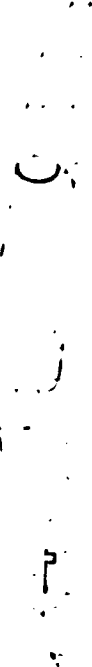


Figure 27. Rigid Rotor Hub Fairing Designed to Reduce Rotor Hub Incremental Drag.

APPENDIX A

DESCRIPTION AND USE OF THE AUTOMATED PANELING TECHNIQUE

PROGRAM Y179A, Y179C

GENERAL DESCRIPTION

The Automated Paneling Technique (APT; Program Designation Y179A) was developed to simplify the generation of a geometric model of any arbitrary shape compatible with Sikorsky Aircraft's three-dimensional potential flow aerodynamic program (Y179L). The program accepts inputs from the user which generally describe cross sections of the body along an axis by combinations of curves and straight line segments. The cross sections are incremented by the program based on specific constraints so that each segment, and consequently each cross section, is approximated by a series of straight line increments. The various increments on adjacent cross sections along the input axis are then connected to form quadrilateral panels which describe the surface of the body as required by the aerodynamic technique. The generation of a proper geometric body is simplified by reducing the user's responsibility for incrementing each cross section and properly identifying every panel and its corner or nodal points. Because of the constraints placed on the incrementing process, the panels generated by the program should approximate the minimum number of panels required to properly model the surface of the body. Figure A-1 illustrates the type of body model generated and the coordinate system used.

As stated previously, the user must describe selected cross sections along the X, Y or Z axis by a combination of curves and straight lines. The curves which the program accepts are shown in Figure A-2. These segments are then incremented by the program based on the following constraints.

1. Minimum and maximum increment length (i.e., the straight line distance between two adjacent points on the incremented cross section as shown in Figure A-3) specified by the user.
2. Maximum increment length based on one-third the separation distance between directly opposing panels. The program assumes the first and last increment at any cross section to be directly opposing. This is not necessarily true for some sections and this constraint may be removed by the user.

3. An increment length may not be more than 130% or less than 70% of the length of increments adjacent to it.
4. An increment must approximate the true curve by a specified tolerance.
5. The total number of straight line increments must equal the number of increments at the cross section to which this section is connected to form the quadrilateral panels.
6. User specified starting or ending increment lengths.

A priority is associated with each constraint and consequently all sections generated may not satisfy every constraint. In this respect, certain constraints represent only approximate restrictions. For instance, for some configurations, the relative size of adjacent increments may not strictly adhere to constraint 3 due to an inability to satisfy all the constraints which have been specified.

Any number of segments may be used to describe a given cross section, but generally the more segments used, the more likely it is that the program will not generate a proper model of the body. For most cross sections, two or three segments are sufficient. The points that must be specified by the user for each segment type are shown in Figure A-2. The open symbols define tangency conditions only and the solid symbols represent actual surface points. A single point is an acceptable input, but cannot be used in conjunction with any other segment. If a single point is used, the program assumes that the section described consists of only that point, and it is normally used to describe the nose of the body. An example of an input section and the resulting output section generated by APT is shown in Figure A-3.

The APT program assumes the body to be symmetric about the Y-Z plane and consequently, only the half of the body in the positive X direction is acceptable as input. The program will automatically perform linear interpolation to generate intermediate body sections along the input axis as requested. This feature allows the user to control panel length without requiring additional input sections.

In addition to the general features already described, APT incorporates several user oriented options. Some options are designed to give the user more control over the distribution of surface panels generated, others are used to input sections which do not conform well with the standard input procedures. Plot options are also available to aid in generating a proper geometric model of the body.

The standard input procedure requires that cross sections along the body axis (Z axis) be described. Often a body or sections of a body would be more easily described and conform to the incrementing process better if cross sections were described along the "X" or "Y" axis. Fuselage sponsons, rotor head fairings and wings are good examples of these types of sections. The program will allow the user to describe these sections along the X or Y axis as requested. If this option is selected, the cross sections must be input from the maximum "X" or "Y" value to the minimum instead of the standard minimum to maximum "Z" values. The proper order for inputting segments at any station along the input axis is shown in Figure A-4.

The program marches along the requested input axis incrementing each section. The section at any one station may be described by a different series of straight line increments, depending on the sections to which it is connected. That is, the number of increments required to connect the section to the previous section may differ from the number of increments required for the section following it. Two sections can be described at one location on the input axis. In this case, the program assumes that the body has a discontinuity at this station and a message stating that normal panels are required will be written (this message will also appear in the punched card output generated). Defining two cross sections at any one location of the input axis is required only when the cross sections to be modeled are of different shapes (for instance, the location of an engine intake or exhaust). Two cross section definitions are not required to alter the number of panels describing the surface upstream or downstream of an input section. The program will not generate panels normal to the input axis and it is the user's responsibility to identify normal panels if a closed body is to be generated.

For basic fuselage shapes without a pylon, wings, or engine nacelles, the body is modeled in one piece. However, portions of a body may be more complex and require several more panels in regions to obtain a proper geometric model. In this case, the more complex regions of a body may be modeled independently and the resulting output combined to form the complete configuration. This is demonstrated in Figure A-5. The Advancing Blade Concept aircraft (ABCTM) main rotor pylon and the engine nacelles were modeled separately for two different reasons. The main rotor pylon required several more input stations along the axis than were required for the fuselage in the same region. Consequently, in order to reduce the number of panels required to model the configuration, the two were modeled separately. A model of the ABC with the pylon was generated prior to the decision to add the engine nacelle models. In order to add the nacelle, the panels describing the fuselage in that region were

simply removed from the data deck and the panels required to interface the nacelle (which was modeled by APT) were substituted. The panels at the wing, pylon, or nacelle intersection with the body must be inputted by the user. The numbering sequence required for the nodal points is shown in Figure A-6. A separate program (Y179C) is used to obtain plots of the final combined configuration.

HELPFUL HINTS

Although the automated paneling technique reduces and simplifies the user's responsibility, care must be taken to insure that the body shape is modeled correctly. The printed output from the program is designed to aid the user in identifying improperly modeled cross sections and nonplanar panels (i.e., surface panels which do not adequately approximate a flat surface). The plotted output also aids in this task. This section is designed to assist the user in proper use of Y179A.

Because of the numerous constraints placed on the incrementing process, certain combinations of segments used in describing a cross section may create an improperly modeled section. The user should also insure that individual segments are described properly.

Experience has shown that two errors in inputting circular and super-ellipse segments occur frequently. The error which occurs most often in describing a circular element is a result of unequal radial distances from the center of the circle to the first and last coordinate points of the circular segment. If the two radial distances vary by more than 5%, the segment inputs are identified as being incompatible and a message to that effect is printed in the output.

The most common error occurring in describing a super-ellipse segment occurs when the third input point does not lie in the triangle shown in Figure A-2. Most often this occurs because of improperly defined tangency lines. If the third point lies outside the given triangle, the segment inputs are identified as being incompatible and this message appears in the output.

Both of the errors listed above will cause the program to omit the cross section at which the error occurs and continue. However, the program will terminate prior to generating the surface panels.

Another error which sometimes occurs in describing the cross section is that of inputting a small straight line segment adjacent to a circular or super-ellipse segment having small curvature. This condition may cause the increments at the segment intersection point to fail the $\pm 30\%$ size relationship. This will not cause the program to terminate but may cause an unsatisfactory increment distribution.

The most common problem encountered in the surface modeling is nonplanar panels generated by the program. If the sections used to form the surface panels are similar in cross section and have no discontinuities in the curvature, this problem is seldom encountered. It is the user's responsibility to insure that the sections used are similar. Often sections used in forming surface panels are quite similar but, as mentioned, discontinuities in curvature are present. This condition will sometimes cause nonplanar panels to be generated.

The program incorporates a planar panel check which will identify what panels fail to satisfy the planar criteria and by what percentage they are nonplanar. The user is responsible for modifying the nonplanar panels if required. This can usually be accomplished by simply changing the quadrilateral panel to two triangular panels. Changing the specified surface maximum and/or minimum often eliminates nonplanar panels and it is recommended that these constraints be varied if nonplanar panels are a problem. Experience has shown that panels within 9 or 10% out of plane are sufficiently accurate for use in Y179L. In addition, nonplanar panels may be identified in regions of the body not of particular interest to the user or in regions where the assumption of potential flow is not valid. In this instance the user may consider the panel representation sufficiently accurate.

Despite the built-in safeguards, the automated paneling technique is not fail-safe and a gradual buildup in the complexity of the bodies modelled is recommended.

INPUT INSTRUCTIONS FOR Y179A

The Fuselage Geometry Definition Program requires punched card input. The input procedure for Y179A is designed to simplify the generation of a data deck describing a general fuselage or body shape for input to the Three-Dimensional Potential Flow Program (Y179L).

DESCRIPTION OF CARD INPUT

<u>Card No.</u>	<u>Columns</u>	<u>Symbol</u>	<u>Description</u>
1	1-72	TITLE	Title card - Any alphanumeric characters acceptable. This title will be used to identify all output generated.
2	1- 4	TYPLT	Plotting unit to be used if plots are requested. (left justified) BLP - Calcomp Plots Blank - No plots generated
	8		Enter "1" if sideview plot is desired

<u>Card No.</u>	<u>Columns</u>	<u>Symbol</u>	<u>Description</u>
	9		Enter "1" if cross section plots are desired
	10		Enter "1" if isometric plots are desired
	12	KARD	Enter "7" if a punched card data deck compatible with Y179L is desired.
	15-21	XSC	Plot scale in the "X" direction if plots are requested. Scale should be inches/user's units based on a <u>positive</u> "X" axis length of 8 inches.
	22-28	YSC	Plot scale in the "Y" direction. Scale in inches/user's units based on a <u>total</u> axis length of 8 inches.
	29-35	ZSC	Plot scale in the "Z" direction. Scale in inches/user's units based on a <u>positive</u> "Z" axis length of 16 inches.
2	36-42	PREQ	Any number >0.0 in this location will cause an "X" to be plotted at each cross section coordinate point generated.
3	8-14 15-21	XPOF YPOF	These numbers will be subtracted from the X, Y coordinates of all panels for plotting purposes. If the minimum, X, Y panel coordinates are greater than or less than 0.0, the user may request an X, Y offset to obtain a larger scale plot of the generated shape.

The following set up the basic input parameters for a body shape.

4	8-14	BSLAST	Enter the location of the last input cross section for this body. The program accounts for a zero offset in the "Z" direction so that actual body station values may be used.
---	------	--------	---

<u>Card No.</u>	<u>Columns</u>	<u>Symbol</u>	<u>Description</u>
	15-21	DSIN	Enter the minimum increment length acceptable for this body. This value is subject to change by later input.
	22-28	DSIX	Enter maximum increment length acceptable for this body. This value is subject to change by later input and/or program requirements.
	29-35	EF	By entering any number >0.0 the user may expand or contract the input coordinates by the value of the number entered.
	36-42	XOVR	Any number >0.0 in this location will override the maximum increment length criteria based on the separation distance of opposing increments.
5	1- 6	CTRANS	<p>If no coordinate interchange option is required enter "Z to Z". If an interchange is required enter:</p> <p>"X to Z" - Cross sections will be input at constant "X" locations from maximum to minimum values.</p> <p>"Y to Z" - Cross sections will be input at constant "Y" locations from maximum to minimum values.</p>

The preceding cards are required for every body shape (for instance, a fuselage, pylon, nacelle or wing) to be generated. The following cards are required for every cross section input location. The card number will be preceded by "IS" to indicate they are required for each input cross section.

<u>Card No.</u>	<u>Columns</u>	<u>Symbol</u>	<u>Description</u>
IS 1	1- 3		Enter BS* to indicate the start of a new body section.
	8-14	BSNS	Enter the body station at which the cross section to be described is located.

<u>Card No.</u>	<u>Columns</u>	<u>Symbol</u>	<u>Description</u>
	15-21	SEG	Enter the number of segments used to describe the cross section. If the inputs for this BS are identical to the previous station, a zero should be entered. No segment inputs are required in this case.
	22-28	DBS	Enter the number of body stations desired to be interpolated between the previously input station and this station.
	29-35	DSMNC	If a change in the minimum surface distance is desired, enter the new DSMN. This change affects this input station and all succeeding stations.
	36-42	DSMXC	If a change in the maximum surface distance is desired, enter the new DSMX. This change affects this input station and all succeeding stations.

One card is required to identify each segment used in describing the total cross section. The total number of "segment cards" should equal the value entered in Columns 15 - 21 on Card IS 1 (SEG). If this value is zero, the inputs are assumed identical to the previous segment inputs and no segment cards are required.

The segment cards have the following format:

<u>Card No.</u>	<u>Columns</u>	<u>Symbol</u>	<u>Description</u>
SEG	1- 3		Enter the number of the segment. The segments should be numbered counterclockwise from top to bottom for the standard "Z to Z" input.
SEG	5	NTYP	Enter the number designating the type of segment to be used. 0 - single point 1 - straight line 2 - circle 3 - super-ellipse (See Figure A-2)

<u>Card No.</u>	<u>Columns</u>	<u>Symbol</u>	<u>Description</u>
	8-14	X1	X1
	15-21	YL	Y1
	22-28	X2	X2
	29-35	Y2	Y2
	36-42	X3	X3 - If a specific number of increments is desired for a straight line segment, enter the number desired.
	43-49	Y3	Y3
	50-56	X4	X4
	57-63	Y4	Y4
	64-70	X5	X5
	71-77	Y5	Y5
	78-80	MREQ	<p>A <u>negative integer</u> entered will cause the length of the first increment of that segment to approximate the product of the integer and the minimum surface distance specified.</p> <p>A <u>positive integer</u> entered will cause the last increment of that segment to approximate the product of the integer and the minimum surface distance specified.</p> <p>If the segment is specified as circular, only a positive value is allowed and the segment is divided into the integer number of increments.</p>

The required cards for the next body station along the input axis follow the last segment card (starting with card IS 1). If the body station entered is equal to the previous body station, the program assumes that this station has been described by two different cross sections and that additional input panels will be required at that station.

A blank card should follow the last body station segment cards if another body shape is to be generated. If no other shape is required enter "END" in column 1-3.

Required CPU time for a typical 400 panel configuration is approximately 1 minute.

INPUT INSTRUCTIONS FOR Y179C

Y179C is an auxiliary three-dimensional body plotting routine. Its purpose is to enable the user to obtain plots of a body shape using card output generated by Y179A.

The card output from Y179A which describes the surface panels for an arbitrary body may be modified and additions to the body may be incorporated. Isometric, cross section, and/or side view plots of the resulting body may then be obtained by using Y179C.

The following cards are required for every body shape to be plotted:

<u>Card</u>	<u>Columns</u>	<u>Description</u>
1	1-78	Title Card - Any alphanumeric data is acceptable.
2	6-10	Total number of panels describing the body shape (N - integer, right justified).

Format for Panel nodal points:

<u>Card No.</u>	<u>Panel No.</u>		
3	1	Node 1 (X,Y,Z)	Node 2 (X,Y,Z)
4	1	Node 3 (X,Y,Z)	Node 4 (X,Y,Z)
$2N+1$	N	Node 1 (X,Y,Z)	Node 2 (X,Y,Z)
$2N+2$	N	Node 3 (X,Y,Z)	Node 4 (X,Y,Z)

(For triangular panels, the fourth point is the same as the first point).
Fields of 10 starting in Column 11.

The panel cards are normally generated by Y179A, but panels may be added or omitted by the user.

<u>Card No.</u>	<u>Columns</u>	<u>Description</u>
$2N+3$		Same as Card 2 of Y179A input.
$2N+4$		Same as Card 3 of Y179A input.
$2N+5$		Same as Card 5 of Y179A input.

The following card is used to identify a coordinate system off set for various panels if required. For instance, if the input panels represent multiple bodies, then the separation distance between bodies may be changed.

<u>Card No.</u>	<u>Columns</u>	<u>Description</u>
2N+6	1- 5	Panel number "NB" (Integer-right justified).
	6-10	Panel number "NE" (Integer-right justified).
	11-20	X ϕ These values will be
	21-30	Y ϕ added to all panels
	31-40	Z ϕ between panels NB and NE.

This card may be repeated as many times as required. A zero value for NB indicates that no more panels require an offset.

A blank card should follow the preceding cards if another shape or shapes are to be plotted. If no other shape is required, enter "END" in columns 1-3.

Required running time for a typical 400 panel configuration is approximately 1 minute.

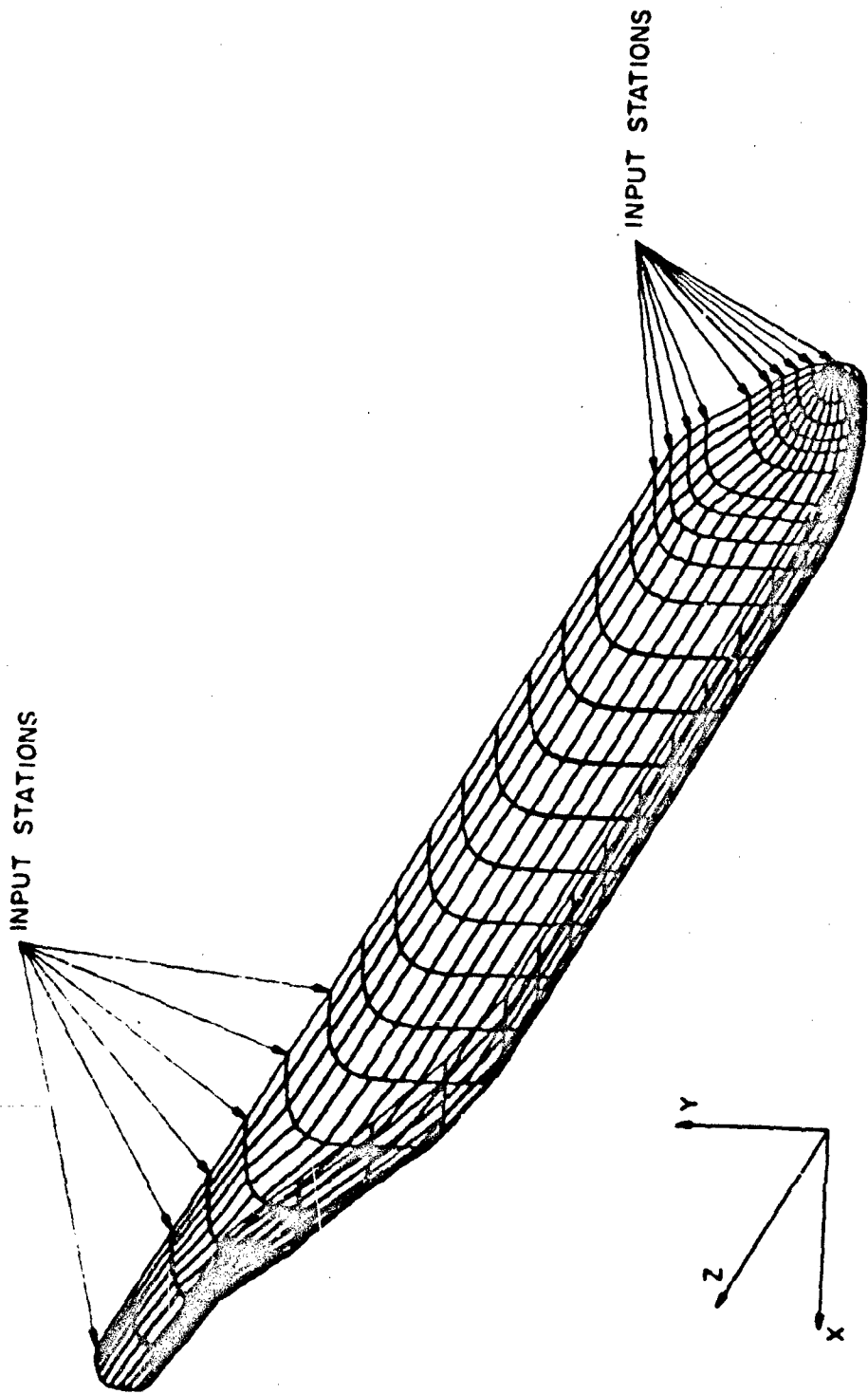


Figure A-1. C-119 Fuselage Generated by Automated Paneling Technique.

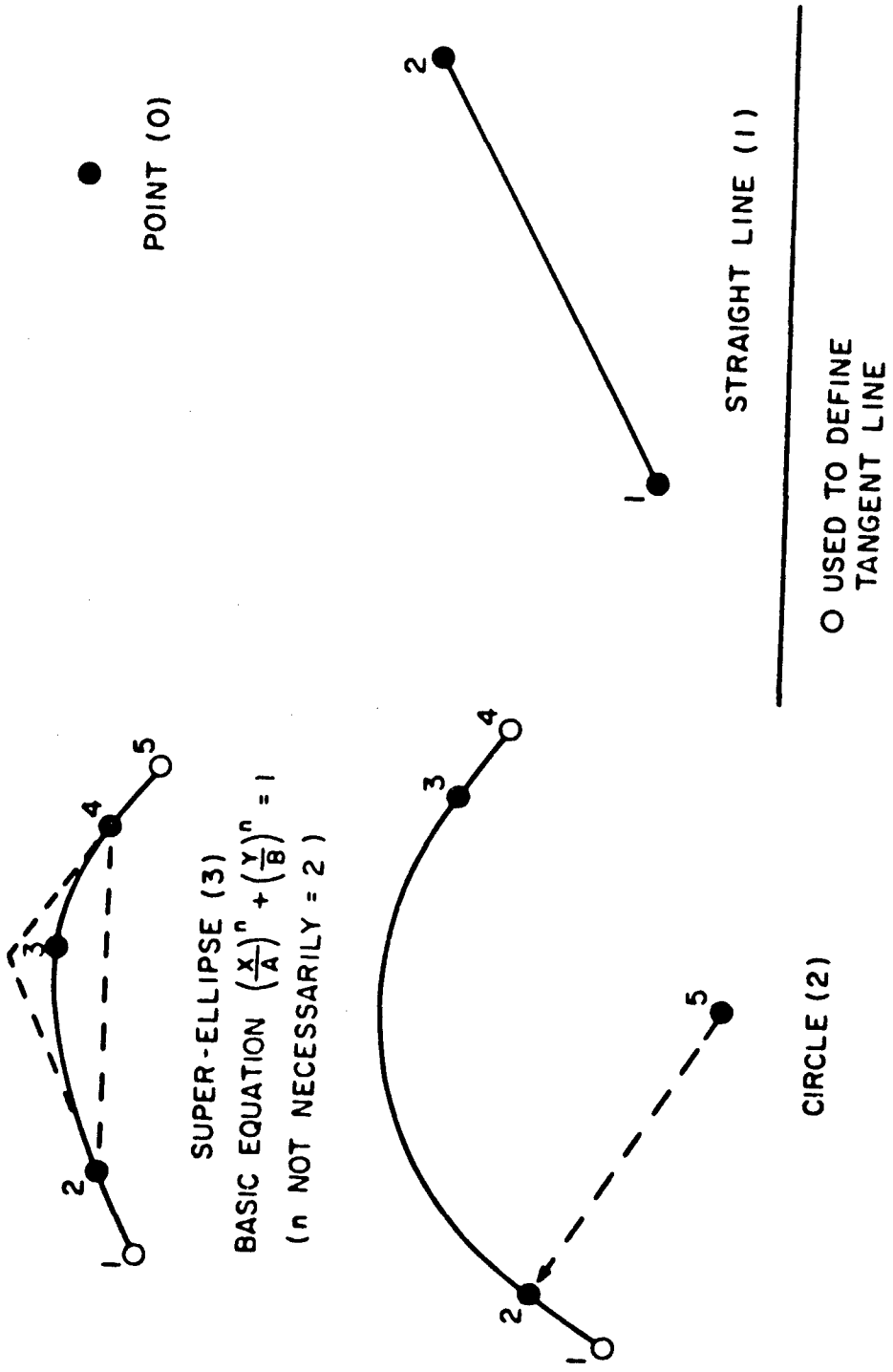


Figure A-2. Description of Segment Types and Input Points for APT.

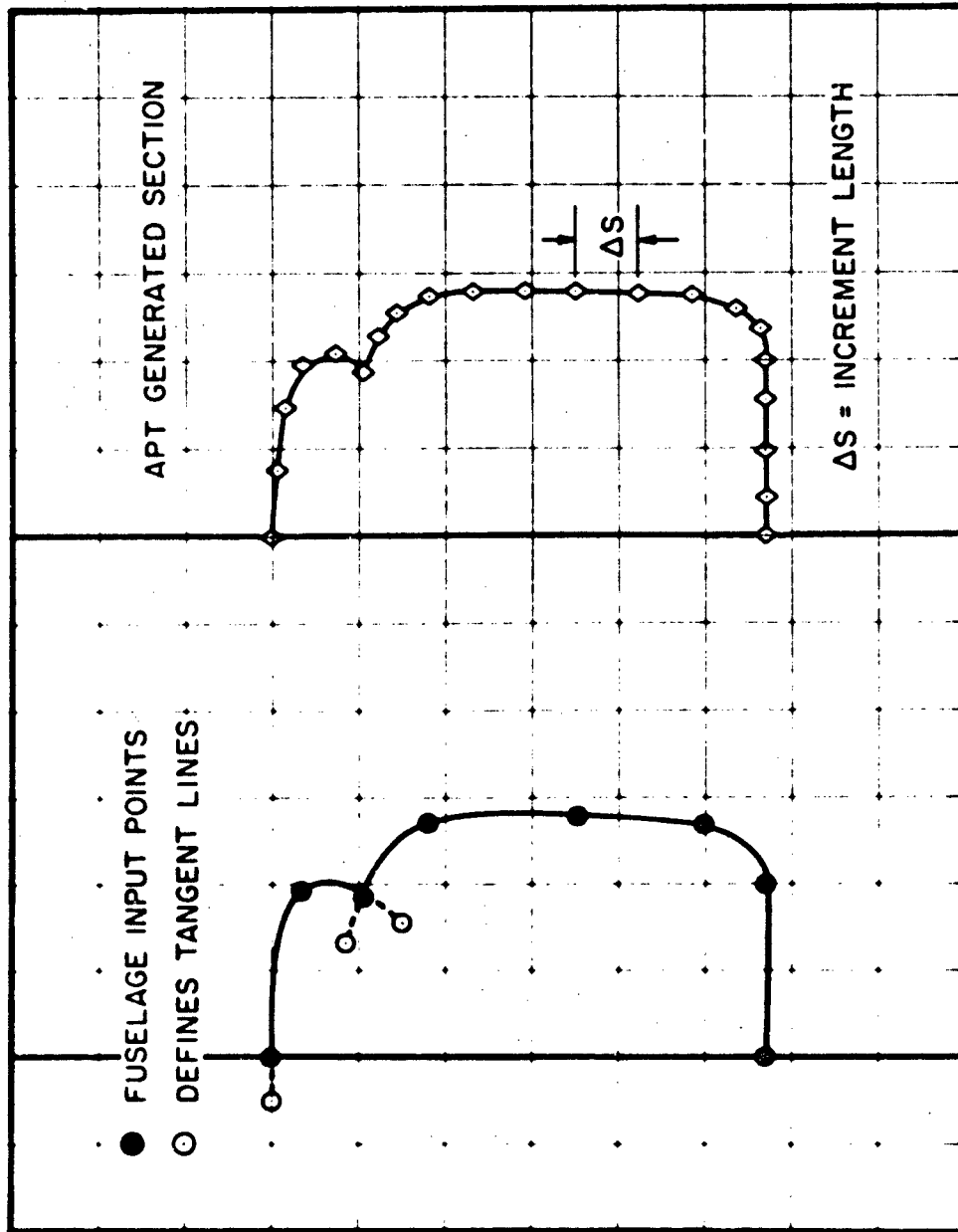


Figure A-3. Sample Input Points and Resulting Output for Cross Section Generated by APT (Rear View).

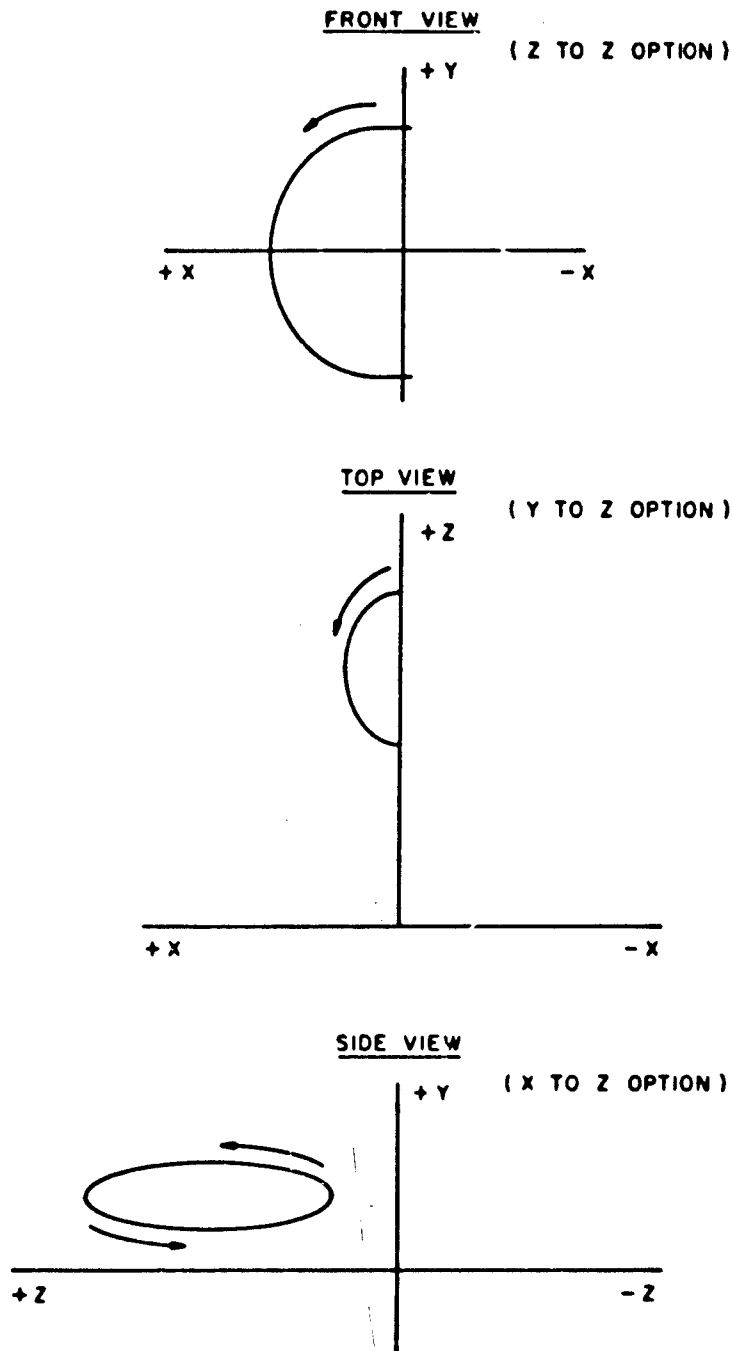


Figure A-4. Required Input Order for Segments Describing a Cross Section.

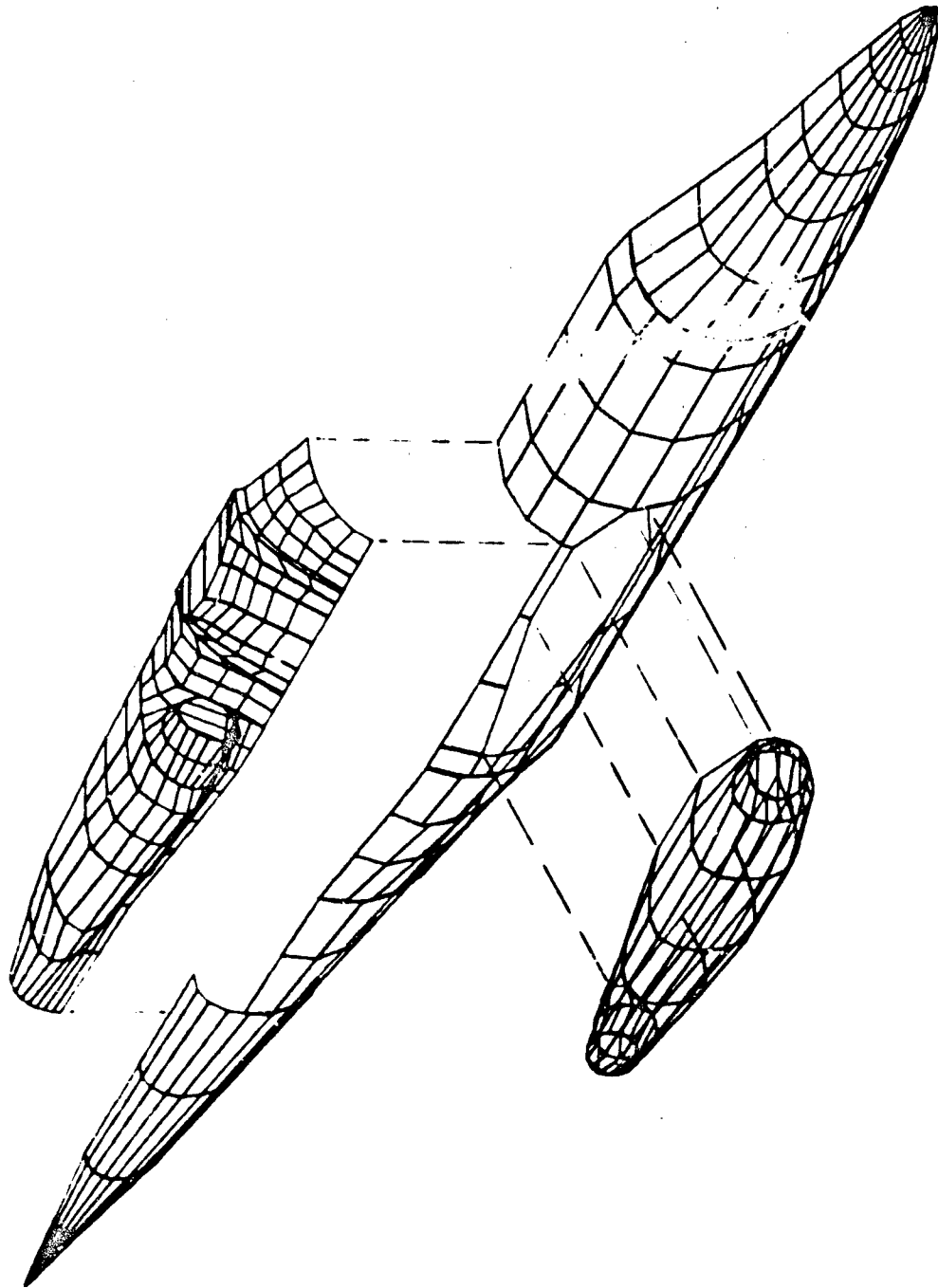
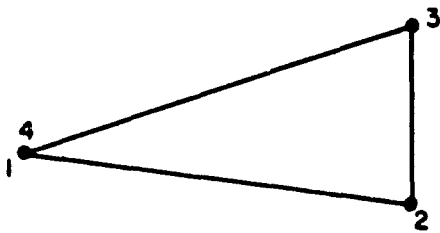
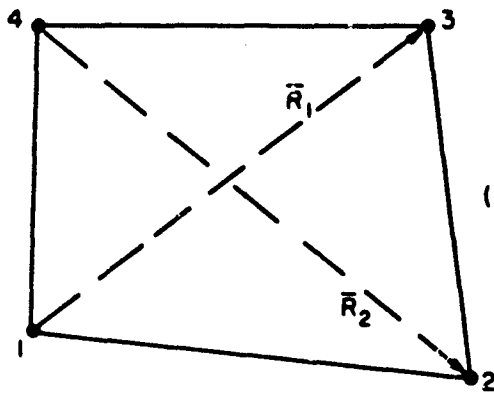


Figure A-5. Example of Fuselage Sections Combined to Form Complete Aircraft.



(TRIANGULAR PANELS)



(QUADRILATERAL PANELS)

PANELS MUST BE SEQUENCED SUCH THAT

$$\bar{R}_2 \times \bar{R}_1$$

IS IN THE SURFACE OUTWARD NORMAL
VECTOR DIRECTION.

Figure A-6. Required Input Order for Corner Points
Describing an Input Panel.

APPENDIX B

DESCRIPTION AND USE OF THE THREE-DIMENSIONAL AERODYNAMIC ANALYSIS TECHNIQUE-PROGRAM Y179L

GENERAL DESCRIPTION

The analytical technique used to predict the aerodynamic flow field on and about an arbitrary lifting or nonlifting configuration is described in more detail in Reference 9. The basic potential flow methods used in the technique are described in detail in References 10 through 12.

The technique requires that the surface of the body be described by a finite number of approximately flat panels as shown in Figure B-1. Any lifting sections such as wings and tail surfaces are also modeled by a vortex lattice system on the mean camber surface as shown in Figure B-2. A constant source strength is distributed uniformly over the surface of each surface panel and the vortex lattice system consists of bound and trailing line vortices. The general solution of the flow field is then obtained by solving a set of linear simultaneous equations relating the influence of each source distribution and line vortex on all the other surface panels, control points and the points at which the Kutta condition is applied for each lifting section. The solution of these equations yields the source and vortex strengths from which the flow velocities and directions about the body or bodies can be calculated.

The aerodynamic program accepts inputs from the user describing the surface panels by their corner or nodal points. The order of input is arbitrary since each panel is described independently. This feature also allows the aerodynamic solution of multiple bodies. The technique accepts triangular as well as quadrilateral panels.

The vortex lattice system for lifting sections is generated by the program, given the spanwise position of trailing vortices and the requested chordwise position of the bound vorticity. The particular vortex lattice technique used requires that the chordwise distribution of vorticity be known. A modified Multhopp lifting surface analysis is employed to determine the vorticity distribution. This feature is inherent in the program and eliminates the requirement for specifying the vorticity distribution. This method is most accurate when applied to thin, high aspect ratio wings and is less accurate for lifting sections that are very thick or have a small aspect ratio. It is, however, considered sufficient for even these shapes since only the chordwise vorticity distribution

is determined by this method and not the vorticity strengths.

The program is capable of handling arbitrary configurations at angles of attack and/or in yawed flow. Engine inflow or exhaust can be simulated by requesting fluid ejection or suction through the surface of individual panels. In addition to these features, the program incorporates several user oriented options for rotating the bodies or coordinate offsets. These features allow the user to vary wing/body incidence, wing dihedral, and fuselage/stores separation distance without generating additional body descriptions.

It is important to emphasize that the program has been exercised extensively for helicopter configurations with complex pylon and engine nacelle configurations, but has not been nearly so well exercised on winged configurations and multiple bodies. It is therefore possible that certain lifting configurations or combinations of configurations may yield unsatisfactory results although none have been identified to date.

The general characteristics required of the panel description of arbitrary configurations are outlined below.

1. Surface panels should be approximately planar.
2. Small panels adjacent to large panels should be avoided since the accuracy of a region is that associated with the largest panel.
3. Long, narrow panels should be avoided in regions where accuracy is considered important.
4. For wings, the trailing edge presents a difficult region to model since the surface panels close very sharply. The trailing-edge panels should be small or the trailing edge should be modeled more bluntly.
5. The only restriction on order of input for a body is that lifting sections must be modeled from outboard to the inboard sections.
6. The trailing-edge bound vortex location should not be greater than 95% of the chord.
7. The point at which the Kutta condition is applied is variable and is determined by the program from the relation,

$$(X/C)_{KP} = (X/C)_{BTE} + .04 \left[(1 - (X/C)_{BTE}) + (X/C)_{TV} \right]$$

- where $(X/C)_{KP}$ = the Kutta condition point
- $(X/C)_{BTE}$ = the chordwise position of the last bound vortex
- $(X/C)_{TV}$ = the length specified for the trailing vortices, c is the chord length.

For instance, for a trailing edge bound vortex at 95% of the chord and a trailing vortex length of 500%, the Kutta point will be applied at approximately the 115% point.

Application and Substantiation

The three-dimensional aerodynamic analysis technique has a wide range of applications to the design and analysis of helicopter configurations. The resulting output supplies surface pressures and the local flow direction on the body. This allows early identification of surface airloads and aids in the placement of airspeed instrumentation and antennae. This information also aids the designer in identifying regions of possible flow separation.

In addition to the flow characteristics on the surface of the body, the velocity magnitude and direction at points off the surface can be computed. This feature allows the designer to investigate the potential interference effects the body may have on the rotor or other helicopter components.

The calculated results from the Y179L program have been correlated for fuselage configurations ranging from simple cylindrical bodies to complex shapes such as the Army/Sikorsky ABCTM with auxiliary engine nacelles and the winged rotary system research aircraft (RSRA) configuration. Typical correlation for the configurations analyzed is shown in Figures B-3 to B-5. Off-body velocities have not been correlated due to lack of experimental data.

The capabilities of the aerodynamic analysis technique have proven extremely useful and have been used extensively in the design and analysis of the ABCTM, RSRA and in particular the Army/Sikorsky YUH-60A and the commercial S-76.

Input Instructions for Y179L

The required input describing the body to be analyzed adheres to the general rules identified in Appendix A. The automated paneling technique (APT) described in Appendix A was designed to complement Y179L and its use is recommended.

<u>Card</u>	<u>Columns</u>	<u>Symbol</u>	<u>Description</u>
1	1-72	TITLE	Any alphanumeric title.
2	1-10	REFA	Desired reference area for force and moment coefficients.
	11-20	REFL	Desired reference length for moment coefficients.
3	1-10	ALPHA	Angle of attack, deg (positive nose up)
	11-20	BETA	Angle of yaw, deg (positive nose right)
4	5	MONLY	1 - Perform Multhopp Analysis only 0 - Perform total analysis
	10	MPRNT	1 - Printer plots of Multhopp analyses requested 2 - Plots and Multhopp influence coefficients requested 0 - Neither requested
	15	NGPRNT	1 - Panel unit vectors printed 2 - Panel coordinates in panel system printed 0 - Neither printed
	20	NPRNT	1 - Solution matrix and constant matrix printed 2 - Panel influence coefficient matrix printed for panels NCM1 to NCM2 0 - Neither printed
	21-25	NCM1	(See above)
	26-30	NCM2	(See above)
	35	MPRNT2	1 - Multhopp loading functions printed 2 - Multhopp wing geometry printed 3 - Wing camber computations printed 4 - Full Multhopp influence coefficient matrix printed 0 - No additional printout

<u>Card</u>	<u>Columns</u>	<u>Symbol</u>	<u>Description</u>
5	5	NSAV1	0 - Do not file geometry data -1 - Geometry data not on file - initiate file write of geometry data (This feature is used to store various geometric characteristics to avoid time-consuming com- putations if subsequent runs are anticipated for this shape). 1 - Geometry data on file - geometry data is to be read from file
	10	NSAV2	0 - Do not file solution -1 - Solutions to various flow conditions are not on file - initiate file write of solution 1 - Solutions for various flow conditions are on file - search file for required solution - calculate solution and write on file if solution is not currently on file.

Various sections of the body or bodies may be inputted independently if desired. The following cards are required for each individual section used (maximum of five sections).

6	1- 5	TYPE	Body Section type: NL,S - nonlifting, symmetric NL,NS - nonlifting, nonsymmetric L,S - lifting, symmetric L,NS - lifting, nonsymmetric
	13-72		Any alphanumeric title describing this section
7	5-10	NOP	Total number of surface panels describing this subsection. (If the section type on card 6 designates a nonsymmetric section, the body is assumed to be in two subsections, one on either side of the Y-Z plane).
8	1-10 11-20 21-30	XOF YOF ZOF	Location of origin in section coordinate system. These values will be added to the panel coordinates to obtain coordin- ates in reference system

<u>Card</u>	<u>Columns</u>	<u>Symbol</u>	<u>Description</u>
8 (cont'd)	31-40	XROT	Angle in degrees which the input coordinates should be rotated about the input X axis.
	41-50	ZROT	Angle which the input coordinates should be rotated about the input Z axis.
9	1-10	-	Not used by program.
	11-20	XC ₁	Coordinates for panel node point 1, first panel.
	21-30	YC ₁	
	31-40	ZC ₁	
	41-50	XC ₂	Coordinates for panel node point 2, first panel.
	51-60	YC ₂	
61-70	ZC ₂		
10	1-10	-	Not used.
	11-20	XC ₃	Coordinates for panel node point 3, first panel.
	21-30	YC ₃	
	31-40	ZC ₃	
	41-50	XC ₄	Coordinates for panel node point 4, first panel.
	51-60	YC ₄	
	61-70	ZC ₄	

Cards 9 and 10 are repeated for each panel describing the particular body section identified. If the body section has been identified as nonsymmetric, cards 7 and 8 are repeated for subsection 2 and cards 9 and 10 are repeated for each panel in subsection 2. Symmetric sections do not require additional inputs in yawed flow. After the last panel input card of the last body section, enter "END OF PANEL INPUT" starting in column 1.

The following cards are inputted after the cards described previously. Since these cards represent panel or point rotation options, they are preceded by an "R".

<u>Card</u>	<u>Columns</u>	<u>Symbol</u>	<u>Description</u>
R1	5	IR	Body section containing points or panels requiring a specific rotation. A zero is required to exit from this option.
	6-10	NR	Number of panels or points requiring rotation. (Integer-right justified.)

<u>Card</u>	<u>Columns</u>	<u>Symbol</u>	<u>Description</u>
	11-20	XR	Location about which panels or points should be rotated.
	21-30	YR	
	31-40	ZR	
	41-50	RX	Angle in degrees which points or panels should be rotated about input X axis.
	51-60	RZ	Angle in degrees which points or panels should be rotated about input Z axis.

If panel node points are to be rotated, repeat the following card for each panel required up to "NR".

R2	1- 5	NP	Panel number for which rotations are required. A zero will exit to card R3. (Integer-right justified.)
	6-10	NOD ₁	Panel node points which should be rotated. (Integer-right justified.)
	11-15	NOD ₂	
	16-20	NOD ₃	
	21-25	NOD ₄	

If specific points on the body are to be rotated, repeat the following card for each desired point.

R3	1-10	A ₁	(X, Y, Z) coordinates of point to be rotated.
	11-20	B ₁	
	21-30	C ₁	
	31-40	A ₂	(X, Y, Z) coordinates of next point to be rotated.
	41-50	B ₂	
	51-60	C ₂	

The program will continue to read cards R1 through R3 until a zero value has been entered for IR on card R1.

Lifting section input (if required) follows the cards previously described. These cards are preceded by an "L" to designate that they are required only if the body contains lifting sections.

<u>Card</u>	<u>Columns</u>	<u>Symbol</u>	<u>Description</u>
L1	5	IV	Body section number requiring lifting section inputs.
	10	LV	Subsection 1 or 2.
	11-15	NSV	Number of trailing vortices for this subsection (enter zero for subsection 2 of symmetric section).
	16-20	NCV	Number of bound vortices for this subsection.
L2	8 fields (8F10.0)	AV	Spanwise positions of trailing vortices - entered outboard to inboard.
L3	8 fields (8F10.0)	BV	Chordwise positions of bound vortices - the last value designates the length of the trailing vortex. Entered from leading edge to trailing edge in percent chord.

The lifting section inputs must be repeated for each lifting section. Only card L1 is required for subsection 2 if the section is symmetric.

The following card(s) are input after the lifting section cards (if applicable). These cards are used to specify fluid ejection or suction for specific panels and will be preceded by an "P".

<u>Card</u>	<u>Columns</u>	<u>Symbol</u>	<u>Description</u>
F1	1- 5	PNP	Panel number requiring fluid ejection or suction (Integer-right justified).
	6-15	PNV	Prescribed normal velocity for this panel entered as a ratio of freestream velocity. Positive velocity is in direction of surface outward normal.

Card F1 may be repeated for a maximum of 50 panels. A zero value for PNP on card F1 is required to designate that no more panels require prescribed normal velocities.

The following cards designate various output options and will be preceded by an "O".

<u>Card</u>	<u>Columns</u>	<u>Symbol</u>	<u>Description</u>
01	1- 5	M	Number of waterlines (Y = constant) along which surface pressures are to be calculated by interpolation between panel control points. (Maximum 16, Integer-right justified.)
	6-10	L	Number of body lines along which surface pressures are to be calculated ($\theta = \text{constant}$) $\theta = 0^\circ$, top centerline; $\theta = 180^\circ$, bottom centerline; where $\theta = \tan^{-1} \left(\frac{X}{Y - YWL} \right)$ (Maximum 16, Integer-right justified.)
	10-15	NOB	Number of off-body points at which velocities are to be calculated (maximum 216, Integer-right justified). If the following option is chosen, NOB represents the number of radial stations on the rotor blade (maximum 12).
	16-20	NPSI	Number of azimuthal positions (0° to 180°) at which to calculate the normal, radial and tangential induced velocities at the rotor blade stations specified ($\Delta\psi = 180^\circ / (NPSI - 1)$). Sign convention for velocities is: normal velocities-downflow is negative radial velocities-positive towards the tip tangential velocities-positive towards the leading edge (maximum 18, Integer-right justified).

If M > 0 repeat the following card as required:

02	8 fields (8F10.0)	WL	Enter the waterline at which surface pressures are to be calculated (eight waterlines per card).
----	----------------------	----	--

If L > 0 enter the following cards:

<u>Card</u>	<u>Columns</u>	<u>Symbol</u>	<u>Description</u>
03	1-10	YWL	Enter the Y value from which the bodyline angles should be computed.
04	8 Fields (8F10.0)	BL	Enter the bodyline angles along which surface pressures are to be calculated (eight values per card).

If NOB > 0 and NPSI = 0, repeat the following card as required:

05	1-10 11-20 21-30	X Y Z	Coordinates of the off-body point at which velocities are to be calculated.
----	------------------------	-------------	---

If NOB > 0 and NPSI > 0, enter the following cards as required:

06	8 Fields (8F10.0)	RAD	Nondimensional radial stations at which induced velocities are to be calculated. Entered from root to tip (eight values per card).
07	1-10 11-20 21-30 31-40 41-50	ZR YR RRT SHAFT CONE	Z location of rotor hub Y location of rotor hub Radius of rotor (units in which body is described). Shaft tilt in degrees, forward tilt is negative. Amount of coning in degrees.

The program requires five auxiliary tape or mass storage units. The units are referenced in the program as units 8, 9, 10, 11 and 12. The data stored on each unit is described below.

<u>Unit(s)</u>	<u>Description</u>
8, 9, 10	Influence coefficients for all the panels and vortex lattices are stored on these units. These are working storage areas and are required for every job executed.

<u>Unit(s)</u>	<u>Description</u>
11	This unit is used to store the solution for various angles of attack and/or yaw. This unit is required only if NSAV2 on Card 5 of the input deck equals -1 or 1. If the body is to be analyzed in yawed flow, a yawed flow condition should be used to initiate solution filing.
12	Unit 12 is used to store various geometric data required for the analysis, such as panel unit vectors and panel coordinates in panel system. This unit is required only if NSAV1 on Card 5 is -1 or 1. (Note: if NSAV1 equals 0, the value of NSAV2 is irrelevant).

Because of the user oriented way in which the panels are described, this aerodynamic technique requires a significant amount of storage. Consequently, only a total of 500 panels may be used to model a given body (250 if yawed flow is desired for a symmetric section). This total includes all surface panels and vortex lattice panels.

The program was originally developed for a UNIVAC 1110 computer system and has been converted to the IBM 360 system at the Army Computing Facility at Ft Eustis, Virginia. The program has been exercised primarily on the UNIVAC 1110 system and therefore an accurate estimate of the run time on the IBM system is not yet available. The approximate run times are shown in Figure B-4. This figure also shows the time savings associated with using the data storage options identified on Card 5. For some winged configurations, the running time may significantly increase if trailing edge surface panels are located very close to a bound vortex element. The running times also vary significantly depending on the options requested on cards 01 to 07.

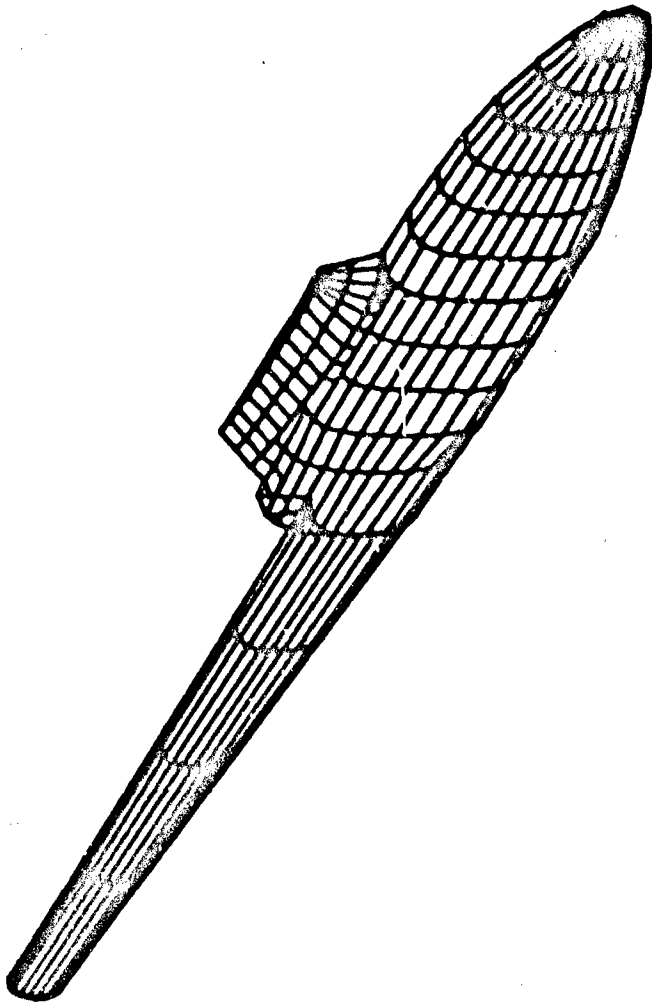


Figure B-1. Panel Representation of Body Used in Three-Dimensional Aerodynamic Analysis Technique (Y179L).

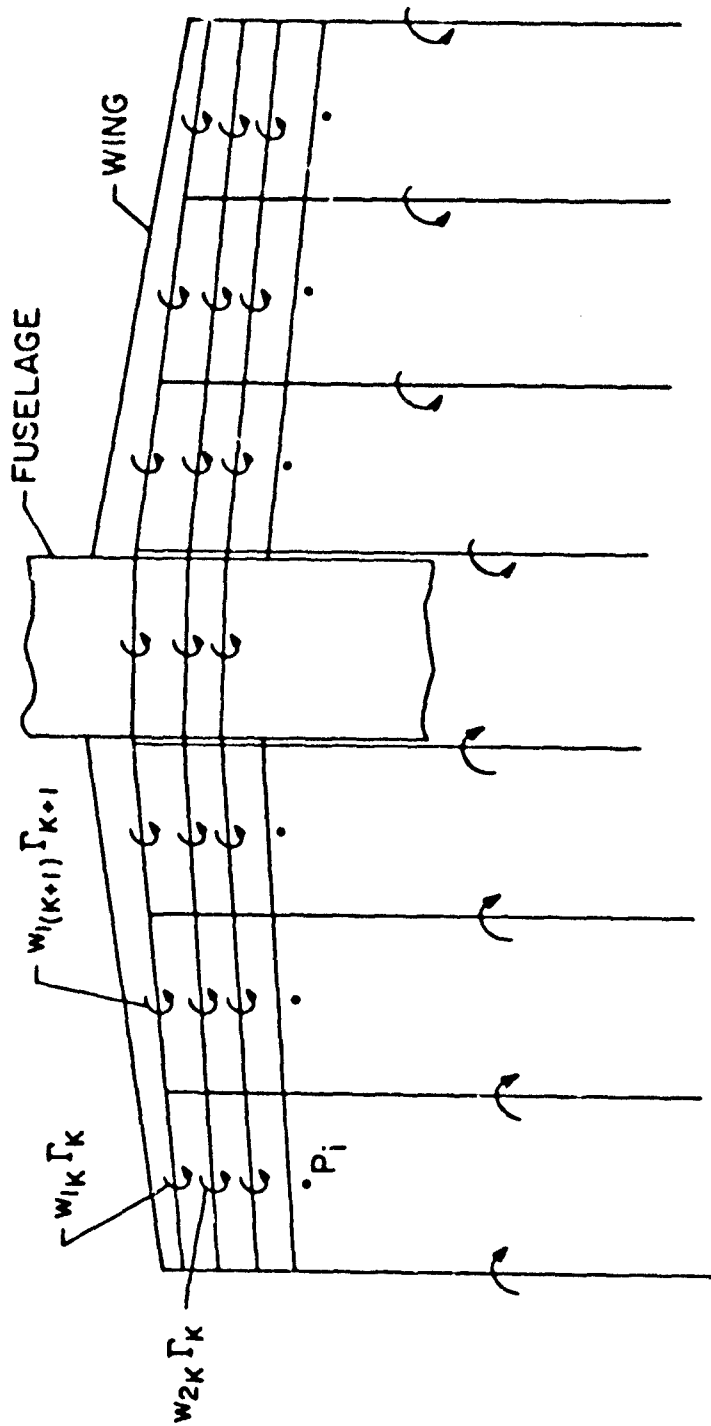


Figure B-2. General Arrangement of Lifting Section Vortex Lattice Network.

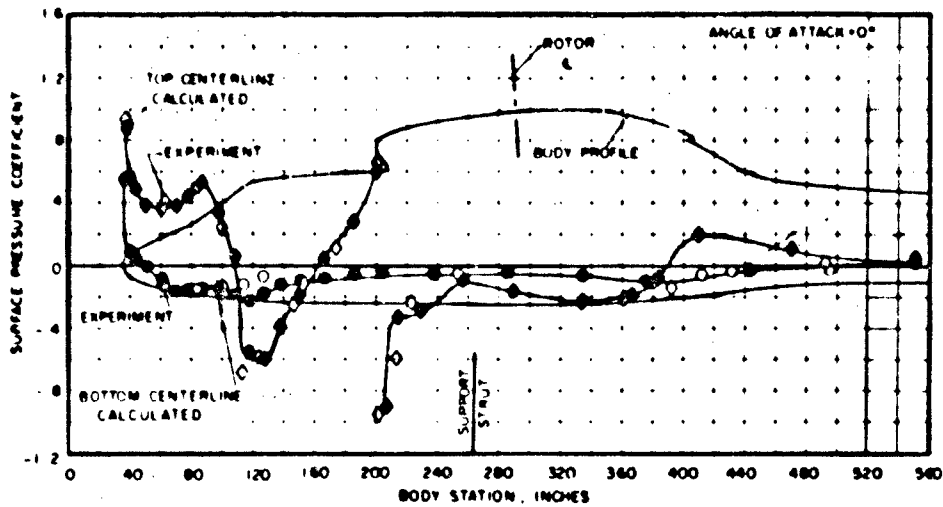


Figure B-3. Comparison of Experimental and Calculated Surface Pressures on RSRA One-Sixth Scale Model.

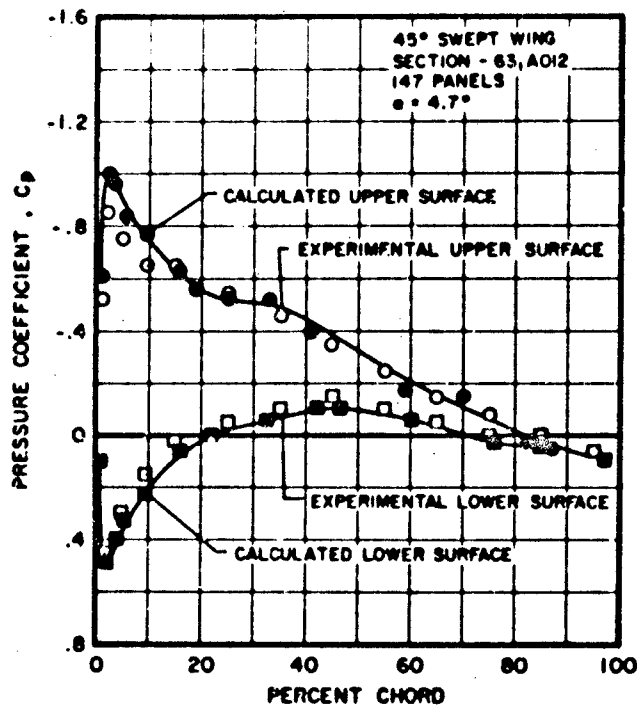


Figure B-4. Comparison of Experimental and Calculated Surface Pressures on a 45-Degree Swept Wing.

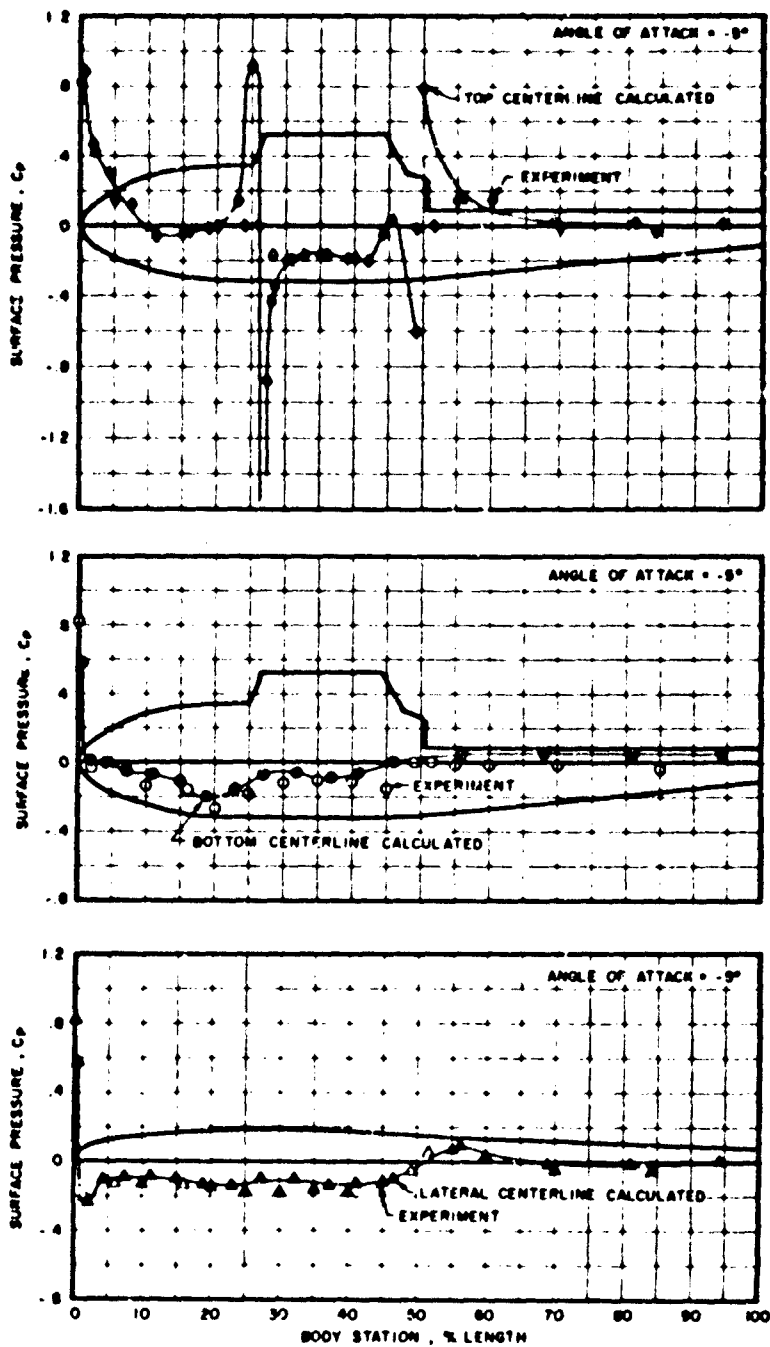


Figure B-5. Comparison of Experimental and Calculated Surface Pressures on Model 1 Fuselage (Reference: NASA TM X-3185).

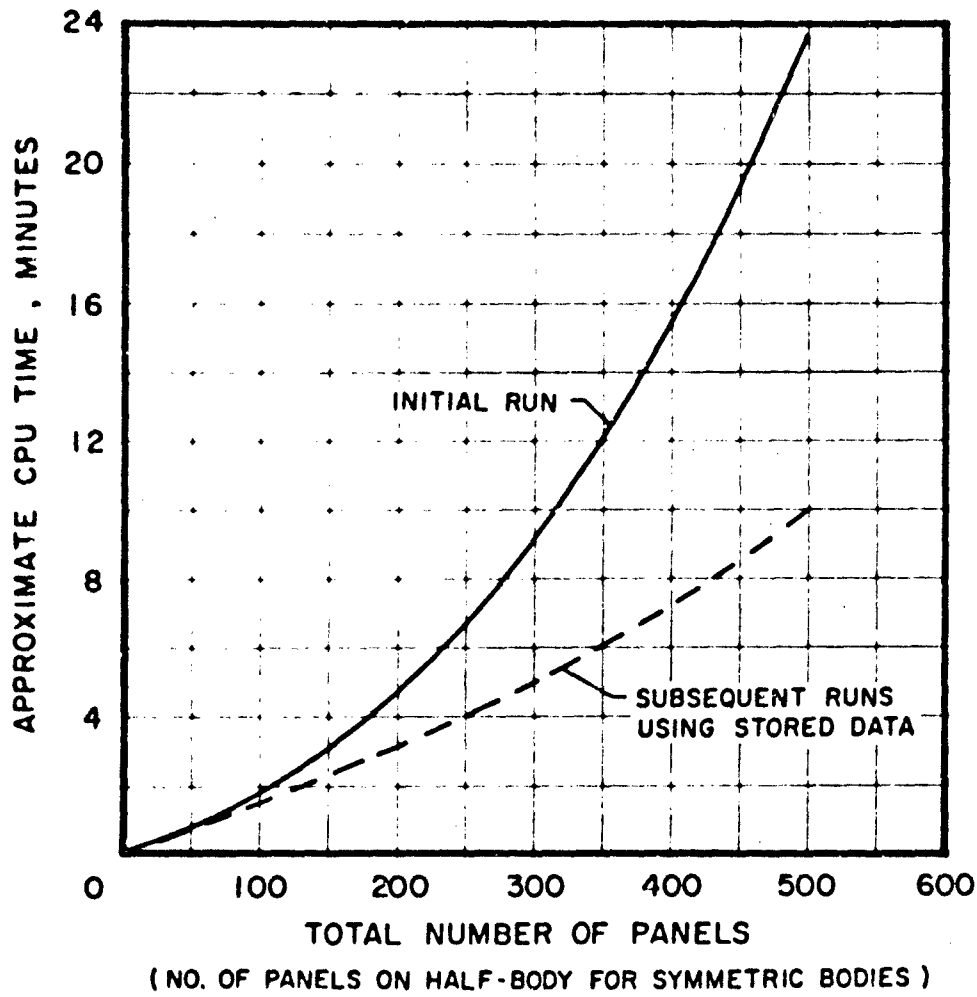


Figure B-6. Estimated CPU Time for Y179L on IBM 360 System.

APPENDIX C

DESCRIPTION AND USE OF THE HUB DRAG PREDICTION

PROGRAM - Y179Z

GENERAL DESCRIPTION

The Hub Drag Prediction Method has been incorporated in a computer program designated Y179Z. The program accepts inputs by the user giving a geometric description of the hub/pylon configuration of interest along with various empirical data if applicable. The program then uses interpolated pylon and fairing surface pressures (if applicable) to predict the total incremental drag of the rotor hub configuration. The program identifies the pylon pressures used in the calculation and produces printer plots of the pressure distribution. The program also allows the user to input a specific pressure distribution although this feature is not normally used because the required calculations can easily be performed if the pressure distribution is known.

Required CPU time for Y179Z is less than one minute.

Input Instructions for Y179Z

<u>Card</u>	<u>Columns</u>	<u>Symbol</u>	<u>Description</u>
1	1-72	TITLE	Any alphanumeric title
2	1	TPC	Type of pylon configuration (i.e., A, B, C). If blank, the program assumes that pylon pressures will be inputted.
	1-10	PC(1)	Pylon length (l)
	11-20	PC(2)	Pylon width (w)
	21-30	PC(3)	Pylon maximum height (h)
	31-40	PC(4)	Axial location of pylon maximum height (Z_M)
3	1- 2	NHUB	Type of hub configuration UF - unfaired hub EF - ellipsoidal fairing RF - rigid fairing
	10-20	HC(1)	Axial location of hub on pylon (Z)
	21-30	HC(2)	Hub frontal area (sq ft) (A_p or A_f)
	31-40	HC(3)	Hub diameter (d)
	41-50	HC(4)	Fairing thickness (t)
	51-60	HC(5)	Fairing skin friction coefficient (C_f)

<u>Card</u>	<u>Columns</u>	<u>Symbol</u>	<u>Description</u>
4	1-10	SC(1)	Shaft height
	11-20	SC(2)	Shaft diameter
	21-30	SC(3)	Shaft frontal area (A_g) (sq ft)
	31-40	SC(4)	Shaft drag coefficient (C_{Dg})

Non-zero values on Card 4 are required for unfaired hubs only if the shaft height is considered sufficient to remove the hub from the local increased velocity region due to the pylon.

5	1-10	BSC(1)	Blade shank length
	11-20	BSC(2)	Blade shank frontal area/ shank. (A_{B_g}) (sq ft)
	21-30	BSC(3)	Blade shank drag coefficient (C_{DB_g})

If the pylon type (TPC) on card 2 is left blank, the following cards are required. These cards will be preceded by a "P" to designate that they are required only if the pylon pressures are to be input.

P1	1- 5	NPP	Number of pylon axial positions for which pressures are to be input (Integer-right justified).
----	------	-----	--

Repeat the following card for each pressure input

P2	1-10	ZL	Location along pylon axis at which surface pressure acts. (Z/L - percent)
	11-20	CPZ	Surface pressure coefficient at this location.

If another hub configuration is to be analyzed, enter a blank card after the preceding cards and enter new data starting with card 1. If no other hub configuration is required, enter "END" in columns 1 - 3.

LIST OF SYMBOLS

A	projected frontal area, sq ft
C _D	drag coefficient referenced to frontal area
C _f	skin friction coefficient
C _p	pressure coefficient
d	diameter
f	equivalent flat plate area, drag/dynamic pressure, sq ft
h	pylon maximum height, in
l	pylon length, in
M	Mach number
q	dynamic pressure, sq ft
R _e	Reynolds number based on hub diameter (unless otherwise stated)
t	hub thickness, in
Z	distance along pylon length, in

Subscripts

BS	blade shanks or cuffs
F	faired rotor hub
H,p	unfaired rotor hub
S	rotor shaft or shaft fairing